AD-A134 192

TECHNICAL REPORT RT-83-4

EXPERIMENTAL MEASUREMENT OF THE NEAR-FIELDS OF A UHF HORN ANTENNA

George R. Edlin
Test and Evaluation Directorate
US Army Missile Laboratory

October 1982

U.S. ARMY MISSILE COMMAND
Redstone Arsenal, Alabama

Approved for public release; distribution unlimited.

SMI FORM 1021, 1 JUL 79 PREVIOUS EDITION IS OBSOLETE

DISPOSITION INSTRUCTIONS

DESTROY THIS REPORT WHEN IT IS NO LONGER NEEDED. DO NOT RETURN IT TO THE ORIGINATOR.

DISCLAIMER

THE FINDINGS IN THIS REPORT ARE NOT TO BE CONSTRUED AS AN OFFICIAL DEPARTMENT OF THE ARMY POSITION UNLESS SO DESIGNATED BY OTHER AUTHORIZED DOCUMENTS.

TRADE NAMES

USE OF TRADE NAMES OR MANUFACTURERS IN THIS REPORT DOES NOT CONSTITUTE AN OFFICIAL INDORSEMENT OR APPROVAL OF THE USE OF SUCH COMMERCIAL HARDWARE OR SOFTWARE.

UNCLASSIFIED

SECURITY CLASSIFICATION OF THIS PAGE (When Data Entered)

REPORT DOCUMENTATION PAGE

READ INSTRUCTIONS BEFORE COMPLETING FORM

1. REPORT NUMBER RT-83-4	2. GOVT ACCESSION NO. AD-A134 192	3. RECIPIENT'S CATALOG NUMBER
4. TITLE (and Subtitle) Experimental Measurement of the Near-Fields of a UHF Horn Antenna		5. TYPE OF REPORT & PERIOD COVERED Technical Report
		6. PERFORMING ORG. REPORT NUMBER
7. AUTHOR(s) George R. Edlin		8. CONTRACT OR GRANT NUMBER(s)
9. PERFORMING ORGANIZATION NAME AND ADDRESS Commander US Army Missile Command ATTN: DRSMI-RT Redstone Arsenal, AL 35898		10. PROGRAM ELEMENT, PROJECT, TASK AREA & WORK UNIT NUMBERS
11. CONTROLLING OFFICE NAME AND ADDRESS Commander US Army Missile Command ATTN: DRSMI-RPT Redstone Arsenal, AL 35898		12. REPORT DATE 1 Oct 82
		13. NUMBER OF PAGES 132
14. MONITORING AGENCY NAME & ADDRESS (if different from Controlling Office)		15. SECURITY CLASS. (of this report) UNCLASSIFIED
		15a. DECLASSIFICATION/DOWNGRADING SCHEDULE

16. DISTRIBUTION STATEMENT (of this Report)

Approved for public release; distribution unlimited.

17. DISTRIBUTION STATEMENT (of the abstract entered in Block 20, if different from Report)

18. SUPPLEMENTARY NOTES

19. KEY WORDS (Continue on reverse side if necessary and identify by block number)

near field
test objective
near zone
electric field
magnetic field

20. ABSTRACT (Continue on reverse side if necessary and identify by block number)

The purpose of this report is to determine quantitatively some of the practical limitations of testing in the near field of UHF horns; in particular, how near to the horn aperture is the field reasonably uniform in amplitude and phase for a given size test object.

This report describes in detail near field measurements of both the electric (E) and magnetic (H) vectors from the aperture of a UHF horn out to

DD FORM 1 JAN 73 1473 EDITION OF 1 NOV 65 IS OBSOLETE

UNCLASSIFIED

SECURITY CLASSIFICATION OF THIS PAGE (When Data Entered) a distance of 4.8 meters. These measurements encompass a rectangular volume of dimensions 2.4m x 3m x 4.8 m. The data spatial separation (i.e., spatial resolution) is 0.1m in each orthogonal direction.

The E and H field data is analyzed and displayed graphically. It is analyzed independently and combined to show the wave impedance behavior in the near zone.

By observation of the data presented, one can immediately develop engineering guidelines for defining the useful test volume in the near zone of a UHF horn. (author)

TABLE OF CONTENTS

LIST OF FIGURES

I. INTRODUCTION

A. Background

The development of numerous high-power radio frequency (RF) emitters in the ultra-high-frequency (UHF) range has proceeded simultaneously with the continuing emergence of increasingly RF susceptible solid-state electronic components (particularly the most recently developed complementary metal-oxide-semiconductor (CMOS) technology). These concurrent technological developments have contributed greatly to increase the number of radio frequency interference (RFI) and electromagnetic compatibility (EMC) problems facing the communications engineers. It is assumed that these problems will loom even larger in the mid 1980's.

These RFI and EMC problems manifest themselves in two major categories when addressed in the particular domain of design, development, and testing of guided missile systems. The two categories are often referred to in the defense community as hazards (i.e., safety) and operational (i.e., functional dependability). In the first, the obvious area of major consideration is personnel safety. The protection and prevention of damage to system hardware and mission success potential are important, but secondary to personnel considerations. The safety problem area is dominated by careful attention to the electroexplosive devices (EED's) which are used to trigger missile launches, automatic eject mechanisms, and weapon detonations. The EED's are susceptible to RF energy and can be activated inadvertently by stray electromagnetic energy. Obviously, premature activation of these triggering systems may be extremely dangerous and is always undesirable. In the second category, system performance is the major consideration. Many external and internal factors influence system operational functions. One of these is inadvertent exposure to significant levels of electromagnetic energy at system critical frequencies (i.e., RFI). This RFI may cause system upset or malfunction. The RF energy levels required to produce undesirable effects in functional dependability are usually significantly lower (often several orders-of-magnitude) than those encountered in hazards (safety) considerations.

Although the problems addressed are most relevant to guided missile systems, the ramifications are pertinent to any military and/or civilian communication and control system which exposes susceptible electronic circuits to potentially dangerous levels of electromagnetic energy in the UHF spectral regime.

Most of the undesirable effects mentioned above are directly related to the intensity of the spurious electromagnetic energy. As nature often seems to dictate, the intensity varies inversely with the distance (or some exponential power thereof) from the source. Consequently, the most serious environments for RFI and EMC effects are often in the near zone of radiating antenna structures. A survey of some pertinent documentation[1, 5, 6, 7] reveals continuing interest in the following areas:

1. Electromagnetic interference in electronic systems in the near field of high-gain microwave antennas.

2. Near field measurements to meet safety requirements.

3. Determination of far field patterns from near field measurements.

4. Mutual gain of multiple antennas in the near field.

5. Radar-cross-sections (RCS's) in the near zone.

An expanded discussion on some of these areas and referenced documents has already been published by this author and is included as Appendix A.

The area designated as number one is of particular interest to the US Army in testing the complex missile systems under development at the US Army Missile Command (MICOM).

As a necessary requirement in testing the complex US Army missile systems for potential RFI and EMC problems, each missile system must be exposed to electromagnetic energy levels with prescribed amplitude, frequency, polarization, and spatial field distribution characteristics. These are identical to or suitably simulate potential environments which the missile system might encounter in actual transportation and/or deployment. This requirement demands RF test capability which includes high-power sources (transmitters of several kilowatts) over a wide range of frequencies (100kHz-10GHz) coupled appropriately with broadband antenna systems (log-periodic, ridged horns, etc.) with selectable polarizations. As previously mentioned, the response of a system to the electromagnetic field imposed on it from an actual source antenna is of keen interest in both hazards and operational test requirements. In order to subject the test item or system to the proper field environment, two fundamental approaches are used. The first is quite straightforward: Equipment to be tested is placed at an appropriate orientation and distance from the actual source antenna, and the spurious effects induced in the test system by the source are measured, recorded, and probable coupling mechanisms are identified. This approach is certainly valid; however, it is often very expensive and sometimes completely impossible from a logistical point of view. The second approach to the testing problem involves the concepts of simulation and/or extrapolation. The system to be tested is placed in one or more potentially "compromising" orientations with respect to a generic type broadband antenna and systematically illuminated with a broad range of frequencies, modulations, and polarizations. System response is again measured, recorded, and analyzed with particular emphasis on the nature of the response as a function of the electromagnetic field amplitude, frequency, polarization, and system orientation. From these general variations, extrapolations are carried out which hopefully predict how the system under test should react to the anticipated actual source of spurious electromagnetic radiation. Although this approach entertains many assumptions and _a priori_ decisions about the test system behavior, it is effective in simulating a wide variety of environments. This approach allows some systems to be tested for which it would be virtually impossible to accomplish by using the first approach discussed. One of the major problem areas associated with the simulation/extrapolation approach is a requirement of a high-intensity field level at all frequencies and polarizations. One of the newer techniques for establishing the required high-intensity field is the major subject of this report.

B. Statement of the Problem

This research report describes an effort to characterize quantitatively the near zone region of a high-gain UHF pyramidal horn antenna and subsequently to use this characterization to outline specific ways in which this information can be used to significantly enhance current technology in EMC/RFI testing.

C. Existing Solution to the Problem

There are two existing solutions to the problem of performing high-level far field testing. The first is to test at lower levels and extrapolate to the higher levels via analysis in conjunction with direct circuit injection. The analysis alone requires complex computations and still cannot account for nonlinear effects such as dielectric breakdown. The use of direct injection can solve the breakdown problem; however, the process is difficult to accomplish due to compact physical constraints and complex impedance matching problems, i.e., the coupling of the test signal can adversely affect the circuit under test.

The second way to accomplish the test is to have the necessary RF transmitting power available to produce the high field levels required at the recommended far field test distance. The normally accepted far-field test distance from the source antenna is given by $2D^2/\lambda$ where D is the largest dimension of the source antenna aperture and λ is the wavelength of the transmitted signal. This generalized formula has been cited in the Navy report, "Near Field and Fresnel Zone Directive Antenna Coupling Program Final Quarterly Report," report #6174D, February 1973. This criterion represents the distance at which there is a reasonably small phase shift across the test volume. In addition, the theoretical wave impedance is approximately 377 ohms. Satisfying these conditions causes the near zone region to extend many meters from the transmitting antenna. The problems with the second approach are the technical and financial constraints. Broadband amplifiers sell for around $50K each, and the band coverage is approximately 200 MHz each from 200 MHz to 1000 MHz. Even these transmitters cannot simulate multikilowatt radar units. Consequently, the test engineer must often forget about continuous frequency coverage and depend on multikilowatt narrow band transmitters. The cost of these units may run several $100K. This approach requires millions of dollars to build a high-level facility. Although technically feasible, this is a very expensive way to accomplish the required objectives.

D. Proposed Solution

The approach this work explores is the utilization of the near zone of large, high-gain transmitting antennas. The use of the near zone requires that the test volume be completely characterized electromagnetically. The methodology of this investigation utilizes accurate spatial resolution amplitude measurements of the three orthogonal components of both the E and H field intensities. The development of small nonperturbing E and H field probes concurrent with high-speed automated data systems has made it possible to make and record the large number of data points necessary to electromagnetically characterize the desired test volume. These experimental measurements are compared to a standard waveguide type aperture model. These results are utilized to develop the wave impedance value as a function of distance from the aperture. The E and H field characteristics are defined in the near zone, and a corrected antenna gain expression is formulated to allow calculation of field strengths for distances as close as $D^2/4\lambda$ from the radiating aperture. At the $D^2/4\lambda$ distance in front of the UHF horn under consideration, a 1-kW transmitter produces the same electromagnetic field strength as a 20-kW transmitter at the recommended $2D^2/\lambda$ distance from the UHF horn aperture.

II. TECHNICAL APPROACH

A. Summary of Technical Approach

The technical approach used for this report is to develop suitable non-interfering, polarization selective, E and H sensors to accurately measure the electromagnetic fields. The next step is to construct a means to spatially position the sensors. An additional requirement is to develop a data acquisition system to read, record, and spatially relate each data point. The final step in this sequence is to process the data and compare the measured data to the theoretical models.

B. Development of the Measurement Techniques

Probe Description - The probes utilized for the characterization of the three orthogonal components of both the E and H fields are polarization selective, paeudo transparent, non-interfering type sensors. Both the E and H sensors use diode detection with carbon filled lines to connect the sensor to a 100 megohm input impedance voltmeter. The H field sensor is a double gapped loop wired electrically to cancel any component of the E field which drives the output gaps. The E field probe is an electrically short dipole which is also diode-detected and interfaced to the same high impedance voltmeter via carbon filled lines. The calibration of the E and H sensors is accomplished by establishing known E and H fields in a Crawford cell. The Crawford cell is an expanded coaxial line which can be used to establish accurate fields. The sensors are placed in known fields and the detected outputs measured and related to the standard field levels. The calibration curves developed are used to relate the raw data to actual field strengths. Appendix B contains complete explanations of the design and calibration of the E and H field probes.

Three-Dimensional Scanner - The three-dimensional scanner is constructed using 6 inch polyvyn chloride (PVC) pipe for the base section as shown in Figure 1. The trolley which moves the probes in the Z direction (toward and away from the antenna aperture) and the vertical support pole are also PVC. The position is indicated to the computer via a microswitch and a 9 volt battery in series with the carbon filled lines. The trip positions are located at precise 10 cm intervals along the Z axis from 0.1 to 4.8 meters away from the aperture. The X position is also transmitted to the HP 9825 controller by the X position (horizontal position) microswitch. The trips for the X position are also 10 cm apart for $-1.5\text{m} \leq X \leq 1.5\text{m}$. Six E or six H probes are mounted 40 cm apart on the vertical support with provision for lowering the support in 10 cm increments three times. This gives

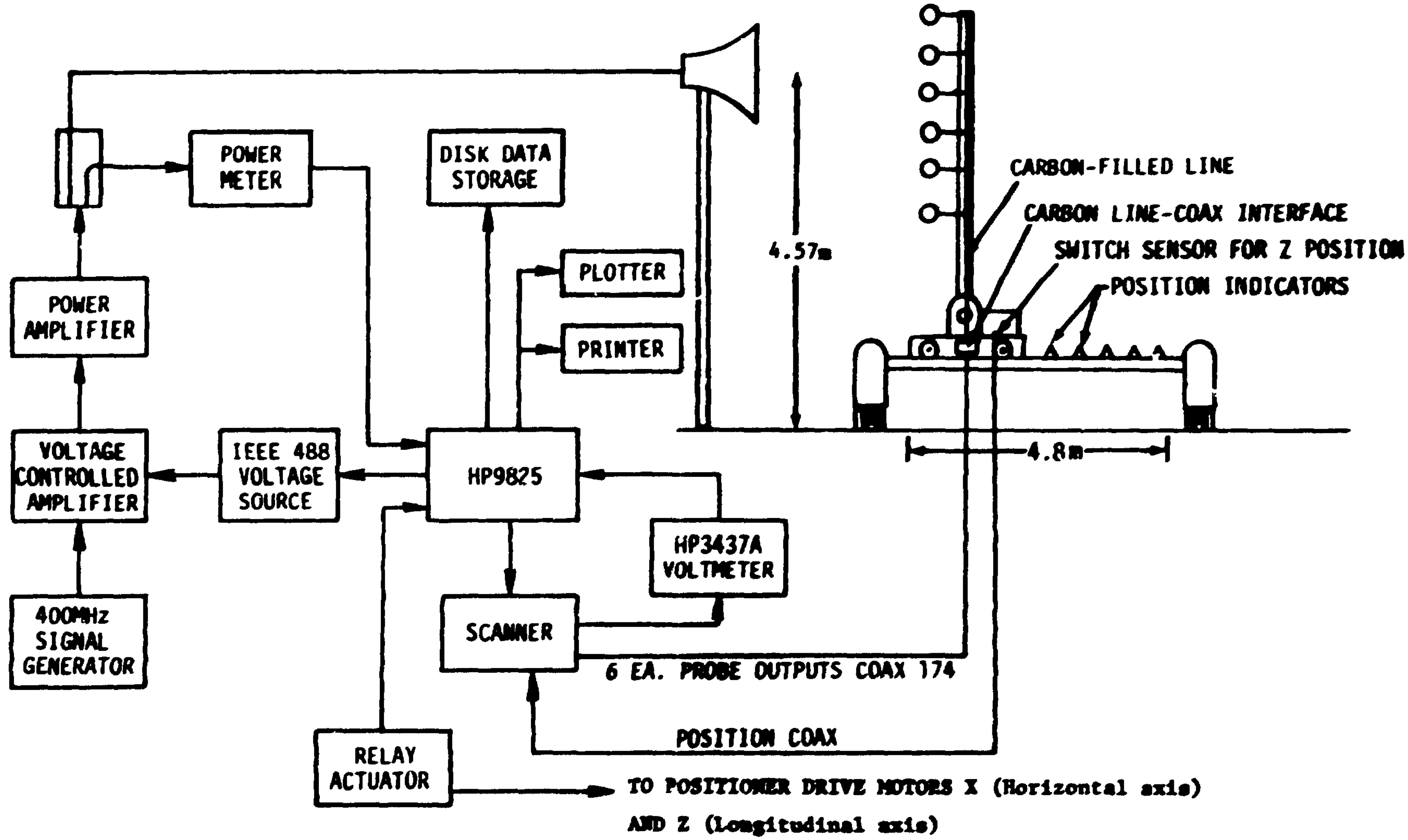

Figure 1. Data acquisition system.

complete coverage for 1.2m above the antenna center line to 1.2m ($-1.2m \leq Y \leq 1.2m$) below the antenna center line. More detailed information on the positioner is included in Appendix C and in the discussion of the data acquisition system.

Data Acquisition System - The data acquisition system consists of a standard gain horn (gain 18 dB nominal, frequency, 300 to 550 MHz) mounted in the vertical E field polarization orientation with the center line 4.57m above the ground. The computer controller is an HP 9825. The excitation for the horn is a Watkins-Johnson (WJ) synthesizer in series with a voltage controlled attenuator. This allows the computer to adjust the excitation level to the solid-state power amplifier. The power is monitored using a directional coupler and an IEEE 488 bus operated HP 436 power meter. In this way the controller is able to monitor and set the power level before each scan. The frequency used is a constant 400 MHz. This frequency is compatible with the horn and field measurement system. The 4.8m probe scanner, along with the HP 3495A scanner, HP 3447A system voltmeter, HP 9825 controller, and 8-inch floppy disk comprise the major hardware components utilized in the data collection system. Figure 1 presents the block diagram for this system. The probe positioner configuration allows for acquiring data precisely every 10 cm for each of the three orthogonal directions. The data measurement matrix results in 37,200 locations for each of six orthogonal components.

The total data system is controlled by the HP 9825 controller. The operator has only to turn on the equipment, set the frequency of the exciter to 400 MHz, and position the mechanical probe positioner to the starting position. The operator then executes the control program and inputs the type probe (E or H) and the component of the field being measured (vertical, horizontal or radial). The operator inserts the proper disk and starts the data acquisition process. The control system automatically adjusts the power to 20 watts into the transmitting system and starts the first scan which is in the Z axis (along the antenna radiation axis). The trip points located at 10 cm intervals along the Z direction synchronize the data readings of each of the six probes mounted on the vertical support. The program reads the raw data and stores it along with the X (horizontal), Y (vertical) and Z (radial) position information after applying proper calibration factors. After the data storage is completed, the positioner moves over 10 cm in the X direction and makes another scan in the Z direction. This process is continued until all the X positions are measured. The vertical probe support is then vertically shifted by 10 cm (Y axis), and the original process is repeated for a total of four times to complete one orthogonal component of the E or H field. A detailed description of the positioner is contained in Appendix C. Each of the orthogonal components are stored on separate 8-inch floppy disks. One complete set of data is 223,200 data points contained on six disks. These data are also printed as they are taken to allow for real-time observation as well as to check for possible disk storage problems.

C. Data Collection

Raw Data - The E field and H field probes have DC outputs on the order of millivolts. The diode detector is a nonlinear device; therefore, the polynomial that relates the field amplitude to the voltage output of the probe is complex and is of the form $F_L = C_1V_0 + C_2V_0^2 + C_3V_0^3$. Where F_L is the field level, V_0 is the probe output, and C_1, C_2, and C_3 are the calibration coefficients determined by putting the probe in known electromagnetic fields at several levels and using a third order polynomial regression program. This polynomial will allow the computer to rapidly compute the correct field level for any probe output voltage.

<u>Data Processing</u> - To convert the data to meaningful information, the potential reading must be multiplied by the appropriate polynomial and stored in data arrays on the disk. Each disk contains a single orthogonal component of the E field or H field. The orthogonal components of the E and H field can then be printed in tables or plotted in two-dimensional or three-dimensional graphs to be analyzed or compared to theoretical plots.

D. Comparison of Collected Data to Theoretical Models

<u>General Discussion of Measured Data</u> - Observation of the data yields some very significant information to the microwave test engineer. First, if one considers the impedance curve shown in Figure 2, one notices that the wave impedance does not vary significantly from the 377 ohm far field values, even as near to the aperture as one meter. This implies that only the E field has to be measured to characterize the power density at test points very close to the antenna aperture. The measured data showing the wave impedance is very well behaved as close as $D^2/4\lambda$ from the aperture. The centerline data plotted in Figure 3 shows that the vertical E field is also well behaved as near as $D^2/2\lambda$ and is reasonably good at distances greater than $D^2/4\lambda$ from the aperture.

<u>Aperture Distribution Model</u> - The analytical model for this was TE_{10} mode amplitude (cosine in X) distribution with a quadratic phase term.

The aperture distribution was used with the vector Smythe-Kirchhoff[3] approximation for diffraction to solve for the spatial representation of the radiated field. This relationship is given in equation (1).

$$\vec{E}(x,y,z) = \frac{1}{2\pi}\nabla x \int (\hat{n}X\bar{E}) \frac{e^{jkR}}{R} da' . \tag{1}$$

Figure 4 shows the horn geometry and aperture associated coordinate system. The TE_{10} waveguide E-Field distribution is given by equation (2).

$$\vec{E}(x,y,0) = E_0 \cos\frac{\pi x}{a} \exp\left[-jk\left(\frac{x^2}{2\ell_H} + \frac{y^2}{2\ell_E} + \alpha\right)\right]\hat{U}_y . \tag{2}$$

Substituting the expression in equation (2) into equation (1) and solving for the associated E field and H field components we have equations (3) thru (9).

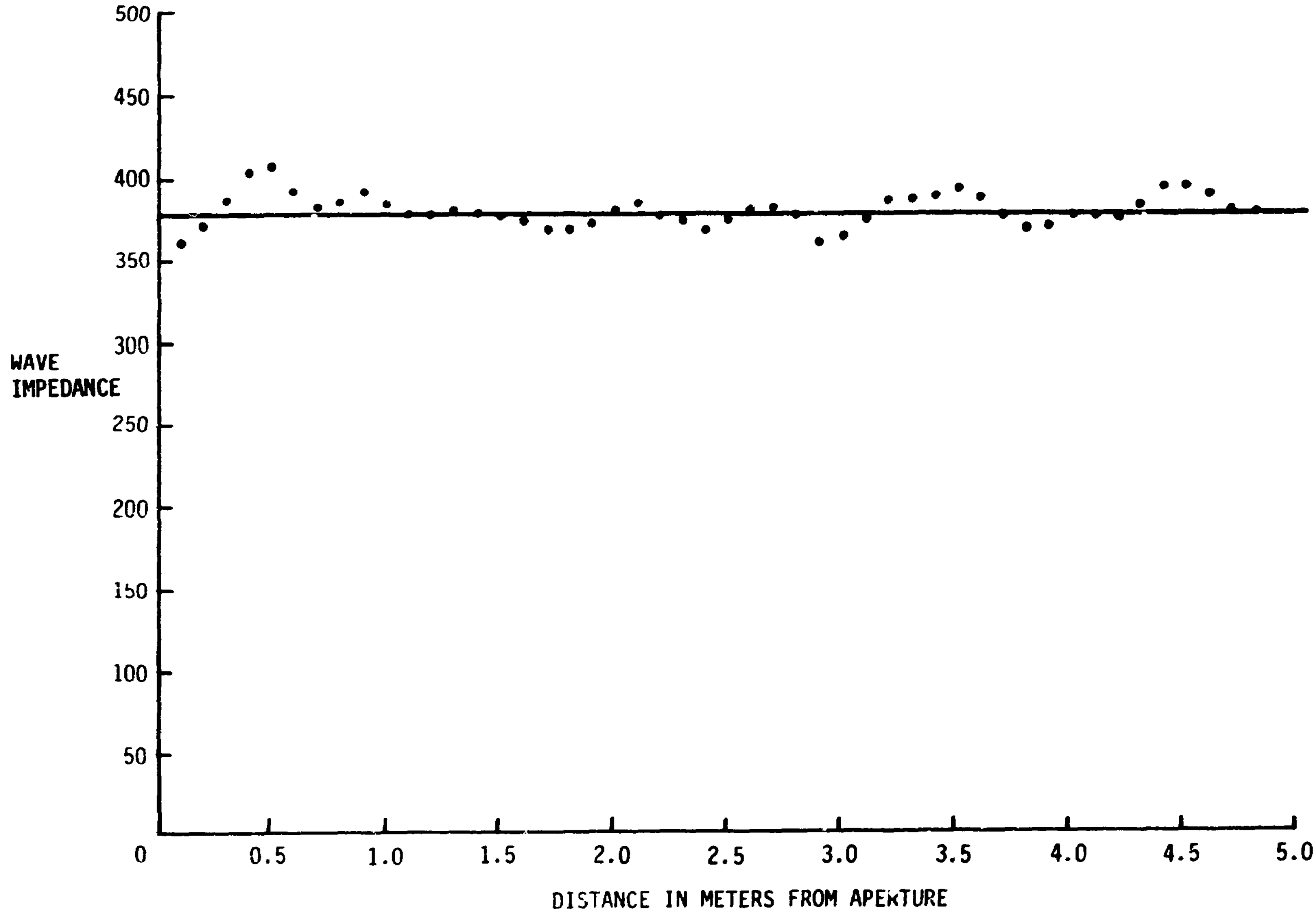

Figure 2. Wave impedance $Z_{o(Ohms)}$ distance (Z) (meters) from the aperture.

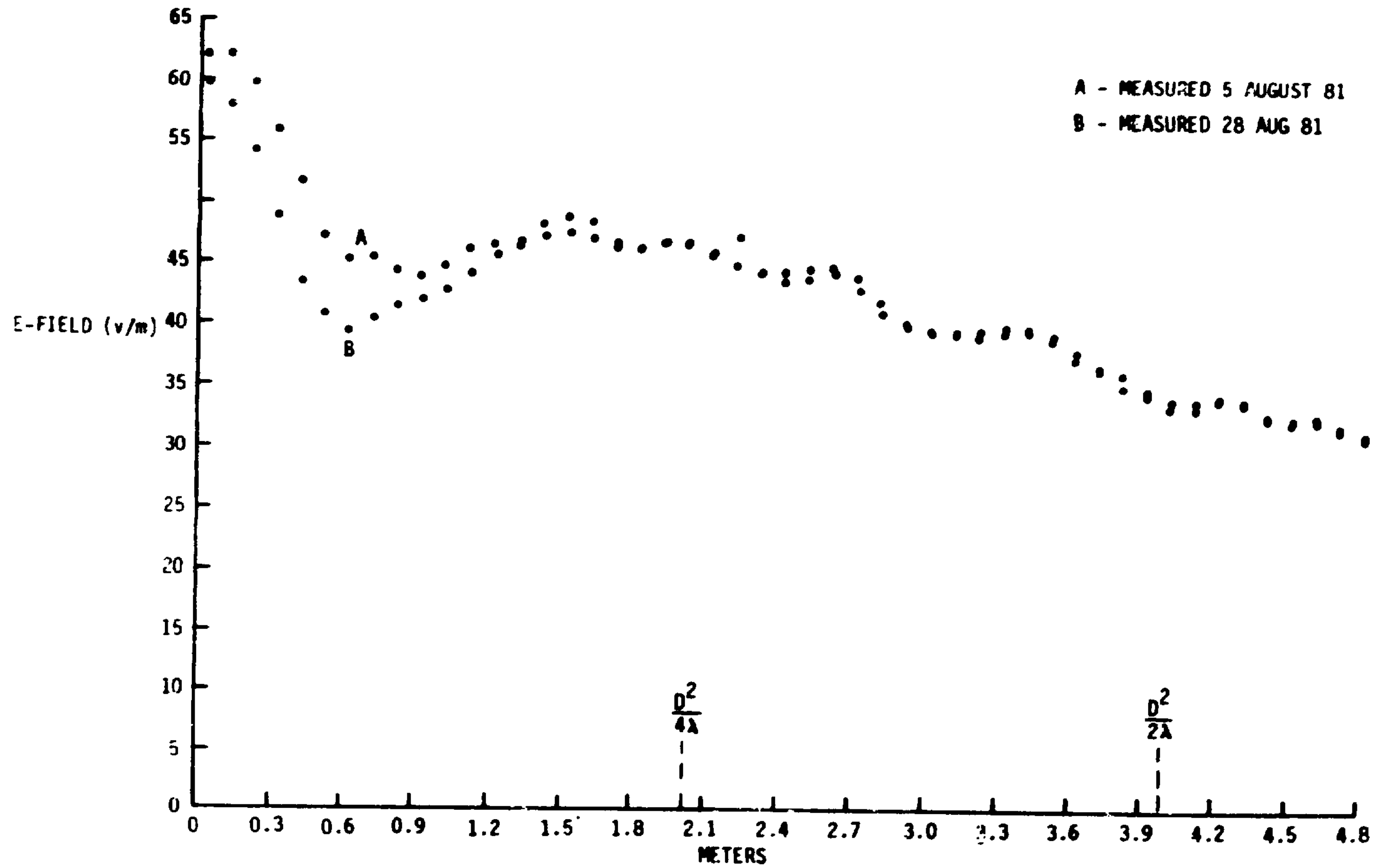

Figure 3. Vertical E-field vs. Z from the Aperture .

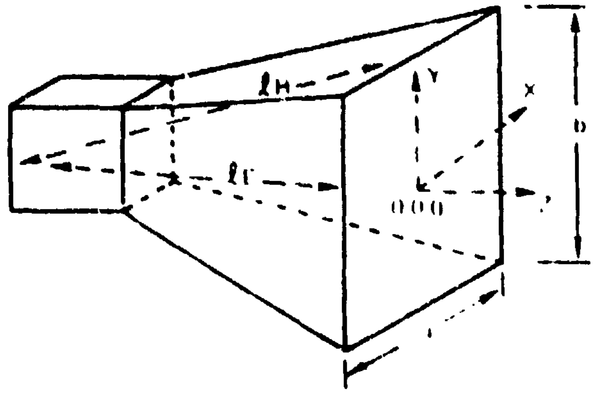

Figure 4. Geometry and coordinate system of UHF pyramidal horn.

$$E_y = \frac{E_0}{2\pi} \iint\limits_{Aper} \cos \frac{\pi x'}{a} \frac{e^{-jkB} z (1-jkR)}{R^3} dx'dy' \qquad (3)$$

$$E_z = \frac{E_0}{2\pi} \iint\limits_{Aper} \cos \frac{\pi x'}{a} \frac{e^{-jkB}(y' - y)(1 - jkR)}{R^3} dx'dy' \qquad (4)$$

where

$$R = \left[z^2 + (x - x')^2 + (y - y')^2\right]^{\frac{1}{2}} \qquad (5)$$

$$B = \left[\frac{x'^2}{2\ell_H} + \frac{y'^2}{2\ell_E} - R\right] \qquad (6)$$

$$H_x = \frac{jE_0}{2\pi\omega\mu} \iint\limits_{Aper} \cos \frac{\pi x'}{a} \frac{e^{-jkB}}{R^3} \left\{\left(k^2 - \frac{3}{R^2} + 3j\frac{k}{R}\right) \left[(y-y')^2 - z^2\right] + \left(1-jkR\right) \right\} dx'dy' \qquad (7)$$

$$H_y = \frac{jE_0}{2\pi\omega\mu} \iint_{Aper} \cos\frac{\pi x'}{a} \frac{e^{-jkB}}{R^3} (y-y')(x-x') \left(k^2 - \frac{3}{R^2} + \frac{j3k}{R}\right) dx'dy' \tag{8}$$

$$H_z = \frac{jE_0}{2\pi\omega\mu} \iint_{Aper} \cos\frac{\pi x'}{a} \frac{e^{-jkB}}{R^3} z\,(x-x') \left(k^2 - \frac{3}{R^2} + \frac{j3k}{R}\right) dx'dy' \,. \tag{9}$$

This model has been utilized by several investigators[2, 4]. A detailed derivation of the commonly accepted analytical model is presented in Appendix D, and numerical evaluations and presentation of the model are included in Appendix E.

Figure 5 compares the measured wave impedance as a function of Z with that obtained theoretically in Appendix E. The measured data do not exhibit nearly as sharp a rise as the computed curve, although it does show a similar shape with perturbations around the 377 ohm line as the distance in the Z direction exceeds 0.75 meters. These small perturbations from 0.75 to 5 meters may be the result of standing waves which seem to be visible in the three-dimensional plot (Figure 6). The fact that the impedance of the measured data does not peak as high or dip as low as the model can be attributed to four main factors: (1) inaccuracies in the model, (2) inaccuracies in the horn construction, (3) spatial integration of the E field amplitudes that change rapidly with Z produced by finite probe size, and (4) standing waves causing constructive and destructive interference in the field amplitudes.

The significance of Figure 5 is two-fold. The first and main point is that the near field wave impedance is essentially the same as far field wave impedance to distances from the aperture of the test horn antenna as near as one meter. In terms of the wavelength of the experimental setup, $D^2/8\lambda$ equals approximately one meter. Secondly, the results of Figure 5 imply that only one of the field components needs to be measured to establish the power density of the radiation field. This fact makes it feasible to utilize the near field for testing purposes. A plot of the analytical model with the measured data as a function of the distance Z (meters) from the aperture is presented in Figure 7. It is very obvious that the measured data do not increase as fast as the model and do not oscillate as much as the model inside the 1 meter or $D^2/8\lambda$ distance from the aperture. This makes the field in the very near zone $D^2/8\lambda$ far more usable than was predicted by the model.

Multipole Model - If one looks closely at Figure 8 which has the $1/r$ relationship plotted along with the measured data, it is obvious that the measured data do not increase nearly as fast as the $1/r$ curve near the aperture. This fact also contributes to the usefulness of the volume near the aperture for testing of small systems, i.e., the rate of change of the E field is not appreciably different at points 2-3 meters from the aperture

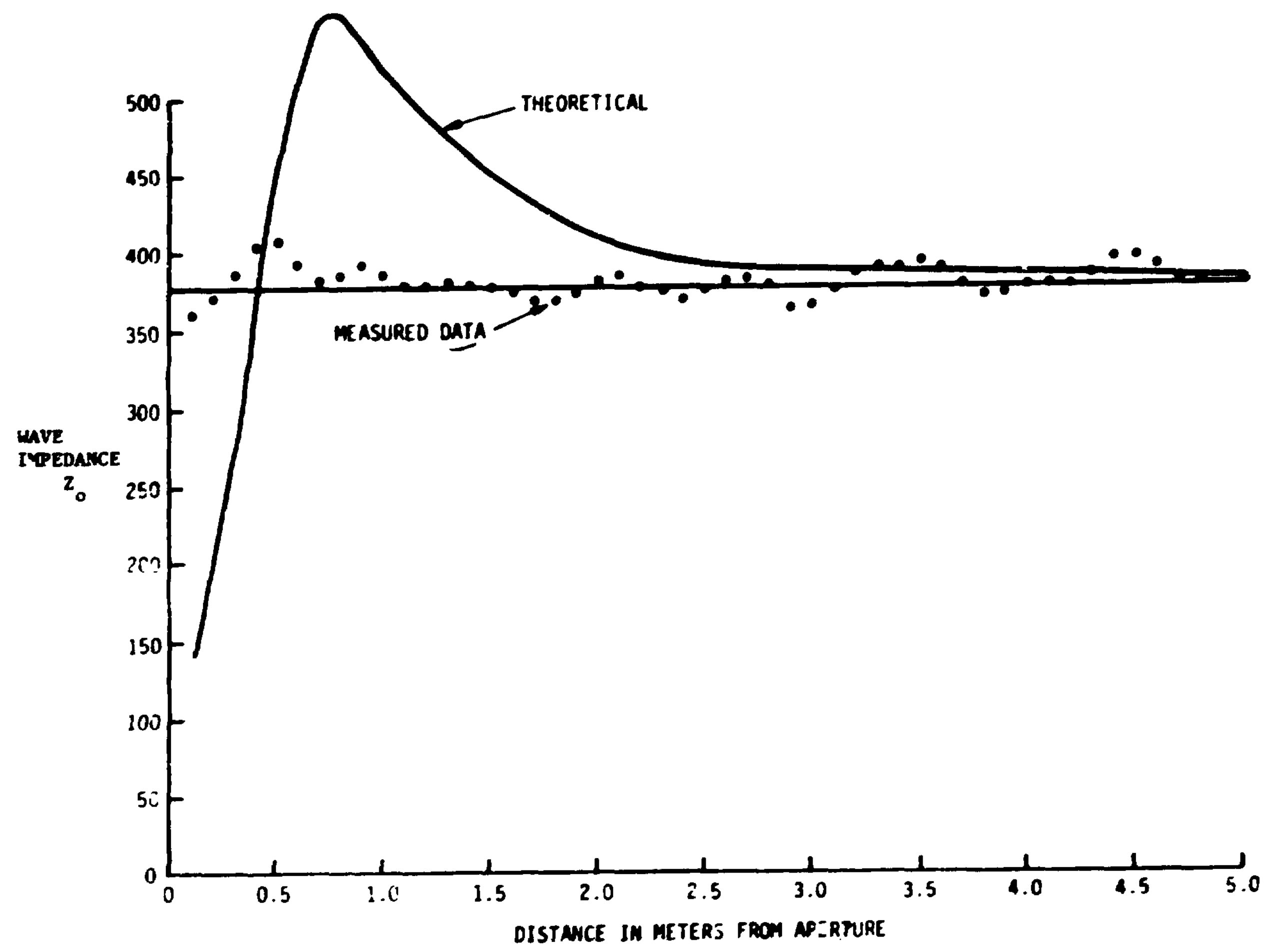

Figure 5. Wave impedance $\left(\frac{Ey}{Hx}\right)$ vs. Z for rectangular pyramidal horn.

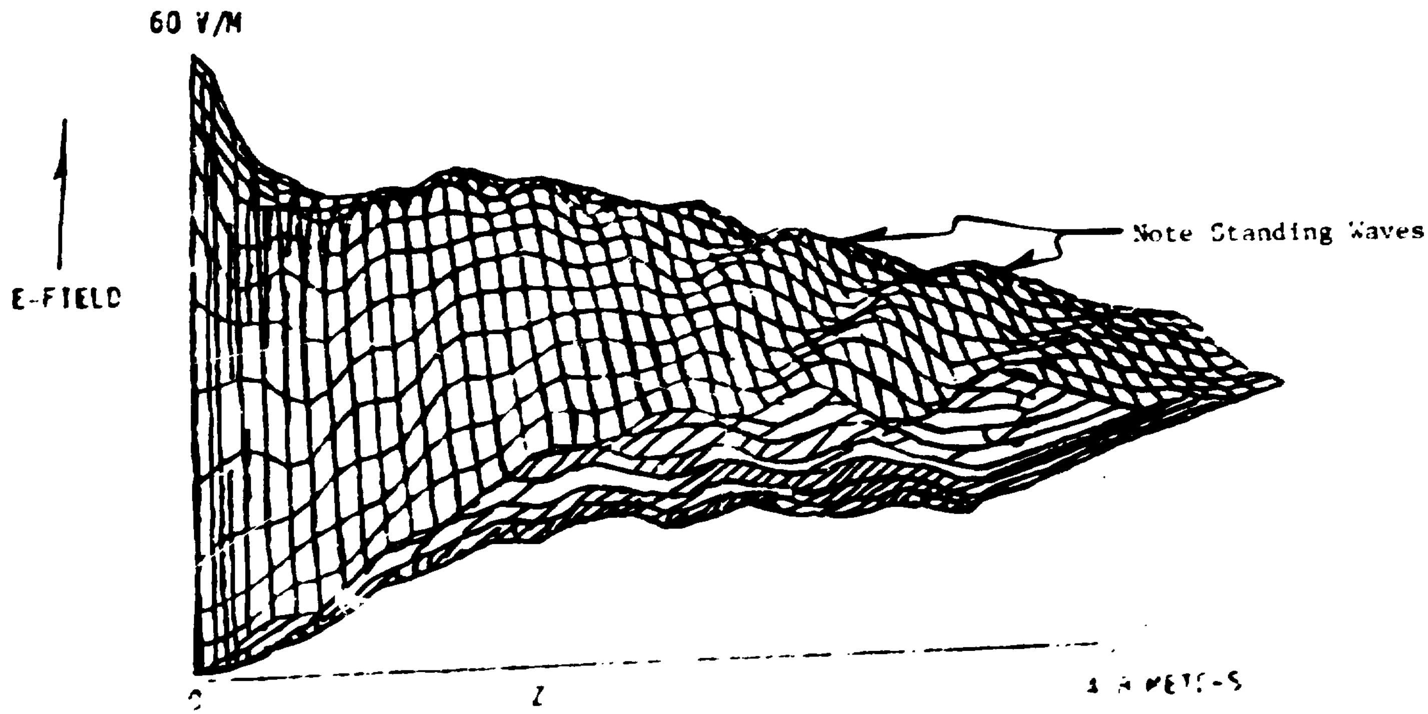

Figure 6. 3-Dimensional plot of E-field (V/m) vs. horizontal position and radial position (side view).

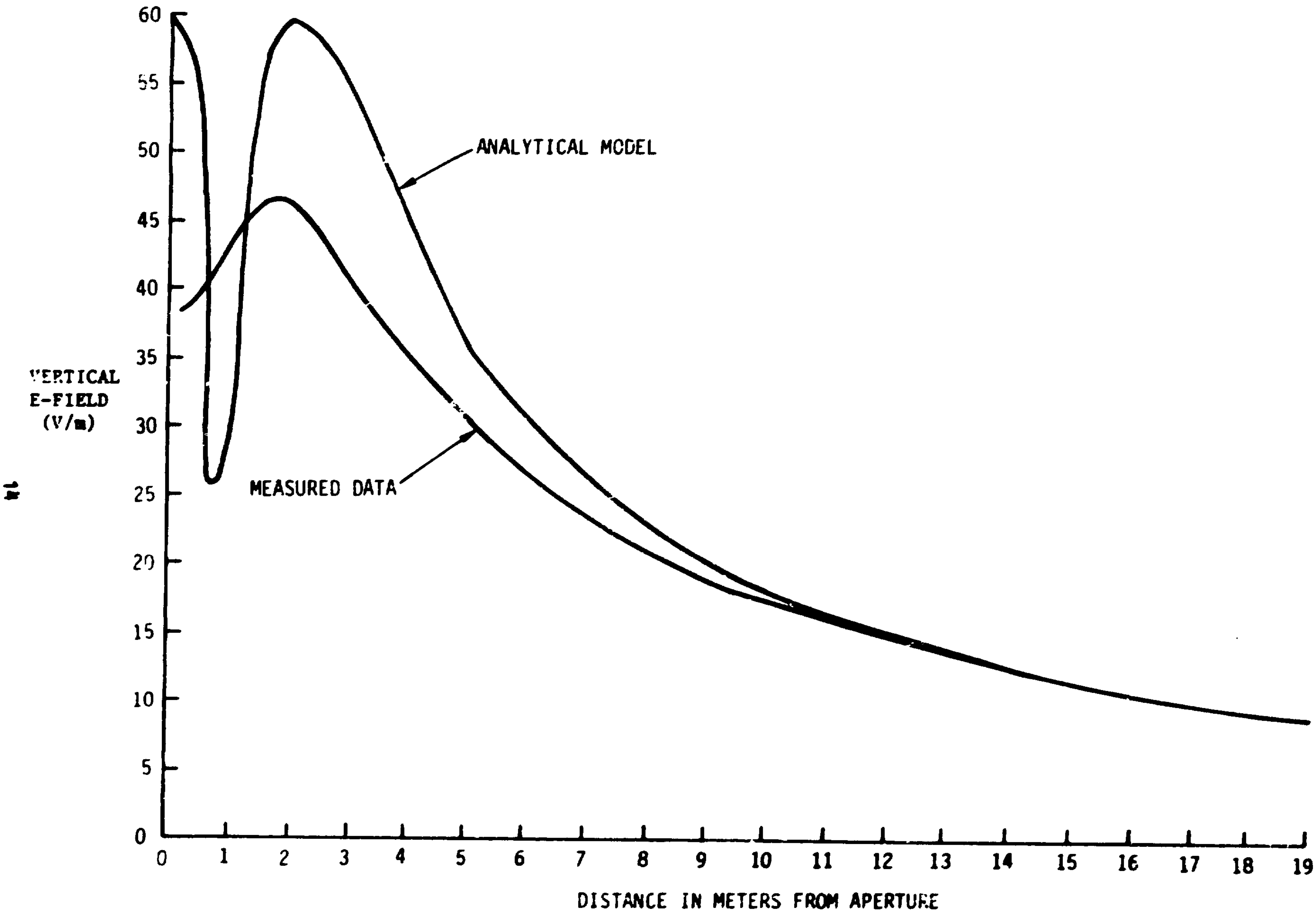

Figure 7. Comparison of analytical model with measured data.

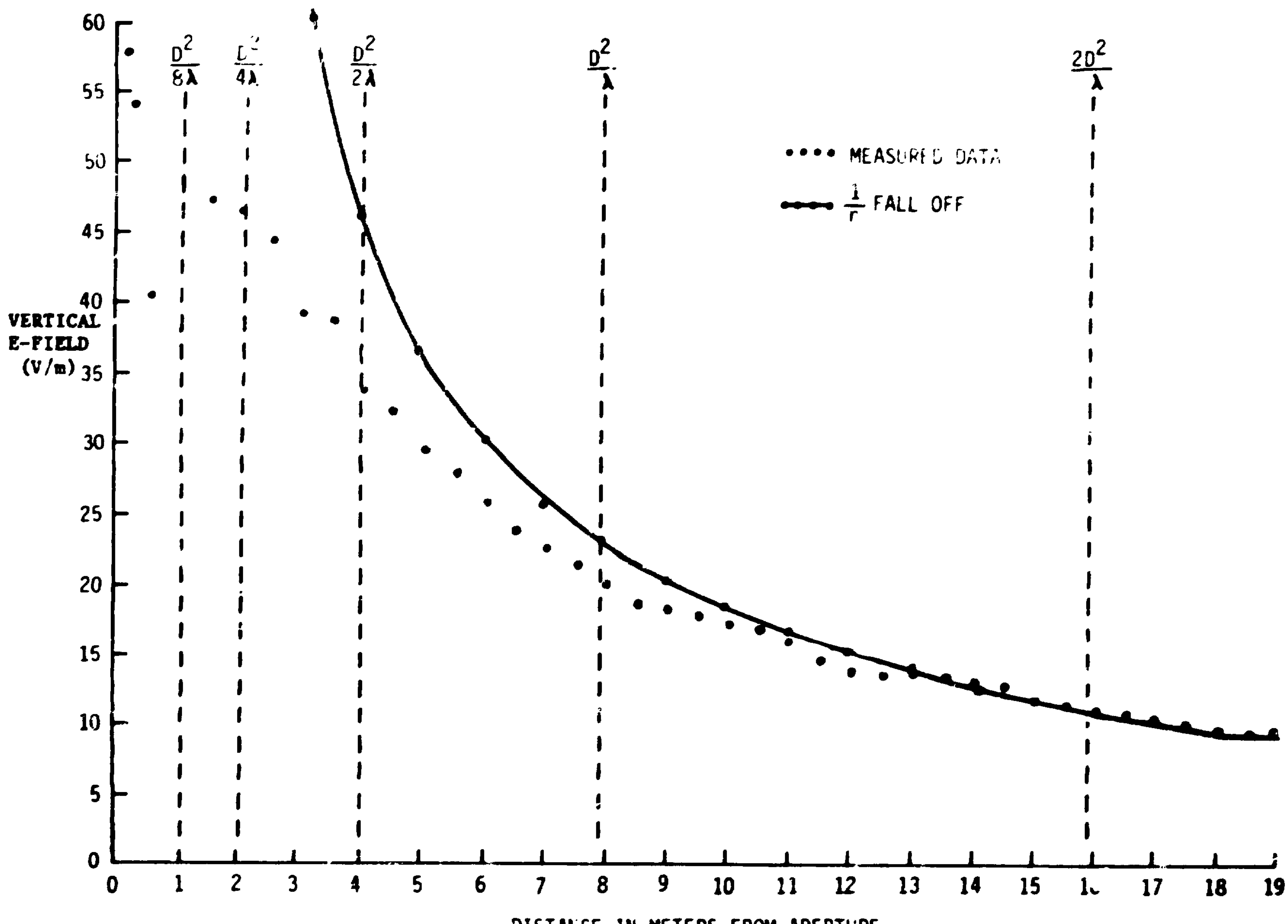

Figure 8. Vertical E-field Amplitude (V/M) vs. Z (Meters)

and points 6-8 meters from the aperture. The advantage of testing in the near zone is very obvious; if one moves in to half the distance, in general, the field strength is effectively doubled, which means to have produced the same field strength at the greater distance would have required a power increase of four times. This simple illustration then implies that for a small system, the test engineer can utilize the near zone, $D^2/2\lambda$, and effectively achieve the same test field with a 1 kW transmitter that would require a 16 kW transmitter at the classical $2D^2/\lambda$ position. It is apparent that the 1/r model is not accurate at radial distances closer than D^2/λ. A useful model which is accurate at a closer distance is the multipole model. The form of the electric field for the multipole model is given as

$$E = \left(\frac{A_1}{r} + \frac{A_2}{r^2} + \frac{A_3}{r^3}\right)(P_T)^{1/2} \tag{1}$$

where

E = E field in volts per meter (V/m)
P_T = power of the transmitter (Watts)
r = distance from the aperture in meters
A_1, A_2, A_3 = experimental constants

A comparison of the multipole model to the experimental data is shown in Figure 9. This model can be used as near as $D^2/4\lambda$ with an accuracy of approximately +0.5 dB. Details of the derivation of this model are presented in Appendix F.

<u>Engineering Model</u> - Since the main objective of this work is to develop a methodology for the utilization of the near zone volume for EM testing, one of the main considerations is to develop an engineering model which would predict the E field at any frequency and radial distance from the antenna.

The E field in the near zone of a UHF antenna predicted by the engineering model is given by equation (2)

$$E = \left\{\left[\frac{G(1 - \exp(-4r/(2D^2/\lambda))}{4\pi r^2}\right] 377P_T\right\}^{1/2} \tag{2}$$

where

E = E-field (in V/m)
r = distance (in meters) from the aperture
D = largest dimension of aperture (in meters)
λ = wavelength (in meters)
P = transmitter power (in Watts)
G = far field gain (absolute, not decibels)

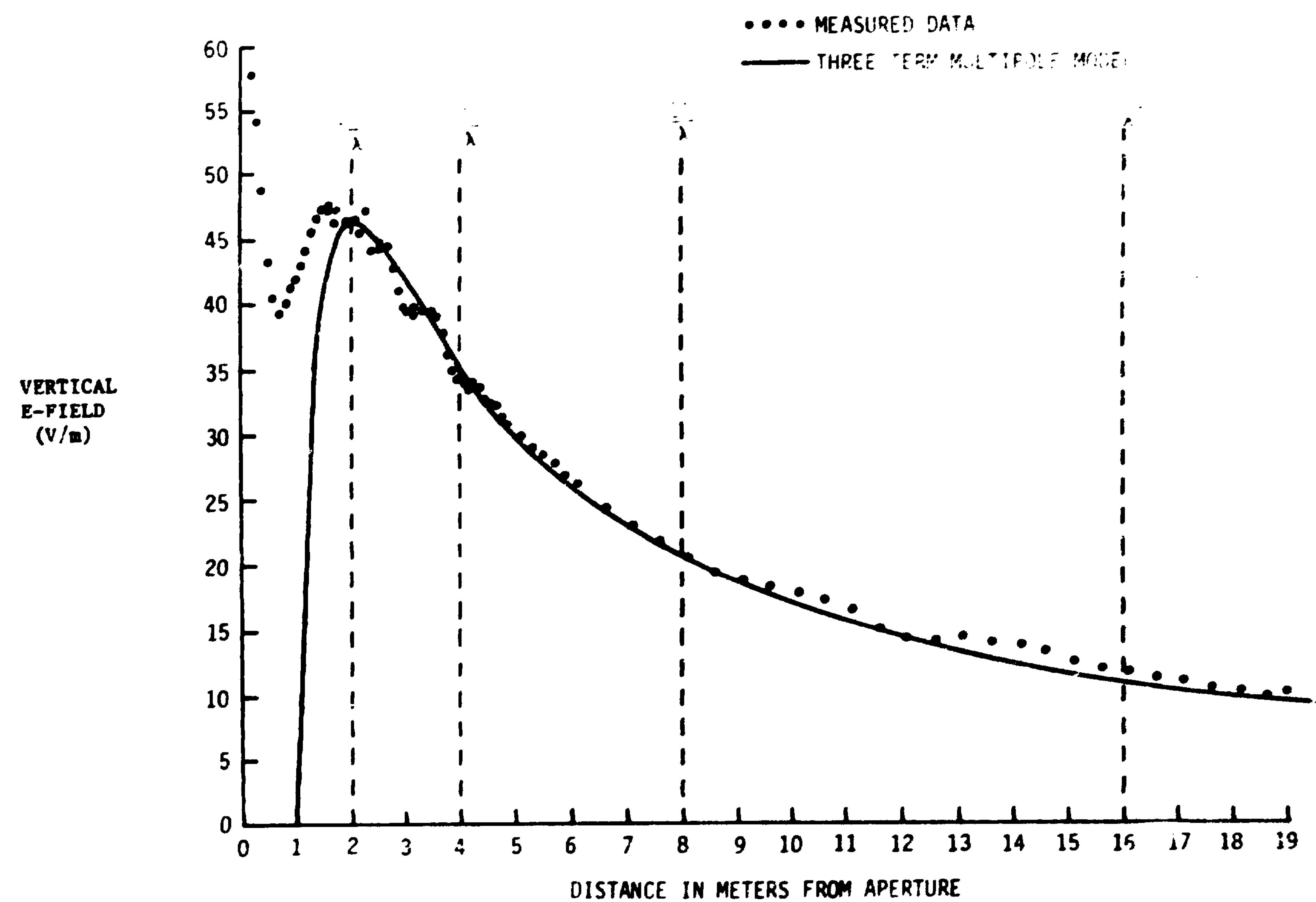

Figure 9. Multipole predicted E and measured data vs. Z.

For additional detail of the engineering model refer to Appendix G. The comparison of the engineering model with the measured data is shown in Figure 10. This model will predict the E field of the test horn in as near as $D^2/4\lambda$ with accuracy of approximately $+1.5$ dB.

Three-Dimensional Data Plots - One of the best ways to show the radial uniformity of vertical E field (E) and horizontal H field (H) is to observe a few 3-D plots. The 3-D plots are presented with the aperture of the horn on the observer's left; with X, the horizontal dimension; field amplitude, the vertical dimension; and Z, the radial dimension from the aperture increasing to the observer's right.

The vertical dimension displays either the amplitude of the E or H field at a selected Y position. This position is always held constant at zero which is center line for the horn for Figures 11 and 12 (see Appendix H). The observation of these figures gives one a visual presentation of the E field shape as a function of X and Z on the center line of the horn from the horn aperture to a separation distance (Z) of 4.8 meters. The intersection points of the cross hatched lines represent the measured data points. These figures are given to show shape and are not scaled. Appendix H contains all plotted data. Explanation of the data correlation is also contained in H. Careful observation of Figures 11 and 12 shows the possible effect of standing waves on E field amplitude. The standing waves referred to are the small perturbations in amplitudes along the Z direction. These waves give rise to some shifting of the wave impedance Z from the far field nominal value of 377 ohms.

The view in Figure 13 shows how the cosine distribution at the aperture diminishes as the radial distance increases. This figure is presented from the same aspect as Figures 14, 15 and 16 which allows the direct comparison of Figures 13 and 14. This comparison gives visual confirmation that the ratio of E to H is consistent across the X dimension of the test volume. Figures 15 and 16 show that the radial H and vertical H are consistent with the radial E and horizontal E shown in Figures 11 and 12, i.e., the vertical H compares with the horizontal E near zero, and the radial amplitude is low and falls off rapidly with increasing distance from the aperture.

III. CONCLUSIONS

A. Near Field Characteristics of the UHF Horn Antenna

Radial Uniformity of the Wave Impedance - The previously discussed Figure 3 shows the radial uniformity of the wave impedance along the center line of the antenna. The maximum deviation is approximately 33 ohms. This occurs near 0.5 meters and is less than 9% different from the far zone value.

The importance of this uniformity cannot be overstressed due to the simplification of the field measurement problem and the understanding of its interaction with various electronic circuits.

Radial Attenuation of the Nonradiative Components - An informative way to view the rapid fall off of the nonradiative component is to observe Figure 12 which shows the 3-D comparison of the radial E field, E_R, with the

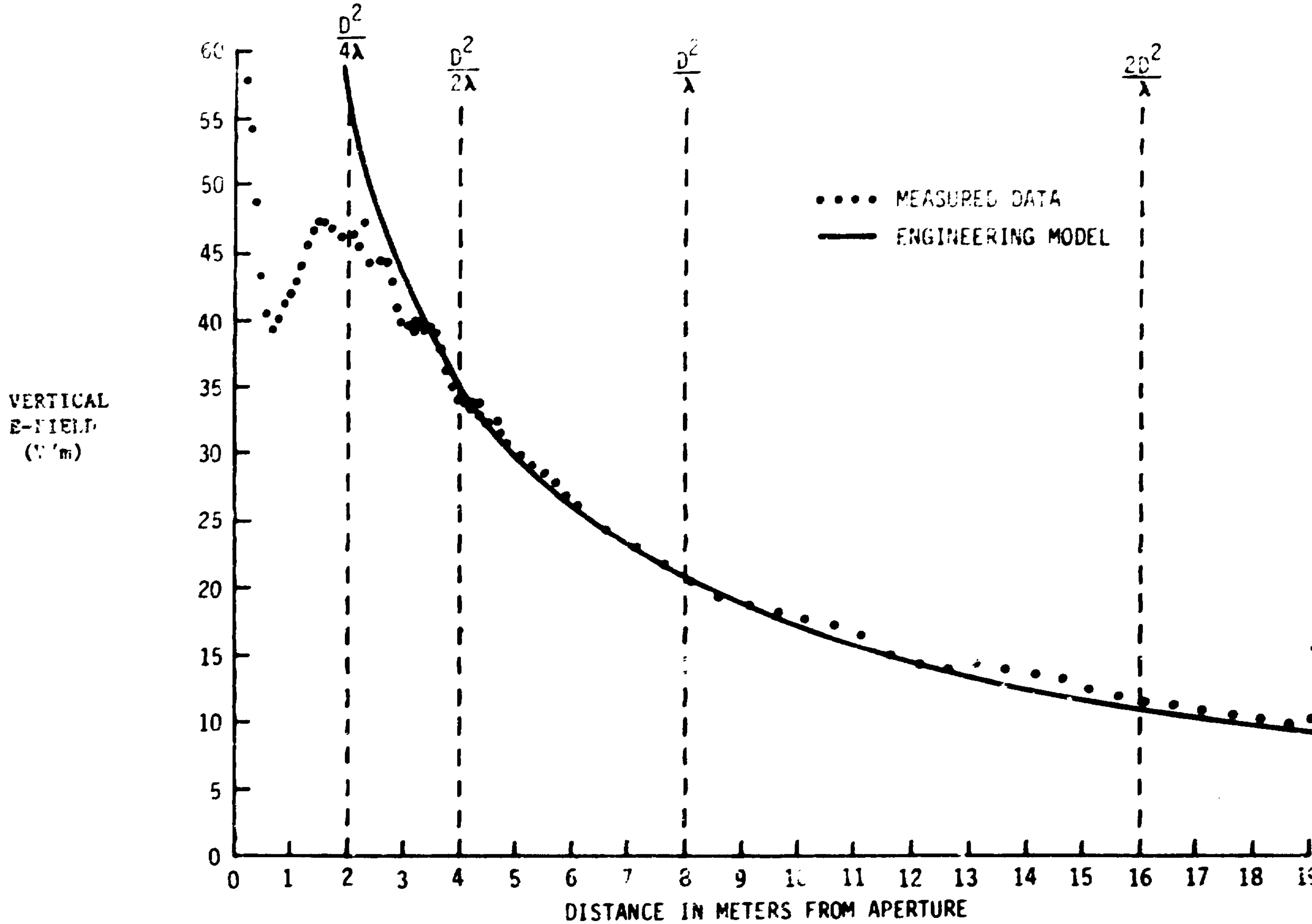

Figure 10. Engineering model compared with measured data.

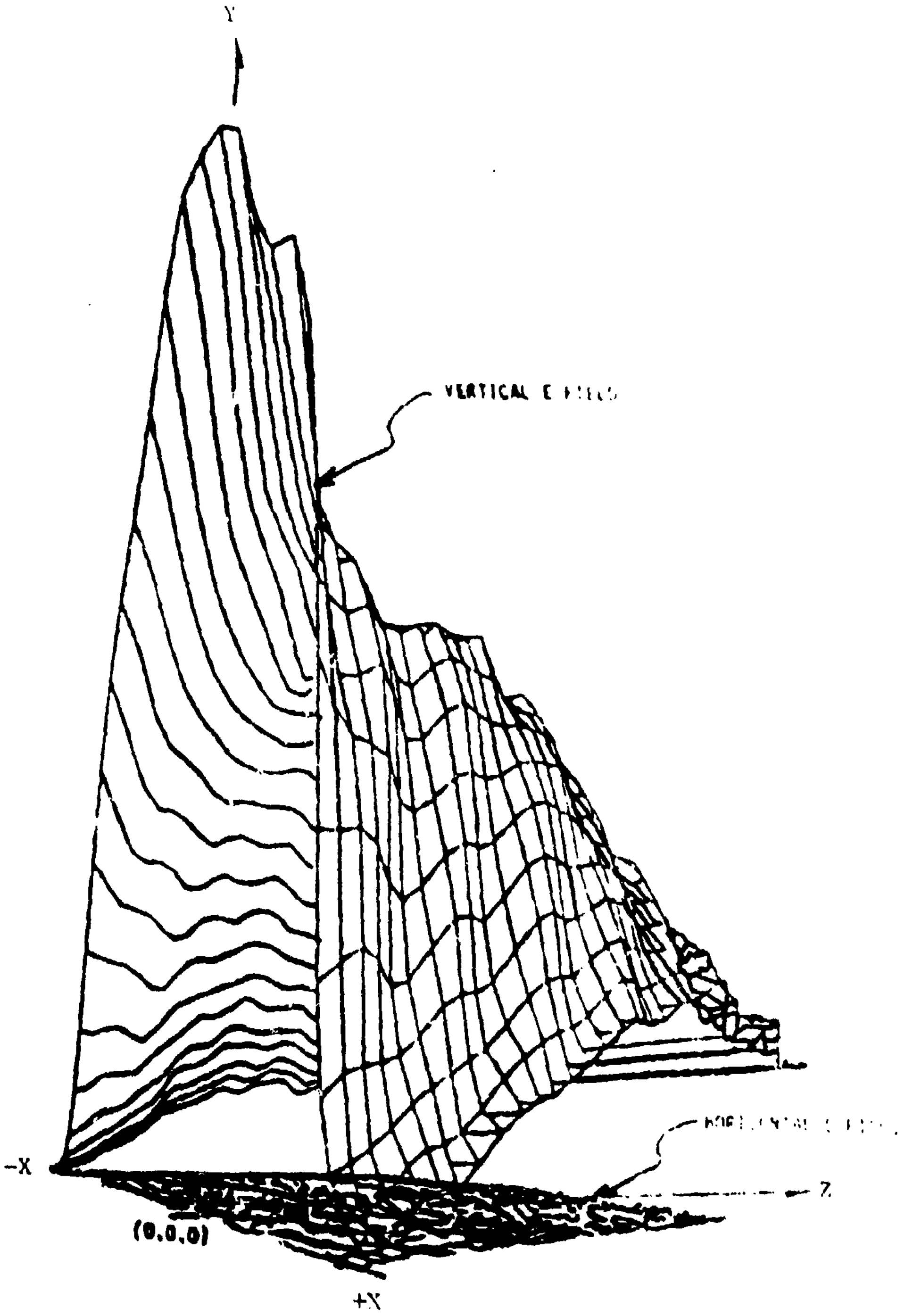

Figure 11. E_V and E_H amplitudes vs. horizontal position (X) and radial position (Z)

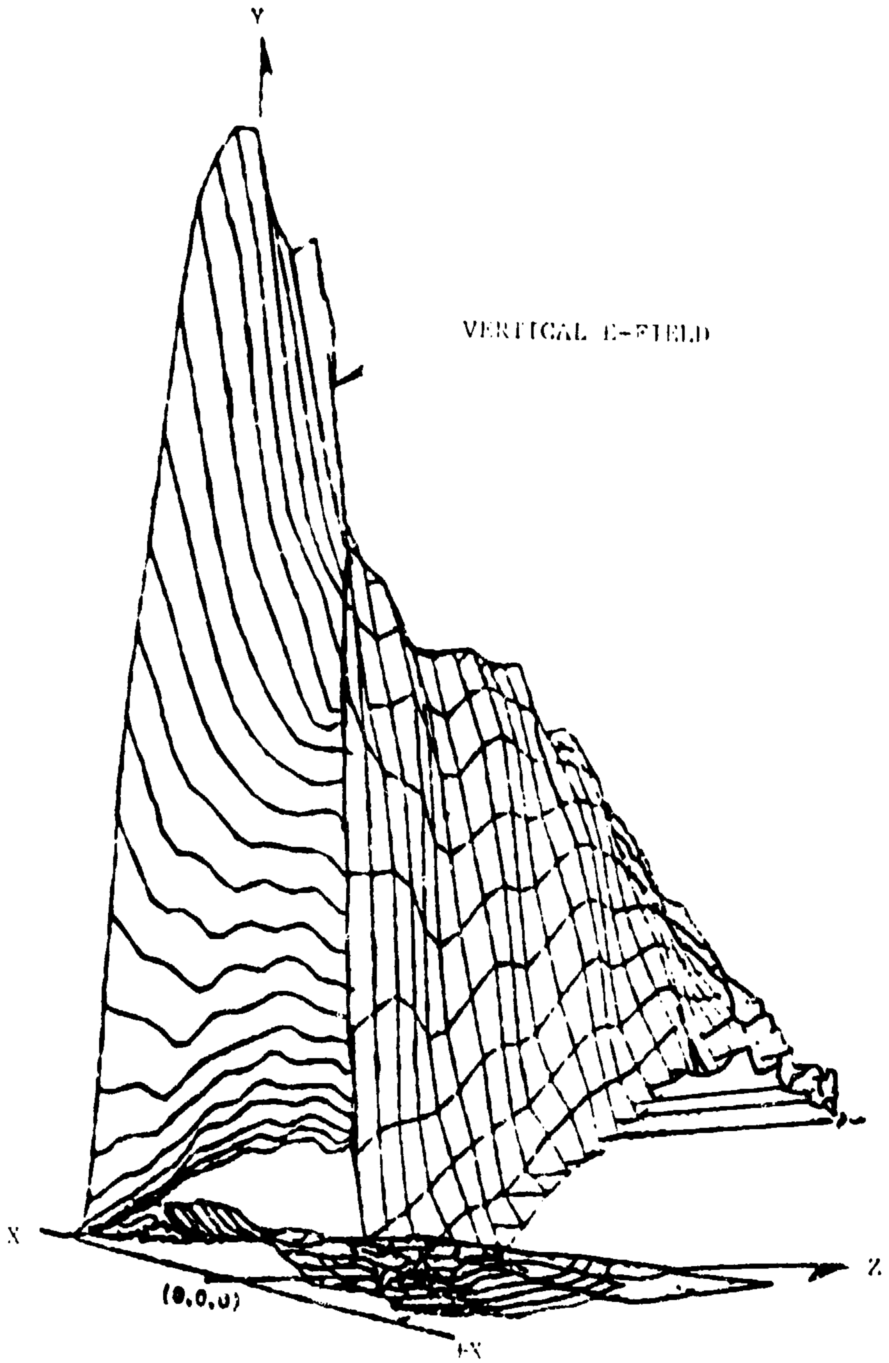

Figure 12. E_V and E_R amplitude vs. horizontal position (X), radial position (Z).

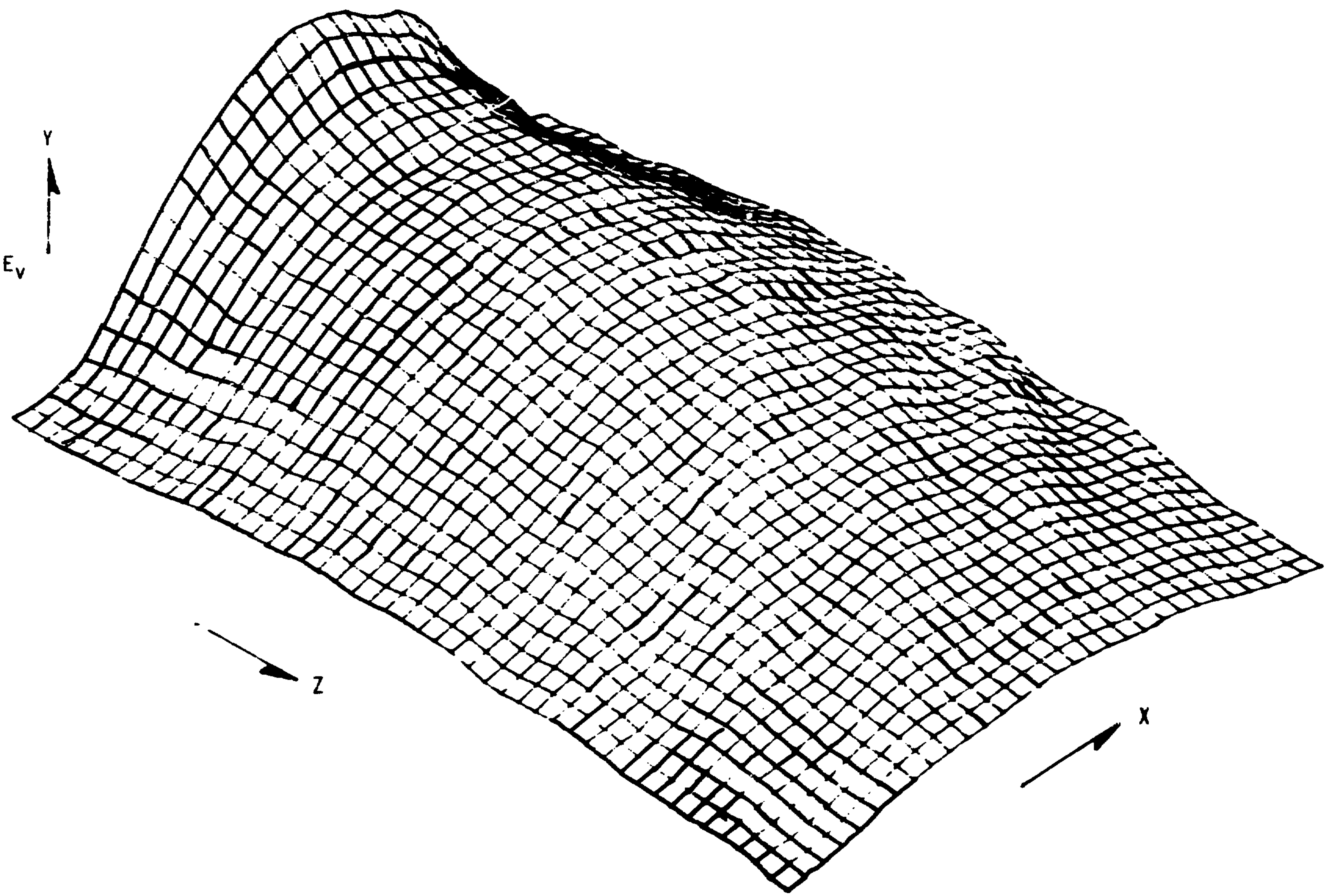

Figure 13. E_v amplitude vs. horizontal position (X) and radial position (Z).

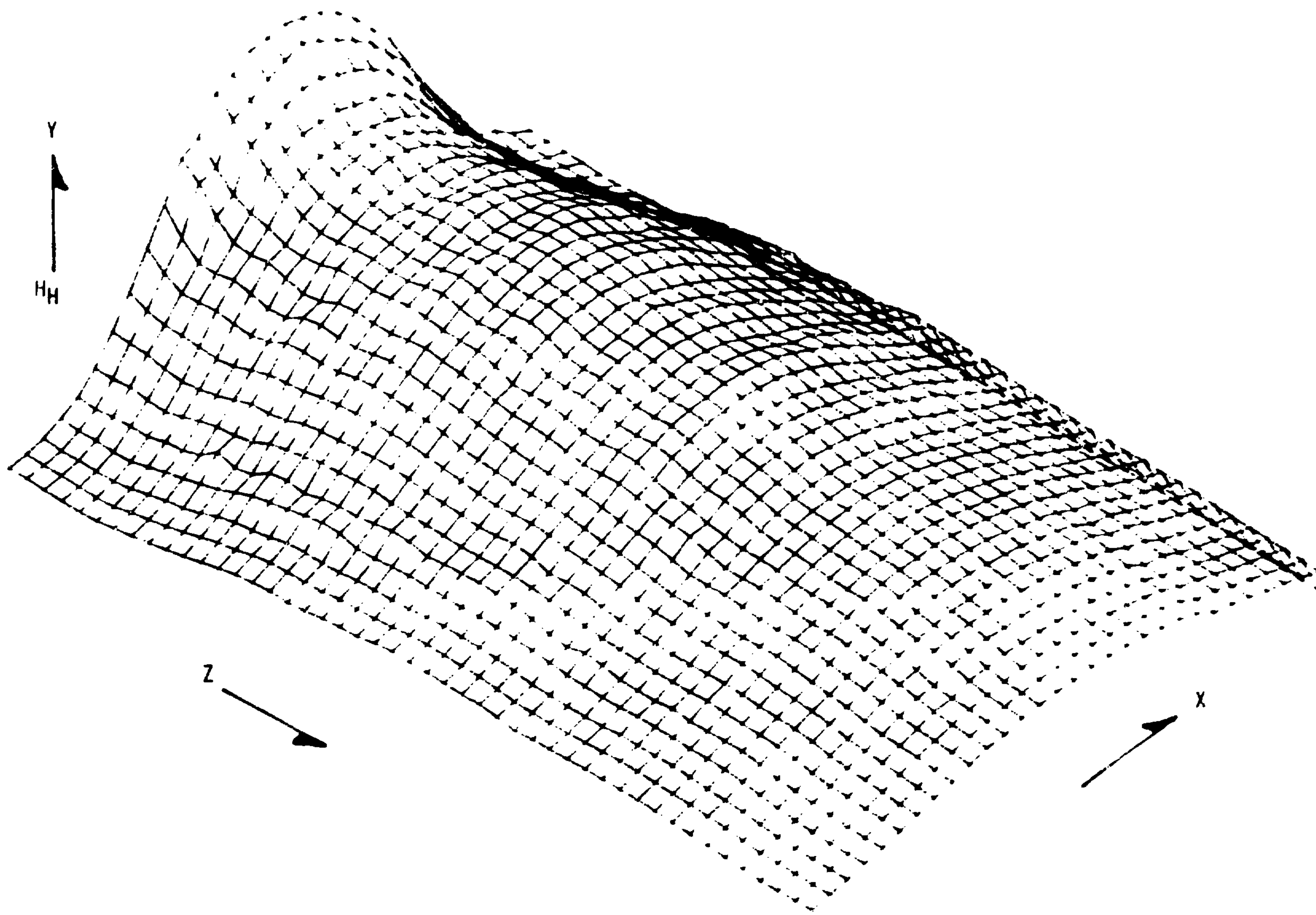

Figure 14. H_H amplitude vs. horizontal position (X) and radial position (Z).

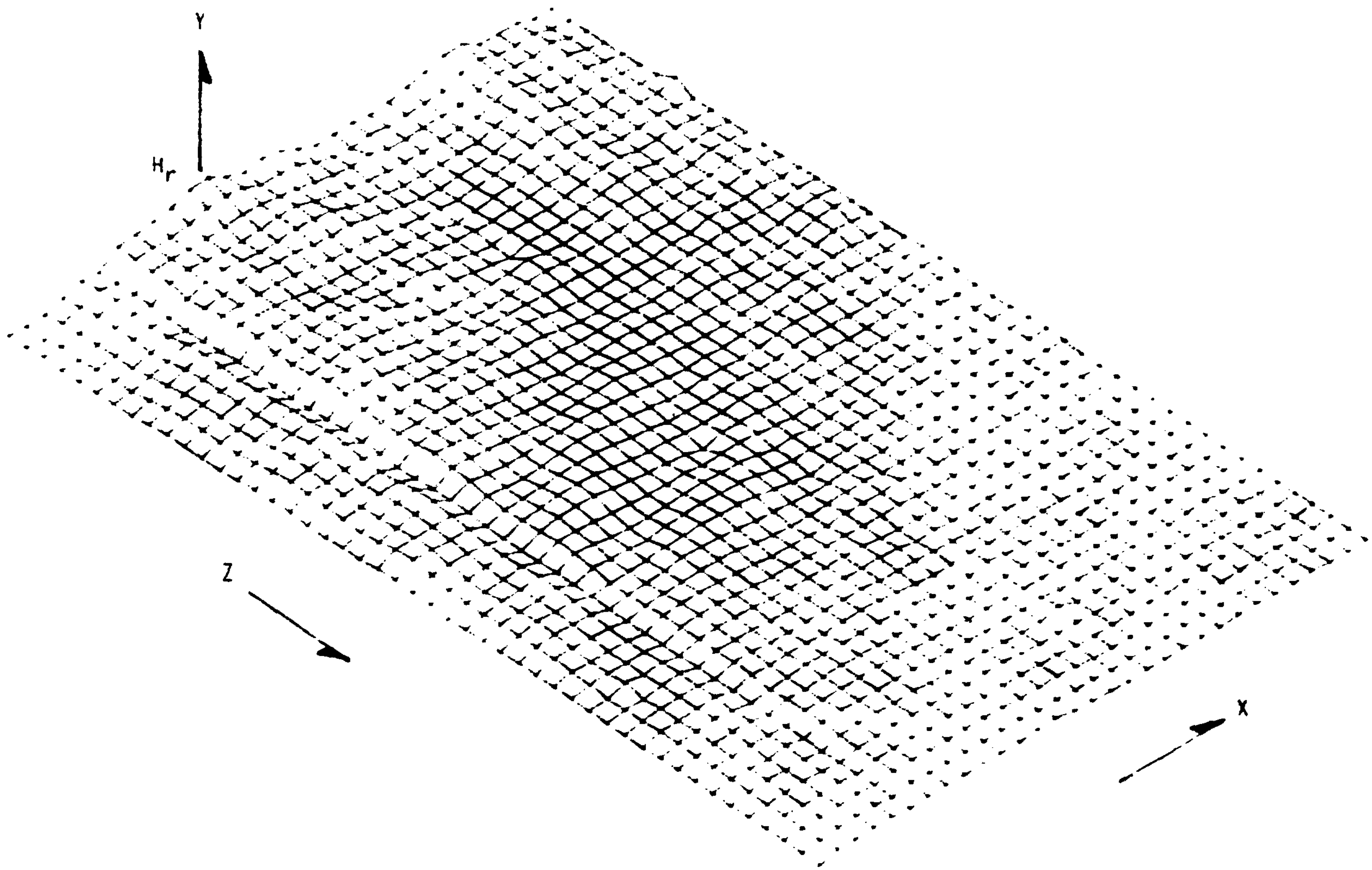

Figure 15. H_R amplitude vs. horizontal position (X) and radial position (Z).

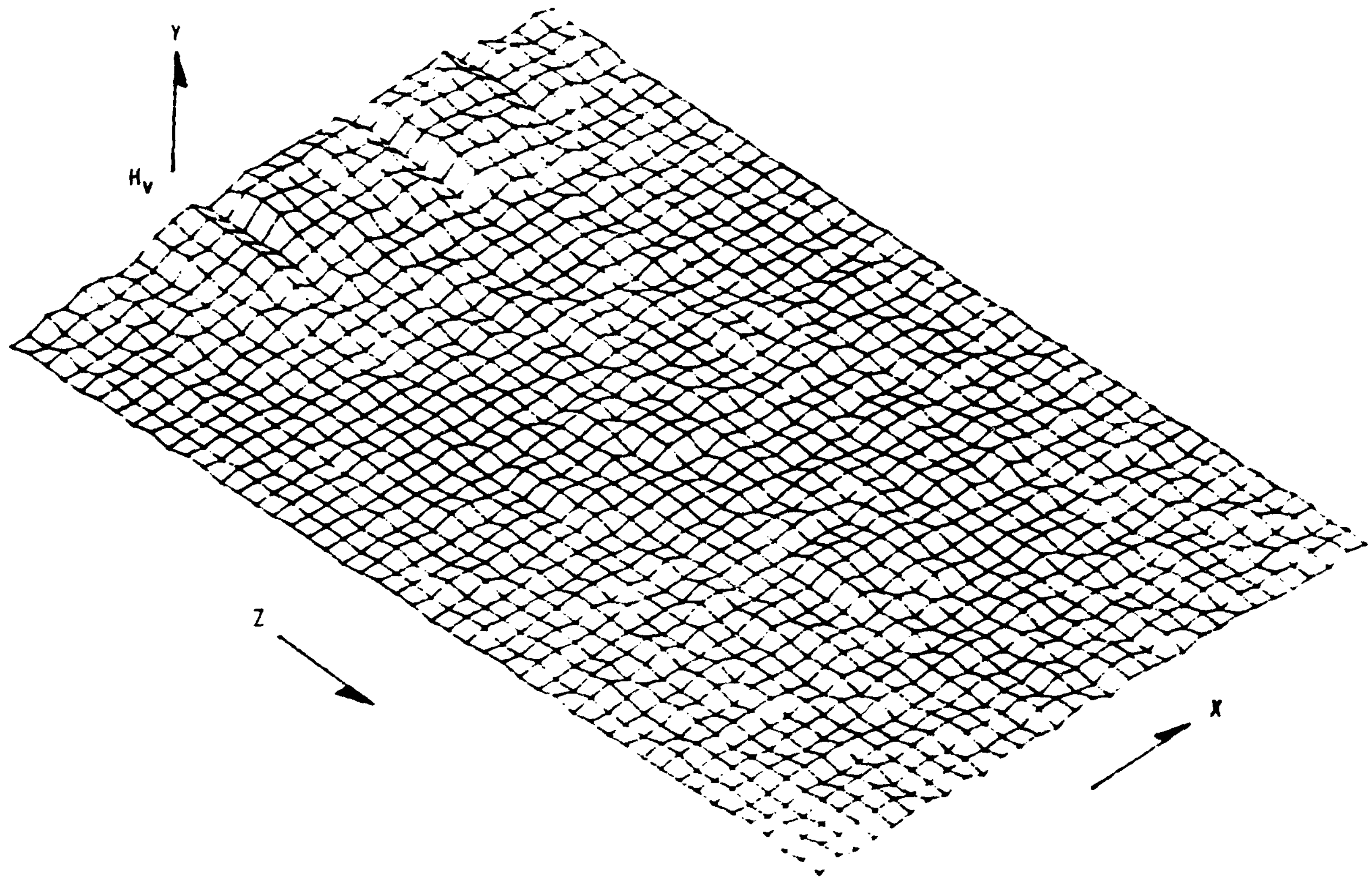

Figure 15. H_v amplitude vs. horizontal position (X) and radial position (Z).

vertical E field, E_V. The E_R is 30 dB below E_V by the two-meter point. The horizontal E field, E_H, is compared to E_V in Figure 11. It is apparent that the E_H is approximately zero. Therefore, these nonradiative components cease to be significant unless the field observation or testing is to be carried out extremely close to the source aperture.

B. Impact on Practical Electromagnetic Testing Techniques

In conclusion, the objective of this work is to characterize the near field volume of a high gain UHF horn for use in electromagnetic testing. This task has been accomplished and the results used to develop a simple engineering model to predict the E field at any radial distance from $D^2/4\lambda$ to the far field interface, at $2D^2/\lambda$. Given a small test object such as a VIPER missile, one could run an electromagnetic hazards test as close as $D^2/4\lambda$ to the aperture. This allows a 1 kW amplifier to produce approximately the same field strength as a 20 kW amplifier at $2D^2/\lambda$, the classical distance for an acceptable field test. Consequently, for the horn used in this work, a small test item could be as close as two meters to the aperture.

The previous example represents the extreme practical limits for the utilization of the near zone test volume. As the test specimens increase in size, the test volume moves out to an appropriate position to produce a more uniform illumination of the test object. It is not necessary for the microwave test engineer to arbitrarily move to $2D^2/\lambda$ to run all of his EMI tests. This work demonstrates that both the E and H fields are well behaved in the near zone of standard gain horns. This allows high level sweep frequency testing which is not possible using the far field distance criteria of $2D^2/\lambda$.

C. Suggestions for Future Research

The process of obtaining and analyzing the data presented in this work has answered some of the basic questions facing the microwave test engineer who wishes to utilize the near zone of a UHF horn antenna. There are, however, other questions and problem areas which need to be explored in detail. One of the most difficult areas of consideration is that of the phase relationship of the E and H field components. To explore the phase relationships one would need to develop non-perturbing E and H field probes that would preserve the phase relationships of the E and H field components.

Another area that warrants consideration is the validation of near field test result, i.e., the direct comparison of specific electromagnetic radiation (EMR) results obtained in near zones with the results observed in far zone tests, thus confirming the validity of testing in the near zone of UHF horns. The validation should address the test object/antenna interactions, i.e., the effects of geometry, distance from aperture, and test object size relative to the test volume. In addition, near field testing techniques need to be extended to other antenna types such as the log periodic and ridged horns.

Development of probe calibration techniques to improve the accuracy of the E and H field measurements would greatly benefit EMR testing. It is also highly desirable to develop automated probe calibration techniques since this would result in a considerable time savings as well as potentially improve the accuracy of probe calibrations.

Additional efforts are needed to validate new and innovative phase controlled multichamber testing as described by Riley, Patent Disclosure No. 4,255,750. The techniques suggested by Riley would greatly simplify testing systems with long interconnecting cables. This disclosure describes, in detail, the technique that needs to be developed and verified.

REFERENCES

1. Balanis, C. A. Antenna Theory Analysis and Design. Harper and Row, 1982. Ch. 12.

2. Chu, T. S., & Semplak, R. A. "Gain of Electromagnetic Horns." Bell System Tech. Jour., March 1965, 44, 527-537.

3. Jackson, J. D. Classical Electrodynamics. John Wiley and Sons, Inc., 1975. P. 438.

4. Meuhldorf, E. I. "The Phase Center of Horn Antennas." IEEE Trans. Antennas Propagation, November 1970, AP-8, 753-760.

5. National Bureau of Standards. "Near Field Electric Energy Density Meter." March 1975, NIOSH-75-140.

6. Naval Ship Engineering Center. "Near Field and Fresnel Zone Directive Antenna Coupling Program Final Quarterly Report." February 1973, Code 6174D.

7. Stutzman, W. L., & Thiele, G. A. Antenna Theory and Design. Wiley and Sons, Inc., 1981. Ch. 8.

BIBLIOGRAPHY

Aldridge, Richard E., "The Design and Construction of a Probe Positioner for Electromagnetic Field Measurements," US Army Technical Report RT-80-18, June 1980.

American National Standards Institute, "Measurement of Potentially Hazardous Electromagnetic Fields-RF and Microwave," US Department of the Navy IEEE, November 1978.

Arthur, C. Ludwig and Richard, A. Norman, "A New Method for Calculating Correction Factors for Near Field Gain Measurements," IEEE Transactions on Antennas and Propagation, September 1973, pp. 623-628.

Baum, C. E., "A Technique for the Distribution of Signal Inputs to Loops," Electromagnetic Pulse Sensor and Simulation Notes, Vol. I, Note 23, Air Force Weapons Laboratory, Kirtland Air Force Base, New Mexico, June 1970.

Baum, C. E., "Maximizing Frequency Response of a B Dot Loop," Electromagnetic Pulse Sensor and Simulation Notes, Vol. I, Note 8, Air Force Weapons Laboratory, June 1970.

Baum, C. E., "The Multi-Gap Cylindrical Loop in Non-Conducting Media," EMP Sensor and Simulation Note 41, Air Force Weapons Laboratory, June 1970.

Baum, C. E., "A Conical - Transmission - Line Gap for a Cylindrical Loop," Electromagnetic Pulse Sensor and Simulation Notes, Vol. 2, Air Force Weapons Laboratory, Kirtland AFB, New Mexico, June 1970.

Cain, F. L., Byers, K. G. Jr., Cofer, J. W. Jr., and Burns, C. P., Investigations of Mutual Gain Statistics for Some Radar Antennas in the Fresnel Zone," Naval Ship Engineering Center, Department of the Navy, Special Technical Report, 1 October 1968.

Chu, T. S. and Semplak, R. A., "Gain of Electromagnetic Horns," Bell System Tech. Jour., Vol. 44, p. 527-537, March 1965.

Draper and Smith, Applied Regression Analysis, John Wiley & Sons, New York, 1966.

Edlin, George R. and Hudson, Wayne T., "The Design and Development of Loop B Dot Sensor," US Army Technical Report RG-75-23, 1 December 74.

Edlin, George R., "Calibration and Use of B Dot Probes for Electromagnetic Measuring," A Thesis, Southeastern Institute of Technology, Huntsville, Alabama, September 1977.

Edwards, J. L., Ryan, C. E., Bodnar, D. G., and Ecker, H. A., "Near Zone Radar Cross Section," AFAL-TR-72-339, prepared for Naval Ship Engineering Center by Atlantic Research, Alexandria, Virginia, December 1972.

Green, F. M., "Development of Electric and Magnetic Near-Field Probes," National Bureau of Standards Technical Note 658, January 1975.

Jackson, J. D., Classical Electrodynamics, John Wiley and Sons, Inc., Second Edition, 1975.

Kerr, John L., "Broadband Horns," US Army Electronics Command, August 1970.

Kerr, John L., "Short Axial Length Broadband Horns," 22 Annual Symposium on US Air Force Antenna Research and Development, October 1972.

Mory, Res, et al, "Development and Production of Multi-Gap Loop (MGL) Series Emp B Dot Sensors," EMP 1-2, Air Force Weapons Laboratory, AFWL-SRE, Kirtland AFB, New Mexico, February 1971.

Muehldorf, F. I., "The Phase Center of Horn Antennas," IEEE Trans. Antennas Propagation, Vol. AP-8, pp. 758-760, November 1970.

Naval Ship Engineering Center, "Near Field and Fresnel Zone Directive Antenna Coupling Program Final Quarterly Report," February 1973.

Ostle, B., "Statistics in Research," Iowa State University Press, Iowa City, Iowa, 1963.

Saad, T. S., Microwave Engineering Handbook, Vol. I, Artech House, Inc., 1971.

Stratton, Julius A., Electromagnetic Theory, McGraw-Hill Book Co., 1941.

Shumpert, Thomas H., "Department of Electrical Engineering," Auburn University, Electrical Engineer, Test & Evaluation Directorate, US Army Missile Laboratory, US Army Missile Command, Redstone Arsenal, Alabama.

Strickland, B. R., Edlin, G. R., and Shumpert, T. H., "Design, Construction, and Calibration of Pseudo-Transparent Non-interfering Electric and Magnetic Field Sensors," Conference Proceedings, IEEE Southeastcon, Huntsville, Alabama, 1981.

Taggart, Harold E., and Workman, John L., "Calibration Principles and Procedures for Field Strength Meters (30 MHz to 1 GHz)," National Bureau of Standards Technical Note 370, March 1969.

Wacker, P. I., and Bowman, R. R., "Quantifying Hazardous Electromagnetic Fields: Scientific Basis and Practical Considerations," IEEE Trans. Microwave Theory and Techniques, Vol, MII-19, No. 2, February 1971.

Whiteside, H. and King, R. W. P., "The Loop Antenna as a Probe," IEEE Transaction on Antenna and Propagation, May 1964, pp. 291-297.

APPENDIX A

A SURVEY OF ADVANCES IN

MICROWAVE NEAR-FIELD MEASUREMENT

Reprint of MICOM Technical Report RT-80-9, June 1980, George R. Edlin.

CONTENTS

I. INTRODUCTION

The development of many high power emitters in the microwave frequency range has led to many problems which cannot be solved using classical far field techniques. The problems of particular interest may be grouped into the following areas:

1. Electromagnetic interference in electronic systems in the near field of high gain microwave antennas.

2. Near field measurements for use in determining far field patterns.

3. Mutual gain characteristics of multiple antennas in the near field.

4. Near field measurements for occupational safety.

5. Determination of Radar Cross Sections (RCS) in the near zone.

Interest in electromagnetic interferences in the Fresnel zone has increased in the past decade due to development of large phased array radars and high gain satellite antennas. Since these antennas are very large with respect to the wavelengths at which they are operated, the far field can extend a great distance from the antenna. The normally accepted distance is given by $2D^2/\lambda$, where D is the largest dimension of the antenna, and λ is the wavelength of the transmitted signal.

It is readily obvious that for antenna sizes in meters and wavelengths in centimeters, the near field zone extends many meters from the transmitting antenna. This causes a large number of electronic systems to be exposed to high level near field electromagnetic radiation. Many times this high level radiation causes circuit malfunction in some solid state systems, either by induction of extraneous signals into the system or by burnout of critical components. This situation has created a need for high level electromagnetic testing in both near and far fields. Since high levels are much easier to obtain in the Fresnel zone, it is desirable to relate the testing accomplished in the Fresnel zone to the appropriate far zone. Two major objectives could be met with this technique. First, only one near field test would need to be conducted. Secondly, by being near the transmitting antenna, the power requirements for producing high level fields would be reduced significantly. This would result in considerable cost savings on the required broad-band transmitters.

The need for determining far field patterns from near field measurements is again due to the development of large higher gain microwave antennas. The testing of these antennas requires very long, unobstructed antenna ranges to obtain accurate patterns and gains. Costs of acquiring and developing such ranges are prohibitive, therefore making development of near field pattern and gain techniques more desirable.

The use of multiple antennas located near each other has created an interest in mutual gain characteristics of microwave antennas. These situations are major problems for large naval ships, Army missile systems, and Air Force systems.

Occupational health considerations have also stimulated a considerable amount of research in the Fresnel zone. This work is necessary to determine how far the hazardous levels of electromagnetic radiation extend from the transmitting antennas.

II. REVIEW OF PREVIOUSLY PUBLISHED MATERIAL

Following is a review of material published in journals, reports, periodicals, and books in the past decade.

A. Mutual Gain Statistics for Microwave Antennas

1. Investigation of Mutual Gain Statistics for Some Radars in the Fresnel Zone[1]

The investigation of mutual gain of microwave antennas in the Fresnel zone is of great importance in any situation where multiple antennas are required. The work by researchers at Georgia Institute of Technology presents measurement results and analysis of the Fresnel zone statistical mutual gain characteristics of four C- and X-band radar antennas. The tests were conducted at ranges of 50 feet and 9 feet. The 9-foot distance was just short of touching due to antenna sizes.

Studies at Georgia Tech have shown that the minor lobe statistical gain characteristics for the horizontal plane patterns are described approximately by the Gaussian cumulative gain distribution curve for ranges well into the Fresnel zone. Some problems occur at very short Fresnel zone distances due to the broadening of the main lobe of the antenna, causing the cumulative gain distribution curves to deviate from the Gaussian type curves.

Previous mutual gain experiments have shown that if the statistical gain distributions of two antennas are approximately Gaussian, this statistical mutual gain distribution of the two antennas is approximately Gaussian. For these tests the shortest separation was 50 feet and no site-effect objects were included. Due to the questions concerning coupling at very short Fresnel distances, two tests were conducted at 50 feet and six at 9 feet. Only C-band tests were conducted at 50 feet; both C- and X-band tests were conducted at 9 feet.

From graphical representation reproduced from this report (Figures 1 and 2), it can be noted that at a range of 50 feet, the measured points and predicted points agree very well. This indicates that if the statistics of the individual antennas are known accurately, the mutual coupling can be predicted very accurately.

The curves at the 9-foot range do not match as well as those at the 50-foot range. The disparity occurs at the top of the curves. This is the result of the main beams broadening near the antennas and thus deviating from Gaussian distributions.

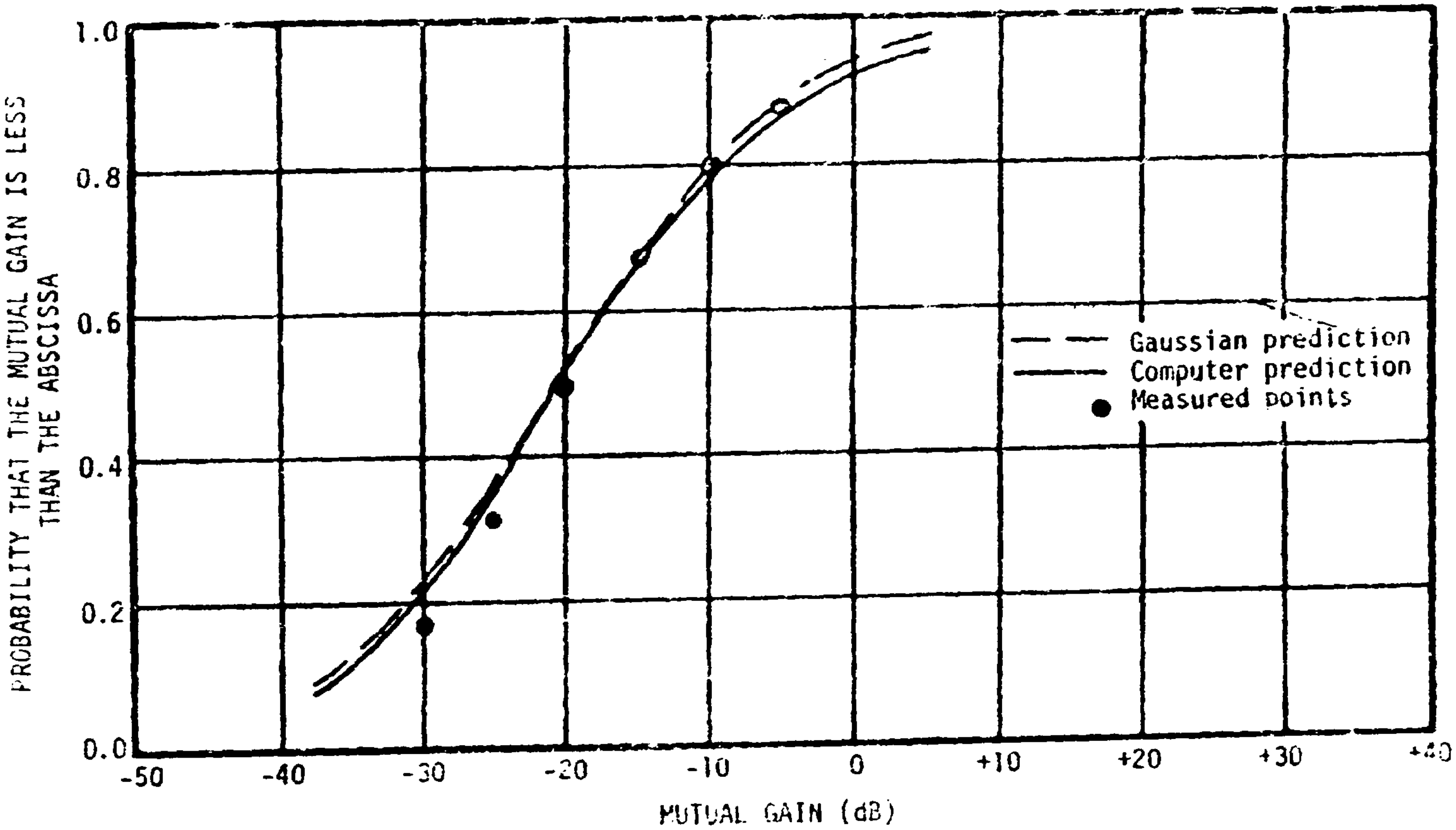

ANTENNAS: GT/AR-4C and GT/AR-6C FREQUENCY: 5.64 GHz RANGE: 50 feet

Figure 1. Measured and predicted cumulative distributions of the mutual gain of the GT/AR-4C and GT/AR-6C antennas for the clear site test at a Fresnel zone range of 50 feet. (Extracted from Reference 1.)

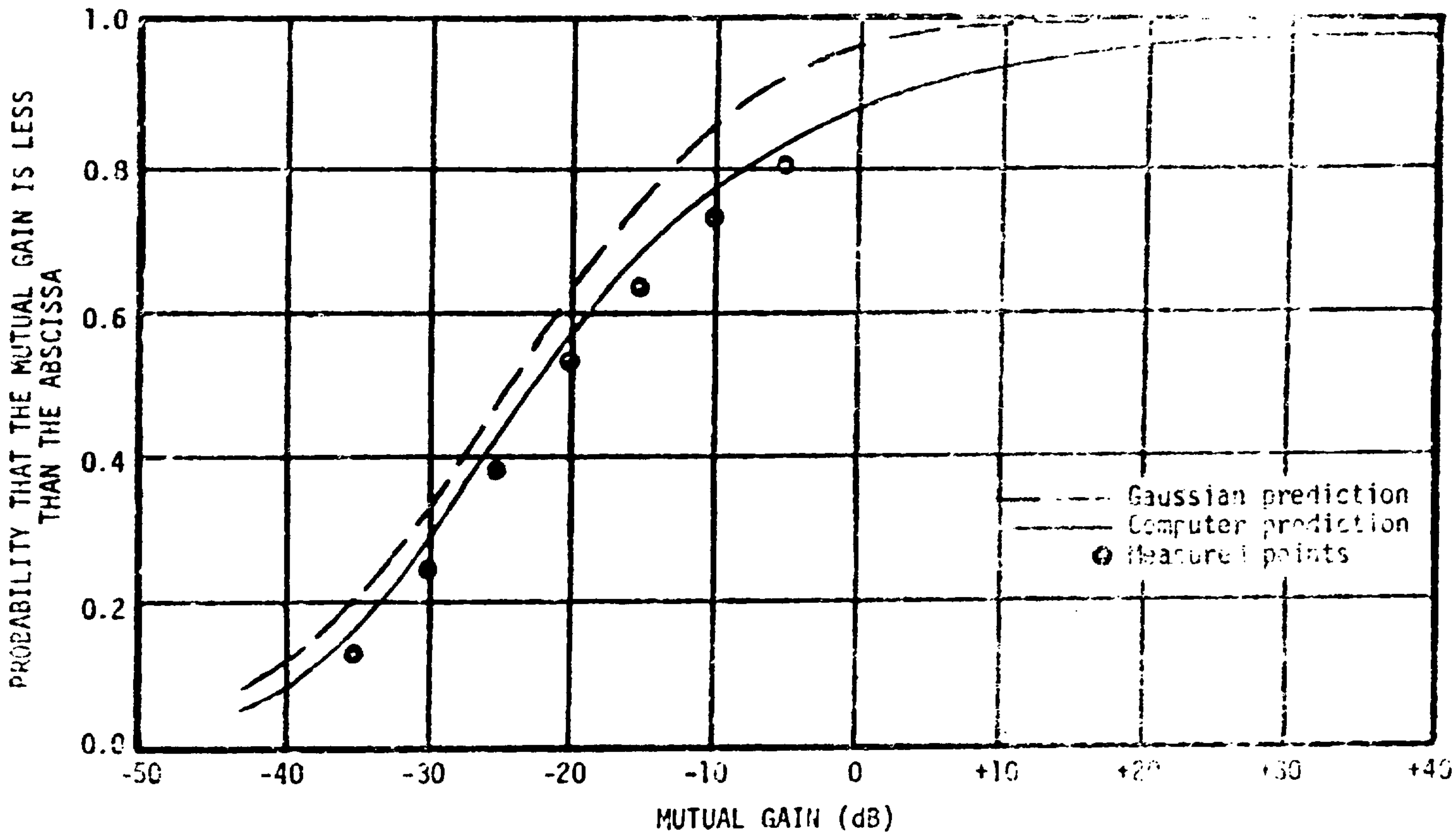

ANTENNAS: GT/AR-4C and GT/AR-6C

FREQUENCY: 5.64 GHz

RANGE: 9 feet

Figure 2. Measured and predicted cumulative distributions of the mutual gain of the GT/AR-4C and GT/AR-6C antennas for the clear site test at a Fresnel zone range of 9 feet. (Extracted from Reference 1.)

Although the Gaussian predictions at very short Fresnel zone ranges do deviate from the measured data points, in many cases the predictions are sufficiently accurate to satisfy the requirements. If the Gaussian predictions are not accurate enough, then the numerical convolution of the cumulative gain distribution can be performed on a computer which gives very good results even at very close ranges.

2. Near Field and Fresnel Zone Directive Antenna Coupling[2]

The electronic systems on naval ships are essential to modern warfare. Due to this fact there is a continued demand for more electronic systems, a large number of which have antennas associated with them. This creates a high potential for electromagnetic interference between systems, due to coupling between the various system antennas. This type coupling is particularly high between antennas in the same bands.

Some of the basic dimensions that must be analyzed are frequency, power, time, and space. The basic frequencies -- harmonics, spurious, and intermodulation -- can all cause considerable interference. The spatial dimension, i.e., relative separation and orientation, as well as scattering, has a considerable effect on the amount of interference. The absolute power of the radiating system is also of paramount importance.

The quantity which needs to be estimated is the coupling factor, which is a loss factor normally given in dB, and is determined from a function of several known parameters. The coupling factor (CF) is given by the following relationship:

$$CF\ (dB) = 10 \log \frac{P_t}{P_r},$$

where P_t is the transmitting power, and P_r is the received power.

The coupling factor can easily be misinterpreted since the effect of increased or decreased "coupling" values is the opposite of "coupling factor." An increase in coupling value corresponds to a decrease in coupling factor and, conversely, an increase in coupling factor corresponds to a decrease in coupling between the antennas.

When conditions are ideal, one can use the coupling factor equation to compute the coupling factor; however, in the practical situation the necessary conditions of far field, free space, and inband frequencies of operation seldom exist. All of these complications give rise to the statistical nature of the coupling factor and make it generally impossible to accurately obtain the coupling factor using a deterministic mathematical treatment. This has led to the use of continuous sampling techniques for determining the mean coupling factor for a given pair of antennas. A spectrum analyzer operating with the time base synchronized to the rotation of one radar is used. This displays the coupling level on a logarithmic scale for an azimuth setting and fixed test frequency of the second antenna. This display is photographed and mean level visually determined by placing a straight edge through the centers of the random variations. This gives a reasonably accurate coupling factor within ±1 dB. The test frequency or the orientation of the fixed antenna is then changed to obtain other values. The average of the mean values then represents a mean coupling factor of a particular situation class for the specific antenna pair. In this manner a data base for mean coupling factor of antenna types and situations is generated.

B. Near Zone Radar Cross Section (RCS)[3]

The objective of this research was to define a generalized technique for ascertaining the near zone RCS of missiles. There are two basic problems which complicate near zone RCS determinations: (1) the target can be illuminated by both planar and nonplanar fields, and (2) the reflected fields can be nonuniform and nonplanar. The near zone RCS is a function of the following parameters: frequency, polarization, range, target size and aspect, and the radiation patterns of the receiver and transmitting antennas. A generalized formulation of the near zone is developed which shows that the near zone RCS is a function of the radiation patterns of the transmitting and receiving antennas, target geometry, and electrical properties which affect the currents induced in it. Sensitivity to the above parameters has been studied and indicates that each is important in varying degrees depending on the existing conditions.

Calculations of scattering properties for simple geometric shapes have been accomplished according to the Geometric Theory of Diffraction which give good agreement with near zone field measurements. Four techniques for determining characteristics of near zone RCS are presented: a direct measurement technique, a computational method, a "Subarea Matrix Method," and a "Modal Expansion Method." The first two can provide good cross section data under limited conditions; however, the third and fourth, in principle, have the capability of providing good data under generalized conditions.

Future work in the near zone RCS area will be concentrated on the Subarea Matrix Method or the Modal Expansion Method. The reason for this decision is that the direct measurement method is only good for specific encounters and the theoretical techniques are limited to simple geometric shapes.

Since neither of the recommended generalized techniques has been developed, it is not possible to guarantee that either will be totally successful. However, it is believed that the Modal Expansion Method has a good chance for success because it has been used successfully in determining radiation patterns of antennas. The data measurement techniques and equipment are presently available at Georgia Institute of Technology. In addition, some of the analytical and sampling criteria have already been established. None of these statements are true for the Subarea Matrix Method; however, the Subarea Matrix Method should not be completely discarded. Some simplified experiments would be worthwhile, although most of the effort is concentrated on the Modal Expansion Method. The method of direct measurement would also be of value for comparison in specific cases, along with the theoretical methods for simple geometric type targets.

C. Correction Factors for Near Field Gain Measurements[4]

The apparent gain of two antennas separated by a finite distance is different from the case of infinite separation, and many researchers have dealt with the problem of correcting for the effect. Most of these analytical methods make various assumptions about the fields which make it difficult to assign a value to the computational accuracy. This paper discusses the use of experimental data instead of assumed field distributions. The results are compared to the method used by Chu and Semplak. Both papers are based on the power transmission formula. The apparent gain of two antennas is given by

$$G_1 \; G_2 = \frac{(4\pi R)^2}{\lambda^2} \frac{P_r}{P_t} ,$$

where G_1 and G_2 are the apparent gains of antennas 1 and 2

R = distance between the antenna apertures

λ = wavelength.

The equations used are exact; therefore, if the fields of the two antennas were known exactly on a common surface S and on the surfaces S_1 and S_2 which inclose antenna 1 and antenna 2, then the near field gain correction factors could be computed exactly.

In the method described in this paper the far field patterns of antennas 1 and 2 are the known data. Thus to obtain the fields of both antennas on a common surface, a spherical wave expansion is matched to the far field patterns. These expansions are then evaluated to determine the E and H field on the desired surfaces.

The approach of the authors was to use the patterns of one antenna transmitting with the other antenna removed. The problem with this approach is that multiple scattering is neglected. This is the only assumption made by this method. It has been shown that multiple scattering can have an appreciable effect. It is also common practice to make several measurements over a small range of antenna separation, and use curve fitting techniques to remove the scattering and multipath effects.

This approach has one other theoretical shortcoming. The method is sensitive to the truncation point of the spherical wave expansion. It is well known that spherical waves exhibit cutoff behavior that limits the number of modes to approximately $N = ka$, where k is the propagation constant, and a is the radius of the smallest sphere that can inclose the source. Two suggested guides for truncation are:

(1) $N = ka + 10$

(2) $N = 7.7\,(2a/\lambda)^{0.78}$ for $1<a/\lambda<15$.

In the first attempts the authors used $N = 25$. It was later discovered that a better choice would have been between $N = 18$ and $N = 22$.

Accuracies on the order of ±0.02 dB appear to be possible. The differences between computed and measured gain correction factors were a little higher, approximately 0.03 dB. This difference could be due in part to measurement error (see Figure 3, extracted from Reference 4). Agreement is quite good and the authors believe that future work will lead to even better agreement.

D. Near Field Measurements for Occupational Safety

1. Near Field Electric Energy Density Meter (EDM)[5]

The EDM-2 electric energy density radio frequency survey monitor was designed to measure electric fields from 10 to 500 MHz. This NBS report describes the problems in collecting and interpreting the monitor readings. A number of sources of error are discussed:

(1) The reactive near field components.

(2) The amount of multipath interference.

(3) Field polarizations.

(4) The field modulation.

(5) The complex interactions between the power source and nearby objects.

The relationship between the electric field and the magnetic field is completely ambiguous when measurements are conducted within one wavelength of the source.

This fact requires that both the electric and magnetic field be measured to obtain the total occupational health exposure. The EDM-2 monitor uses a set of three orthogonal dipoles to obtain the required isotropic response. The output of the dipoles is fed to the monitor electronics by special high resistance conductors to reduce the monitor's interaction with the RF field. The meter displays electric energy density from 0.003 to 30 $\mu J/m^3$. These values equate to plane-wave equivalent power density from 0.1 to 1000 mW/cm^2. The monitor is calibrated in units of microjoules per cubic meter. This choice was made because it simplified the circuit as well as providing useful RF data on an easily readable dial. The units are easily related to milliwatts per square centimeter of equivalent plane-wave field by the following relationships:

(1) $S(\mu W/cm^2) = 60.0 U_E (nJ/m^3)$

(2) $S(mW/cm^2) = 60.0\ U_E(\mu J/m^3)$

(3) $10\ mW/cm^2$ (plane wave) $= 0.3\ \mu J/m^3$

(4) $E(V/m) = 475.33 \left\{U_E(\mu J/m^3)\right\}^{1/2}$

(5) $E(V/m) = 15.03 \left\{U_E(nJ/m^3)\right\}^{1/2}$

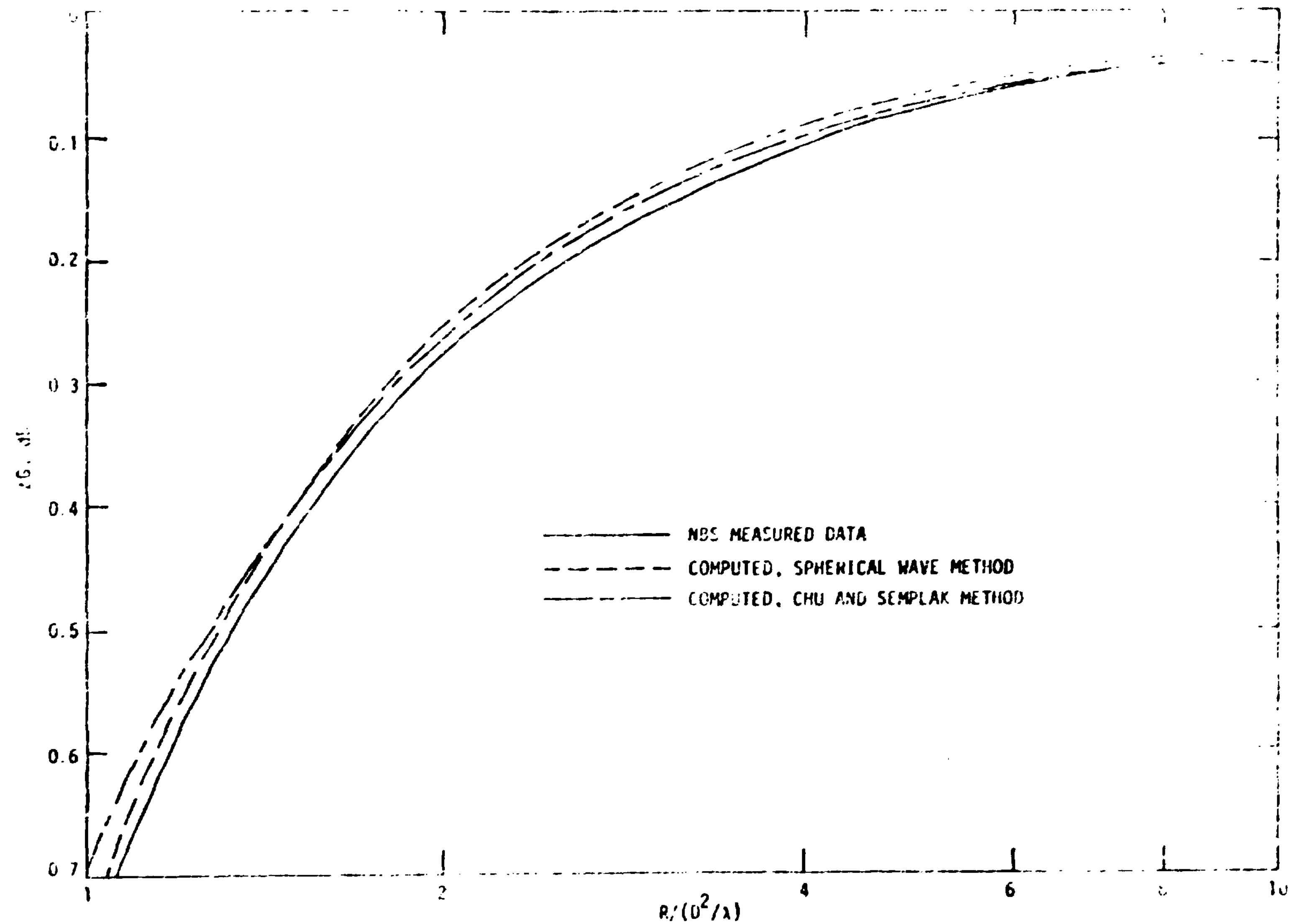

Figure 3. Measured and computed near field gain correction factors. (Extracted from Reference 4.)

The EDM-2 represents an improvement over existing monitors. It has a faster rise and fall time for pulse response, a dynamic range of 50 dB, reduced temperature sensitivity, low noise preamplifiers, and a response flatness of ±1 dB from 10 MHz to 500 MHz.

2. Measurement of Potentially Hazardous Electromagnetic Fields--RF and Microwave[6]

The measurement of electromagnetic fields from 1 MHz to 100 GHz is discussed in this draft ANSI Standard, dated November 1978. This document was written to replace older documents which did not cover frequencies below 300 MHz or problems associated with the accurate measurements in the near field. This was due in part to the unavailability of instruments capable of making accurate measurements in the near field.

For the frequencies above 300 MHz meaningful data can be measured at distances greater than a^2/λ, where the probe dimension is less than a. a is the largest aperture dimension and λ is the wavelength.

Power density is used as the hazard indicator; however, no existing instrument measures power density directly. The techniques used are usually to measure one or more components of the electric field E or the magnetic field H and infer a power density based on the plane-wave far field relationships.

Measurements are required in the reactive or radiating near field region where standing waves occur. Since hazards are due to energy absorption, the parameters $|E|^2$ and $|H|^2$ can be measured. The energy densities $U_E = \varepsilon'|E|^2/4$ and $U_H = \mu'|H|^2/4$ are also representative of the amount of hazard, where ε' and μ' are the real parts of the dielectric constant ε and the magnetic susceptibility μ, with the energy Joules/meter^3 (J/m^3). This choice conveniently allows both E and H to be expressed in the same units.

The typical situations in which near field measurements are required are:

(1) Leakage fields from waveguides.

(2) Radiation fields from large antennas.

(3) Reactive fields from large low frequency horns.

"Leakage" refers to unintentional leakage of energy, whereas "radiation fields" refers to intentional radiations. The "reactive fields" exist in both the leakage and radiation fields and are generally stronger near inefficient radiators. The problem of multipath interference is another complication that exists to some degree in every situation.

Summary of Measurement Techniques. Some of the factors which determine the electromagnetic environment are: the direction of energy propagation with respect to the sources, polarization, frequency, type of modulation, and power of sources. The variable nature of these effects as well as their effects on the resultant electromagnetic environment make it difficult to design and operate instruments which can measure the electromagnetic environment with sufficient accuracy to insure personnel safety.

The near fields of radio frequency sources are characterized by the combination of both reactive and radiation components. These components have spatial and temporal variations which are functions of the physical environment and the type sources that generate them. These variations create many unique situations which make calculations of near field intensities impractical. Therefore, one must rely on measurements.

III. COMMENTS ON NEAR FIELD LITERATURE SURVEY/CONCLUSIONS

In light of information contained in existing literature, it is obvious that the need discussed in Section I, i.e., electromagnetic interference in the near field of large microwave antennas, has not been investigated to sufficient depth to answer certain fundamental questions. Since these questions are of tremendous importance to a large number of defense systems and a growing number of commercial electronic systems, further research in this area seems appropriate. It is apparent that much of the material surveyed applies to near field testing phenomena. This material provides a sound basis and a strong impetus for future research.

REFERENCES

1. F. L. Cain, K. G. Byers, Jr., J. W. Cofer, Jr., and C. P. Burns, Investigations of Mutual Gain Statistics for Some Radar Antennas in the Fresnel Zone, Naval Ship Engineering Center, Department of the Navy, Special Technical Report, 1 October 1968.

2. Near Field and Fresnel Zone Directive Antenna Coupling Program Final Quarterly Report, Naval Ship Engineering Center, Code 6174D, February 1973.

3. J. L. Edwards, C. E. Ryan, D. G. Bodnar, and H. A. Ecker, Near Zone Radar Cross Section, AFAL-TR-72-339, prepared for Naval Ship Engineering Center by Atlantic Research, Alexandria, Virginia, December 1972.

4. Arthur C. Ludwig and Richard A. Norman, "A New Method for Calculating Correction Factors for Near Field Gain Measurements," IEEE Transactions on Antennas and Propagation, September 1973, pp. 623-628.

5. Near Field Electric Energy Density Meter, National Bureau of Standards, NIOSH-75-140, March 1975.

6. American National Standards Institute, Measurement of Potentially Hazardous Electromagnetic Fields--RF and Microwave, US Department of the Navy and IEEE, November 1978.

DEFINITIONS

Antenna - A device used to radiate or receive radio waves.

Antenna Array - An antenna system which uses multiple antennas to obtain directional effects.

Antenna Gain, Relative - The ratio of the power gain of an antenna relative to a half-wave dipole or isotropic antenna.

Beamwidth, Half-Power - The half power beamwidth is measured in the plane containing the lobe maximum. It is the angle between the two directions in that plane that intersects the 3 dB points of the maximum lobe.

Dipole - An antenna that produces a pattern that is similar to an elementary dipole. It is usually a $^1/_2$ λ straight radiator, which is fed at the center.

Electric Field - A vector field of the electric field strength.

Electric Field Strength - The magnitude of the electric field vector.

Far Field Region - That part of the field of an antenna where the angular field distribution is nearly independent of the distance from the antenna, which is sometimes defined by $2D^2/\lambda$.

Isotropic - Having the same properties in all directions.

Magnetic Field Strength - The magnitude of the magnetic field vector.

Magnetic Field Vector - Given by the division of the magnetic induction by the permeability of the medium.

Microwaves - Normally are radio waves that range in frequency from approximately 1 GHz to 200 GHz.

Near Field Region, Radiating - The region of an antenna between the reactive near field region and the far field region. In this region the angular field distribution is dependent on the distances from the antenna. If an antenna is focused at infinity, this region is sometimes referred to as the Fresnel zone -- due to the analogy to optical terminology.

Near Field Region, Reactive - That part of the field immediately surrounding the antenna. For most antennas the region exists to a distance of $\lambda/2\pi$ from the antenna's surface, where λ is the wavelength.

Radar - Refers to a system which radiates electromagnetic waves and receives the reflections of the waves from distant objects. These reflections are utilized to determine the existence of the objects and their positions.

APPENDIX B

DESIGN, CONSTRUCTION, AND CALIBRATION OF PSEUDO-TRANSPARENT NON-INTERFERING ELECTRIC AND MAGNETIC FIELD SENSORS

This entire appendix appeared as a paper in the Proceedings of IEEE Southeastcon 1981, pages 120-124 by Brian R. Strickland, George R. Edlin and Thomas H. Shumpert.

DESIGN, CONSTRUCTION, AND CALIBRATION OF PSEUDO-TRANSPARENT, NON-INTERFERING ELECTRIC AND MAGNETIC FIELD SENSORS

Abstract

For non-uniform, non-planar electromagnetic fields, knowledge of the magnitude and phase of each of the three orthogonal components of both the electric field and the magnetic field is required to completely characterize the field. Electrically small, polarization selective, electric and magnetic field sensors for measurement in the UHF band have been designed, constructed, and calibrated. These sensors are short dipoles (for electric fields) and small loops (for magnetic fields) with RF diodes across their gaps. The rectified RF is transferred down semiconductor (carbon-filled) lines to a DC voltmeter. Calibration of the sensors was accomplished in a "TEM cell" transmission line. Complete discussion of the various phases of this work is included in the paper.

Design

Two characteristics of the B Dot probe need to be considered: namely, frequency response and voltage output. (See Reference 3)

$$f_{max} = \frac{0.35c}{2\pi a} \tag{1}$$

where c is the speed of light and a is the radius of the loop, and

$$|V_p| = \frac{2\pi A E_o f}{c} \tag{2}$$

where A is the area of the loop and E_o is field density. Since

$$E_o = Bc \tag{3}$$

where B is the flux density in webers per square meter, equation (2) becomes

$$|V_p| = 2\pi \; fAB \tag{4}$$

Clearly, equations (1) and (4) are area dependent.

The voltage and frequency relationships of a dipole antenna can be derived from the equations given by Taggert and Workman (Reference 1) as follows:

$$\ell_{eff} = \frac{\lambda}{\pi} \tan \frac{\pi \ell}{\lambda} \tag{5}$$

where ℓ_{eff} = the effective length of the antenna, ℓ = the antenna half-length in meters. For a half-wave resonant antenna $\ell = \lambda/4$. For this condition, equation (5) reduces to

$$\ell_{eff} = \frac{\lambda}{\pi} \tag{6}$$

However, shorter non-resonant antennas cannot be treated in this manner as the effective length is reduced by the tangent function. For very short antennas using tan $\Theta \approx \Theta$ for small Θ $\ell_{eff} = \ell$ which indicates a region where V_{OC} is independent of frequency. This indeed was verified by the data. Furthermore,

$$V_{oc} = E\ell_{eff} \tag{7}$$

where

V_{oc} = open-circuit antenna voltage in volts

E = electric field in volts per meter.

Signal detection should occur at the probe as attempting to extract an RF signal from a field could introduce severe interference problems. It is suggested that the detecting element be mounted directly across the gaps in the case of the B Dot probe and directly between the elements of the dipole antenna (see Figure 1).

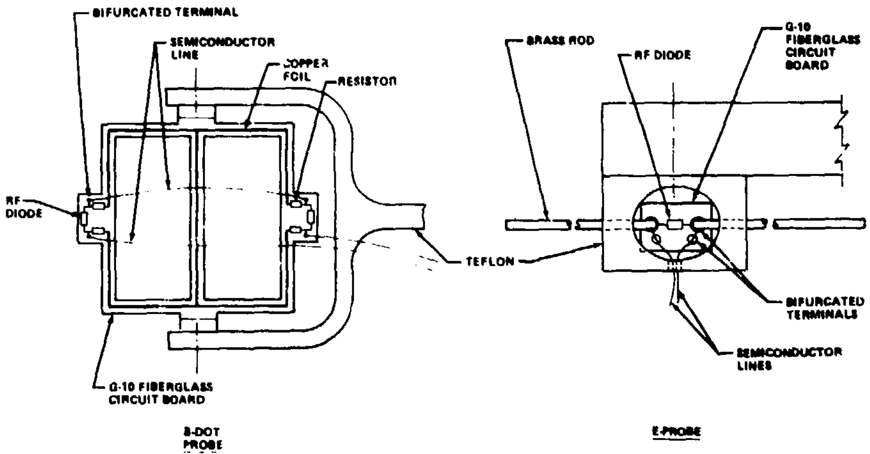

Figure 1. Geometrical and electrical configuration of E and B field probes.

Clearly, no metallic conductor should be used in removing the detected signal from the field. However, carbon filled, or semiconductor lines, may be used with virtually no effect on the field. One disadvantage of semiconductor lines is the high resistance/length. Typical values of resistance for 5-10 meters is 300 KΩ. This problem can be alleviated by either use of a very high impedance voltmeter (we used 100MΩ) or use of precision high input impedance buffer amplifiers.

The above equations, 1 through 7, were used to obtain dimensions of the two probes for operation in the desired frequency range of interest. Another factor to consider is the requirement for noninteracting or nonperturbing probes. This placed an upper limit on the dimensions.

Construction

Construction of a ruggedized B Dot as well as E probes was accomplished. Teflon was used for all possible portions of the probe. The elements of the probes are constructed from single sided G-10 epoxy fiberglass printed circuit board. The B dot probe used the double gap design to cancel the effect of the E field across the gap. The major change in design was to go to a two dimensional design since transmission line matching was no longer required. Also because of the ease of construction, a square instead of circular loop was used. Therefore, equation 1 will be modified slightly for the new probes. The E field probe used a 3/32 brass rod for the elements. For each probe, the dimensions were kept short ($\ell<.1\lambda$) to assure that the probe does not resonate. IN832 RF diodes were used in both cases: two for the B dot and one for the E field probe.

Accurate measurement of the orthogonal components of the B and E fields requires that the probes are capable of horizontal, radial or vertical orientation with the same phase center. Therefore, freedom of movement is necessary in three planes and the probe mounts were constructed to provide this movement without changing the phase center. Figure 1 gives the details of the probes.

Calibration

There are several methods of calibration of field measuring probes (Reference 1). Among these are the standard antenna method, the standard field method and the injection method. Basically, the standard field technique involves placing the probe in a known standard field and determining a calibration factor or antenna coefficient from the magnitude of the known field and the output of the probe. The antenna equations must be solved for 'E', and

$$K = \frac{E_m}{E_k} \tag{8}$$

where

K = the antenna coefficient

E_m = the measured field

E_k = the known field.

To calibrate an antenna using the standard antenna method, the calibrating field is measured first using a standard antenna. The antenna under test is then substituted in place of the standard antenna. From these data, the antenna coefficient can be determined. With the injection method, a low impedance voltage source (less than 0.1 ohm) is used to inject a known voltage in series with the antenna. By calculating the effective length of the antenna and knowing the injected voltage, the antenna coefficient can be determined. This method is the least accurate, while the standard field method is the most accurate. A complete discussion of calibration techniques can be found in reference (1).

Calibration was performed using the standard field method. A Narda Microwave Corporation TEM Transmission Cell was used to establish the standard field. With this TEM cell the standard field method can be used with great accuracy since the only field perturbations are caused by the probe itself and no other sources of reflection and interference such as the ground are present.

TEM Cells (Reference 2) are sections of a two conductor transmission line which operate in the transverse electromagnetic mode. TEM cells are sometimes referred to as Crawford Cells after their developer, Myron Crawford of the National Bureau of Standards. The cell is structured from a rectangular outer conductor and a flat center conductor. The center conductor, or septum, is located midway between the top and bottom walls. The ends of the cell taper down to precision type N connectors at each end. Dimensions and tapers of the cell are chosen to provide a 50 ohm impedance from end to end. The field at the center of the cell is uniform and very close to the 377 ohm impedance of free space. The electric field intensity in volts per meter at the center of the cell, midway between the septum and outer wall is given by the equation

$$E = 47.1\sqrt{P_n} \tag{9}$$

where P_n is the net power transmitted thru the cell. The electric field is polarized normal to the plane of the septum. The probe to be calibrated is placed in the cell and the output voltage is measured thru the ports provided in the cell.

It was desired to obtain a quick and accurate calibration technique. The first step in this procedure was to obtain a general idea of probe output voltage variations with frequency, field level, temperature, and RF diodes. This was accomplished by hand measurement of Vo while the four parameters were varied. The TEM cell was placed inside an environmental chamber where temperature and humidity could be varied and measured. The humidity was kept relatively constant. Five E field probes and five B field probes were used to obtain the effect of different RF diodes on Vo. If Vo were plotted vs. frequency, field level, and temp., we would have a three parameter family of curves which would require a three dimensional graph to display. Since the desired end result was to obtain

$$F_L = f(f, Vo, T) \tag{10}$$

where

f = frequency

F_L = field level (B or E)

Vo = Probe output voltage

T = temperature,

we needed to determine the interdependence of variables and determine a way to computer process the data to obtain equation (10). A standard polynomial regression technique would not work because it does not extend to more than one variable. Also it was not clear how to present the data in two dimensional graphs to best show off the data and bring out significant hidden facts and data trends. As a result many different presentations were examined, i.e., Vo vs. f with F_L as a parameter, F_L vs. Vo with f as a parameter, F_L vs. Vo with T as a parameter, etc. Since we have four different parameters, 4! = 24 number of possible permutations exist, i.e., there are 24 possible ways to present the data.

After examination of the data the temperature variations seemed to vary from diode to diode and no pattern could be recognized. The temperature variation seemed to be a random function of the diode. All 24 permutations were not used (8 would have T as a variable) so it is possible that a pattern could exist and merely not be discovered. This aspect will be investigated more fully at a later date. Based on this it was determined to leave T out and determine equation (10) with T fixed. Either equations could be determined at several different temperatures or an equation could be determined immediately prior to use at ambient temperature. This is feasible since determination of the equation will only take about 10-30 minutes. Styrofoam would need to surround the probes for ruggedization and to prevent heating or cooling due to wind or direct sunlight. Removal of T as a variable greatly reduces the data problem. Now only 6 different permutations exist (actually only 3). It was decided to plot Vo vs. f with F_L as a parameter. For brevity only the E field probe is discussed in the remainder of the paper. A typical plot is shown in Figure 2.

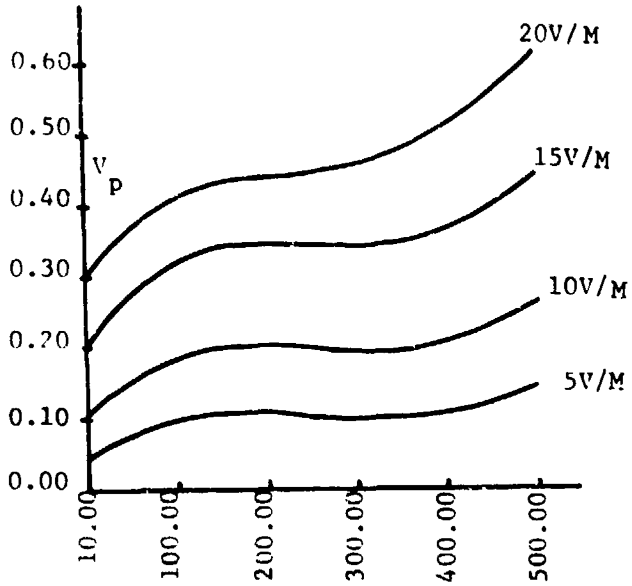

Figure 2. E Probe frequency response.

The Hewlett-Packard 9825 microcomputer is utilized to control the operation and the Hewlett-Packard Interface Bus is used throughout the system. The block diagram of the computer calibration system is shown in Figure 3. Data is taken by the computer as follows:

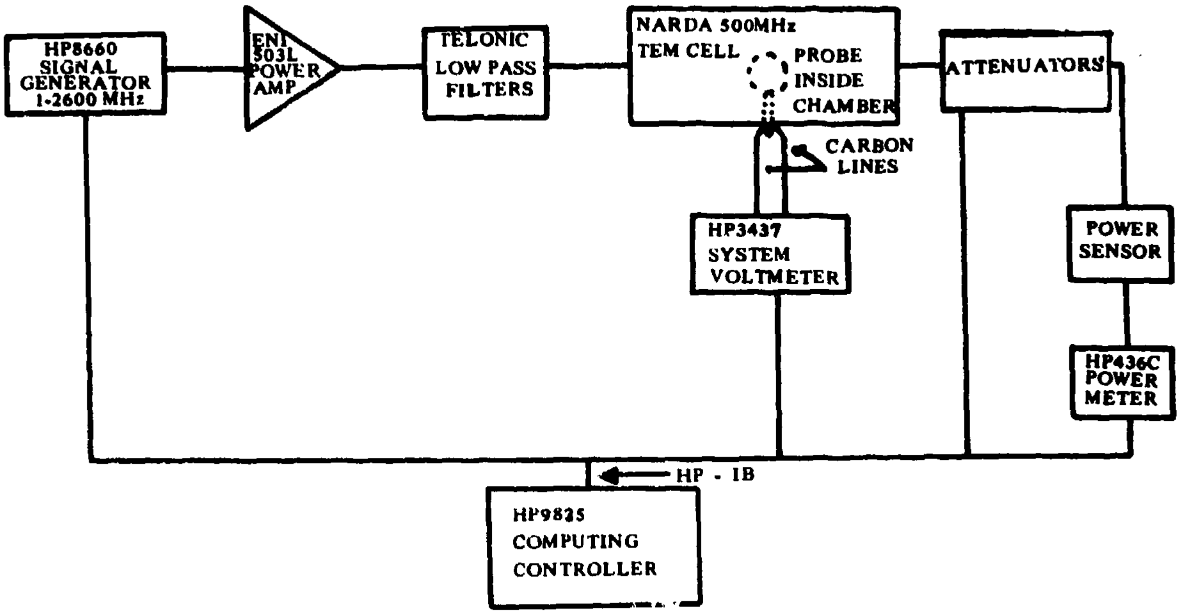

Figure 3. Probe calibration configuration.

1. A given F_L is set within ±.5 db (since the signal generator has a 1db step attenuator).

2. The frequency is set.

3. Vo, f and F_L are stored in an array.

4. The frequency is stepped and 3 repeated.

Assume for illustration purposes 9 frequency points and 9 field levels are used. This gives a 9 x 9 x 3 tensor or 3 dimensional array with 81 rows. If f and F_L are independent, we can change equation (10) to

$$F_L = f(f)\ f\ (Vo)\ . \tag{11}$$

This is approximately true and will lend itself to polynomial regressions around a given F_L and f, and if f and F_L are not allowed much deviation from these values, equation (11) will give negligible error. However, a more general and accurate equation was desired so we must go back to equation (10).

Since f is the only truly accurate variable left to us (F_L is ± .5 db from the set value so), a polynomial regression is performed on the data 9 times for each frequency point giving a series of equations as follows (assuming 3rd order polynomial regression):

$$F_L = C_{11} Vo^3 + C_{12} Vo^2 + C_{13} Vo \quad , f = f_1$$

$$F_L = C_{21} Vo^3 + C_{22} Vo^2 + C_{23} Vo \quad , f = f_2 \tag{12}$$

$$F_L = C_{91} Vo^3 + C_{92} Vo + C_{93} Vo \quad , f = f_9 \quad .$$

Now the original 9 x 9 x 3 tensor is discarded if program memory is a problem and we have a new 9 x 4 matrix composed of the C's in equation (12). Note in equation (12) that a constant term does not exist. This is because it is desired to force $F_L = o$ when $Vo = o$. Now a single equation is obtained from equation (3) by using a polynomial regression on each column of the new 9 x 9 matrix giving 3 equations for the 3 columns as a function of frequency

$$F_L = C_1(f)Vo^3 + C_2(f)Vo^2 + C_3(f)Vo \quad . \tag{13}$$

Referring to equation (13) and Figure 2, it is expected that F_L will follow a $-f^3$ curve, therefore $C_1(f)$, $C_2(f)$, $C_3(f)$ will follow an f^3 curve which indicates that $C_1(f)$, $C_2(f)$, $C_3(f)$ need to be 3rd degree polynomials. It is also noted that F_L vs. Vo is also linear as is expected from equation (7) so the first two columns of the matrix in equation (12) can be dropped without causing appreciable error if computer memory or time is a constraint.

This type of analysis is also used with the B dot probe to determine the degrees of the four polynomials used.

REFERENCES

1. Taggart, Harold E., and Workman, John L., "Calibration Principles and Procedures for Field Strength Meters (30 MHz to 1 GHz)", National Bureau of Standards Technical Note 370, March 1969.

2. Narda Microwave Corporation, Plainview, New York, Test Data certification and procedural literature for Model 8801 TEM cell.

3. Edlin, George R., "Calibration and Use of B Dot Probes for Electromagnetic Measuring", A Thesis, Southeastern Institute of Technology, Huntsville, Alabama, September 1977.

4. Aldridge, Richard E., "The Design and Construction of a Probe Positioner for Electromagnetic Field Measurements", US Army Technical Report RT-80-18, June 1980.

APPENDIX C

THE DESIGN AND CONSTRUCTION OF A PROBE POSITIONER FOR ELECTROMAGNETIC FIELD MEASUREMENTS

Report of MICOM Technical Report RT-80-18, June 1980, George R. Edlin and Richard Aldridge.

CONTENTS

I. INTRODUCTION

The purpose of the project is to design and construct a test fixture to measure the characteristics of the near field emitted from a standard gain horn. This report consists of a discussion of the probes used for measurement, possible designs of the support structure, methods of positioning the probes, and data acquisition techniques. A discussion of a working model is also included.

II. DISCUSSION OF ELECTRIC AND MAGNETIC PROBES

Characterization of an electromagnetic field requires that the orthogonal components of both the B and E fields be accurately measured and recorded. This is true for the far field as well as the near field environment. These measurements can then be used to determine the power density of the field. Conventional measurement of these fields is performed using the B Dot probe (antenna) and calibrated dipole antennas (E probes).

Two characteristics of the B Dot probe need to be considered; namely, frequency response and voltage output. By the equations given in Reference 1

$$f\ max = \frac{0.35\ c}{2\pi\ a} \tag{1}$$

where c is the speed of light and a is the radius of the loop, and

$$|Vp| = \frac{2\pi\ AE_o f}{c} \tag{2}$$

where A is the area of the loop and E_o is the field density. Since

$$E_o = Bc \tag{3}$$

where B is the flux density in webers per square meter, equation (2) becomes

$$|Vp| = 2\pi fAB \tag{4}$$

clearly, equations (1) and (4) are area dependent.

The voltage and frequency relationships of a dipole antenna can be derived from the equations given by Taggert and Workman (Reference 2) as follows:

$$l_{eff} = \frac{\lambda}{\pi} \tan \frac{\pi \ell}{\lambda} \tag{5}$$

where

l_{eff} = the effective length of the antenna,

ℓ = the antenna half-length ($\frac{\lambda}{4}$) in meters for a self-resonant antenna (half wavelength).

For this condition, equation (5) reduces to

$$l_{eff} = \frac{\lambda}{\pi} .$$

However, shorter nonresonant antennas cannot be treated in this manner as the effective length is reduced by the tangent function. Furthermore,

$$V_{oc} = El_{eff} \tag{6}$$

where

V_{oc} = open-circuit antenna voltage in volts,

E = electric field in volts per meter,

l_{eff} = effective antenna length in meters.

Accurate measurement of the orthogonal components of the B and E fields requires that the probes are capable of horizontal, radial or vertical orientation with the same phase center. Further, the probes must be moved spatially throughout the field; that is, in the longitudinal and transverse planes. This introduces physical mounting problems which will be considered later.

Signal detection should occur at the probe as attempting to extract an RF signal from a field could introduce severe interference problems (Reference 3). It is suggested that the detecting element be mounted directly across the gaps in the case of the B Dot probe and directly between the elements of the dipole antenna (see Figure 1). RF diodes, light emitting diodes or liquid crystals could be successfully used for detection. A filter may be desirable, but is not essential for accurate field measurements.

Clearly, no metallic conductor should be used in removing the detected signal from the field. However, carbon filled or semiconductor lines, may be used with virtually no effect on the field. One disadvantage of semiconductor lines is the high loss introduced into the system. While not excessive, this loss must be considered in the probe calibration factor. In the case of the light-emitting diode or liquid crystal detectors, fiber optic lines could be used to transmit the signal out of the field with the advantage of a high degree of isolation between the probe and the load of the measuring device. This method, however, is much more complex and the cost is considerable. If cost and complexity can be overlooked, the fiber optic system seems to be the most desirable. Another possible configuration would be to convert the detected signal to a frequency modulated audio tone to be transmitted out of the field. No effort to prove or disprove this method was expended during this research, but it certainly seems to warrant future investigation.

There are several methods of calibration of field measuring probes (Reference 2). Among these are the standard antenna method, the standard field method and the injection method. Basically, the standard field

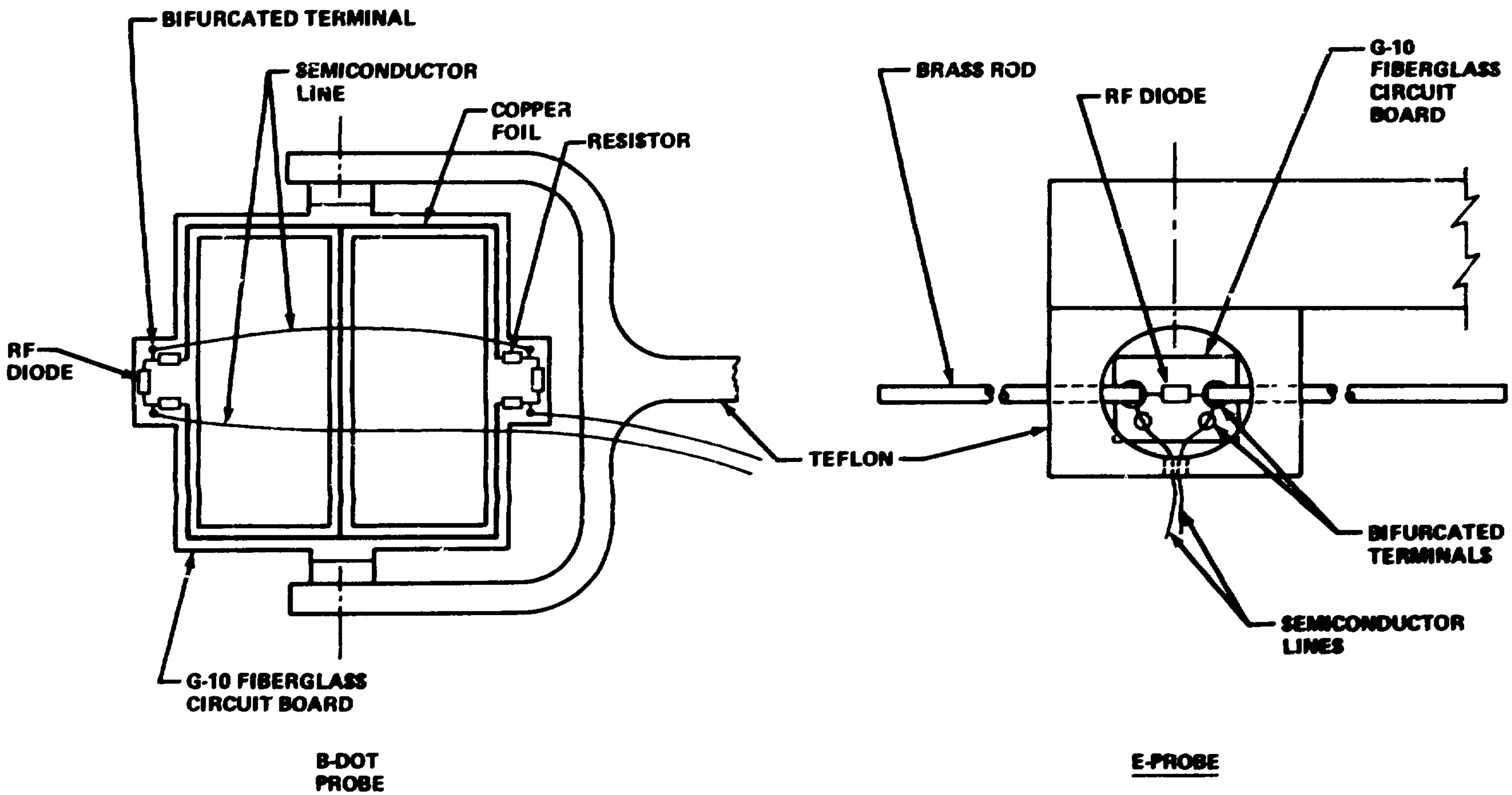

Figure 1. Geometrical and electrical configuration of E and B field probes.

technique involves placing the probe in a known standard field and determining a calibration factor or antenna coefficient from the magnitude of the known field and the output of the probe. The antenna equations must be solved for 'E', and

$$K = \frac{E_m}{E_k} \tag{7}$$

where

K = the antenna coefficient

E_m = the measured field

E_k = the known field.

To calibrate an antenna using the standard antenna method, the calibrating field is measured first using a standard antenna. The antenna under test is then substituted for the standard antenna. From these data, the antenna coefficient can be determined. With the injection method, a low impedance voltage source (less than 0.1-ohm) is used to inject a known voltage in series with the antenna. By calculating the effective length of the antenna and knowing the injected voltage, the antenna coefficient can be determined. This method is the least accurate, while the standard field method is the most accurate. A complete discussion of calibration techniques can be found in Reference 2.

III. DESIGN OF PROBE SUPPORT STRUCTURE

The primary problem encountered in measuring an electromagnetic field is distortion of the field by the measuring equipment. Metallic materials are completely ruled out for use as a probe support structure since ground planes are easily established on metallic surfaces, particularly at higher frequencies. Therefore, it is desirable to use materials which are insulators.

Several possibilities exist for probe support using non-metallic materials such as ceramics, wood, and many types of plastics. While ceramic material is useful, cost and fragility would limit its use in ruggedized systems. Wood has been in use for such applications for a considerable period of time; however, there are some disadvantages. Dimensional instability due to moisture, heat, and light make wood a difficult material to use for probe positioners. Plastic while far from ideal, seems to be one of the better alternatives. Unless extremely heavy grades of plastic are used, the slightest wind can cause it to flex. If plastic materials have an advantage, it is their ability to endure exposure to weather.

IV. PROBE POSITIONING AND DATA ACQUISITION

Another major problem encountered in field characterization is position control and data acquisition. For the present project, the required precision is ± five millimeters. Measurements will be made in three directions and in three orientations. Over the required distances, this amounts to some 216,000 data points. The mass of data and the required precision dictate that a computer be used to control the test. A complete discussion of computer control is beyond the scope of this paper; however, a summary of the method used will be discussed later.

Position indication can be accomplished by analog or digital means. Analog methods involve the use of a multi-turn potentiometer in the motor drive train. Several problems are encountered with this method. Slippage, motor starting torque and the necessity of A to D conversion make this method undesirable.

By far, the better method of position indication is direct digital pulse generation. Pulses can be generated either optically, electrically, or mechanically. The optical method involves a light source passing over a coded area of the positioner frame such that the light might be reflected or not reflected from the frame. A photo diode could be used to receive the light pulses. These light pulses could also be transmitted via a fiber optic line to the controlling system. Encoded electrical tones could be used to indicate position by much the same methods. However, for both optical and electrical methods, decoding at the computer introduces an additional processing step. A mechanical position indicator could also be used. One method is to use a small micro-switch with a roller arm that rolls over trip points on the stationary portion of the positioner frame. These switch closures are simply counted by the computer so that the computer can keep track of where the positioner is located. Again, the use of semiconductor lines is necessary to avoid disturbance of the electromagnetic field being measured.

Construction of the probe positioner began with the stationary frame. Six-inch poly vinyl chloride (PVC) pipe was used for the support uprights and the rails. Nylon bolts and PVC cement were used to assemble the pipe. Since PVC pipe will sag unless supported, several braces were installed using metal screws for rigidity. Other fastening methods may have been more desirable from an interference standpoint, but these small amounts of metal close to the ground level did not adversely affect the field.

The dimensions of the frame are shown in Figure 2. The length of the frame was conveniently chosen to make use of standard lengths of PVC. This length allows a measurement distance of 4.8 meters which is adequate for the test.

It was necessary to be able to move the positioner periodically during construction and testing. However, because of the positioner's weight, swivel casters were installed to facilitate movement. To construct these casters, a round wooden block was placed upright inside the support and a plastic plate attached to the bottom of the block. The wheel assembly was then attached to the plastic plate.

The mast trolly assembly was constructed of PVC and two-inch redwood and was assembled entirely with nylon hardware (Figure 3). The runners were made by cutting a 220° segment of eight-inch PVC pipe. The redwood was used for crossmembers. The mast bracket is 3/8" PVC sheet with redwood spacers. Wheel mounting brackets were cut from plexiglass blocks. When using these materials, careful and accurate alignment was absolutely essential.

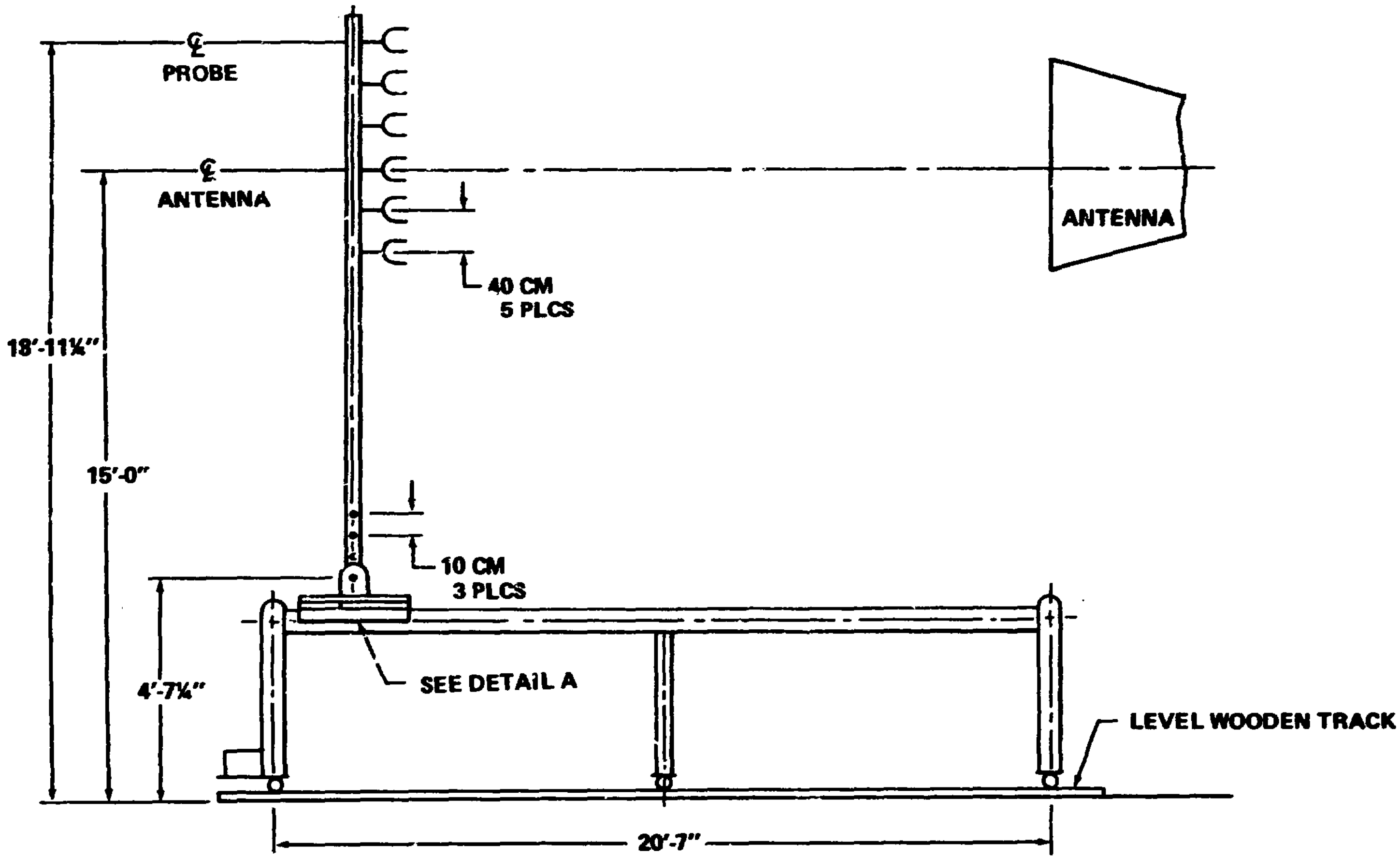

Figure 2. Dimensional sketch of probe positioner.

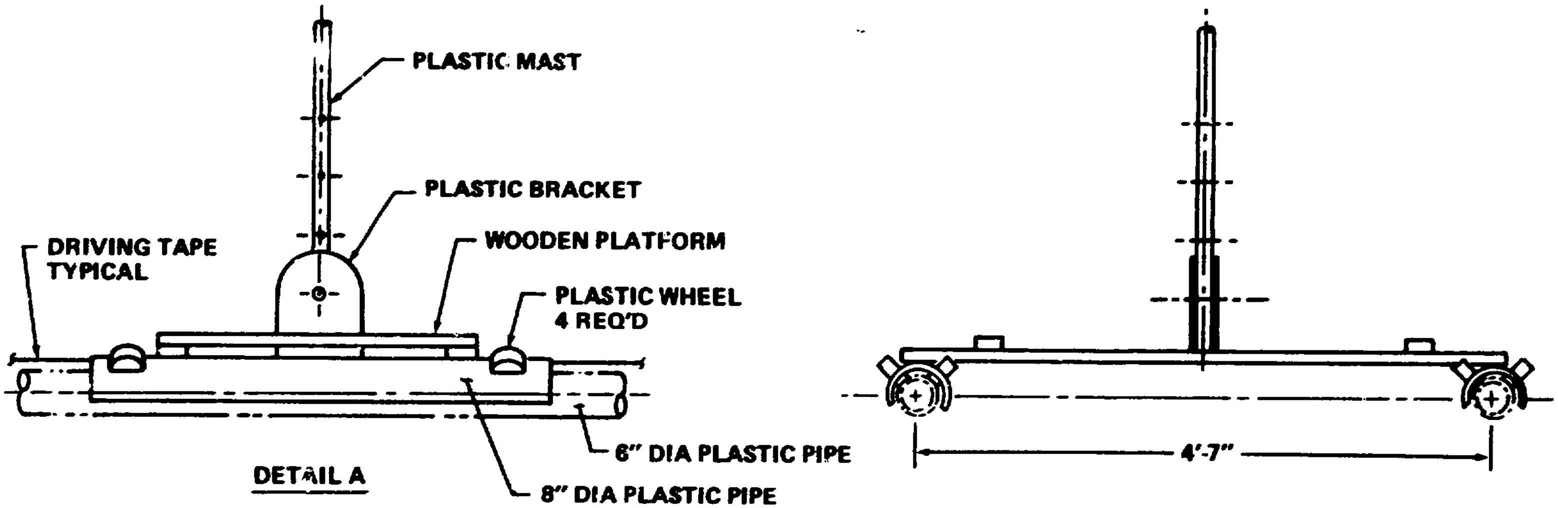

Figure 3. Detail of mast trolley.

The mast consisted of a piece of two-inch PVC pipe. Guy ropes were necessary to keep the mast from bending as the trolly moved along the positioner.

According to Reference 5, "Use of B Dot as a standard field measuring probe has given rise to a need for a ruggedized probe. The development of a more durable probe would save considerable time on repair and checkout of damaged probes." With this in mind, construction of a ruggedized B Dot as well as E probes was accomplished. Teflon was used for all possible portions of the probe. The element of the B Dot probe is constructed from single sided G-10 epoxy fiberglass printed circuit board. The output of this probe compares favorably with the output of a standard B Dot probe of comparable size. A similar construction technique was used for the E probe. A 3/32" brass rod was used for the elements. For each probe, the length is kept short ($\ell < 0.1\lambda$) to ensure that the probe does not resonate. Freedom of movement is necessary in three planes and the probe mounts are constructed to provide this movement without changing the phase center. Figures 1, 4, 5, 6 and 7 give the details of the probes which are mounted to the mast with $^1/_2$" nylon bolts. All semiconductor lines from the probes are brought to a common junction box at the base of the mast where they are converted to shielded lines. Two separate masts were constructed to reduce probe damage during testing. The B Dot probes are mounted on one mast and the E probes are mounted on the other.

At the time of this writing, calibration of the probes had not been completed. However, an outline of the procedure to be used follows.

Calibration will be performed using the standard field method. A Narda Microwave Corporation TEM Transmission Cell will be used to establish the standard field. TEM Cells (Reference 4) are sections of a two conductor transmission line which operate in the transverse electromagnetic mode. TEM Cells are sometimes referred to as Crawford Cells after their developer, Myron Crawford of the National Bureau of Standards. The cell is structured with a rectangular outer conductor and a flat center conductor. The center conductor, or septum, is located midway between the top and bottom walls. The ends of the cell taper down to precision type N connectors at each end. Dimensions and tapers of the cell are chosen to provide a 50-ohm impedance from end to end. The field at the center of the cell is uniform and very close to the 377-ohm impedance of free space. The electric field intensity in volts per meter at the center of the cell, midway between the septum and outer wall is given by the equation

$$E = 47.1 \sqrt{P_n} \tag{8}$$

where P_n is the net power transmitted thru the cell. The electric field is polarized normal to the plane of the septum. The probe to be calibrated is placed in the cell and the output voltage is measured through the ports provided in the cell.

A motor assembly is installed at the base of one of the support uprights of the positioner frame using a gear reduction and tape drive system to move the mast trolley. The tape used is plastic banding material which does not stretch appreciably and is very durable. It was determined that moving the

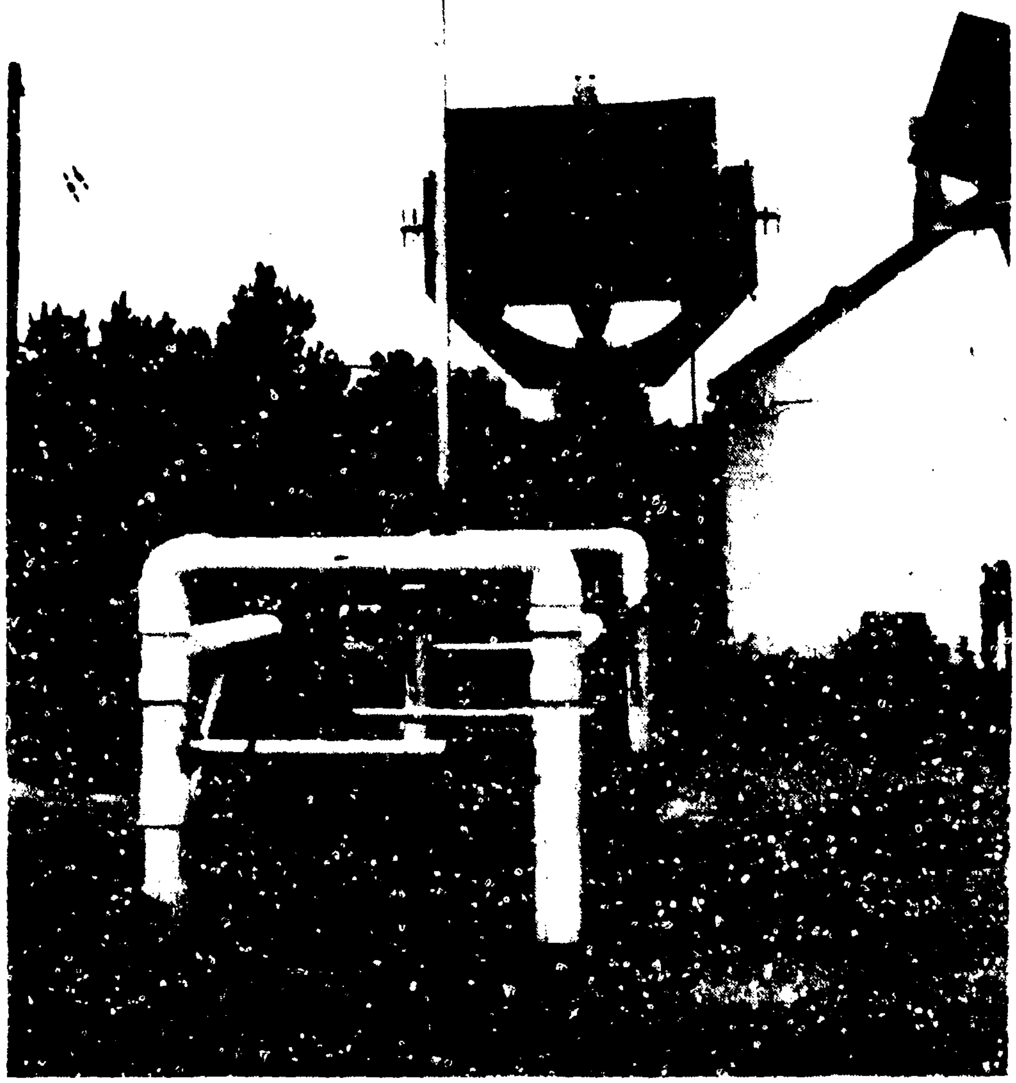

Figure 4. Actual probe positioner in foreground with UHF high gain pyramidal horn in background.

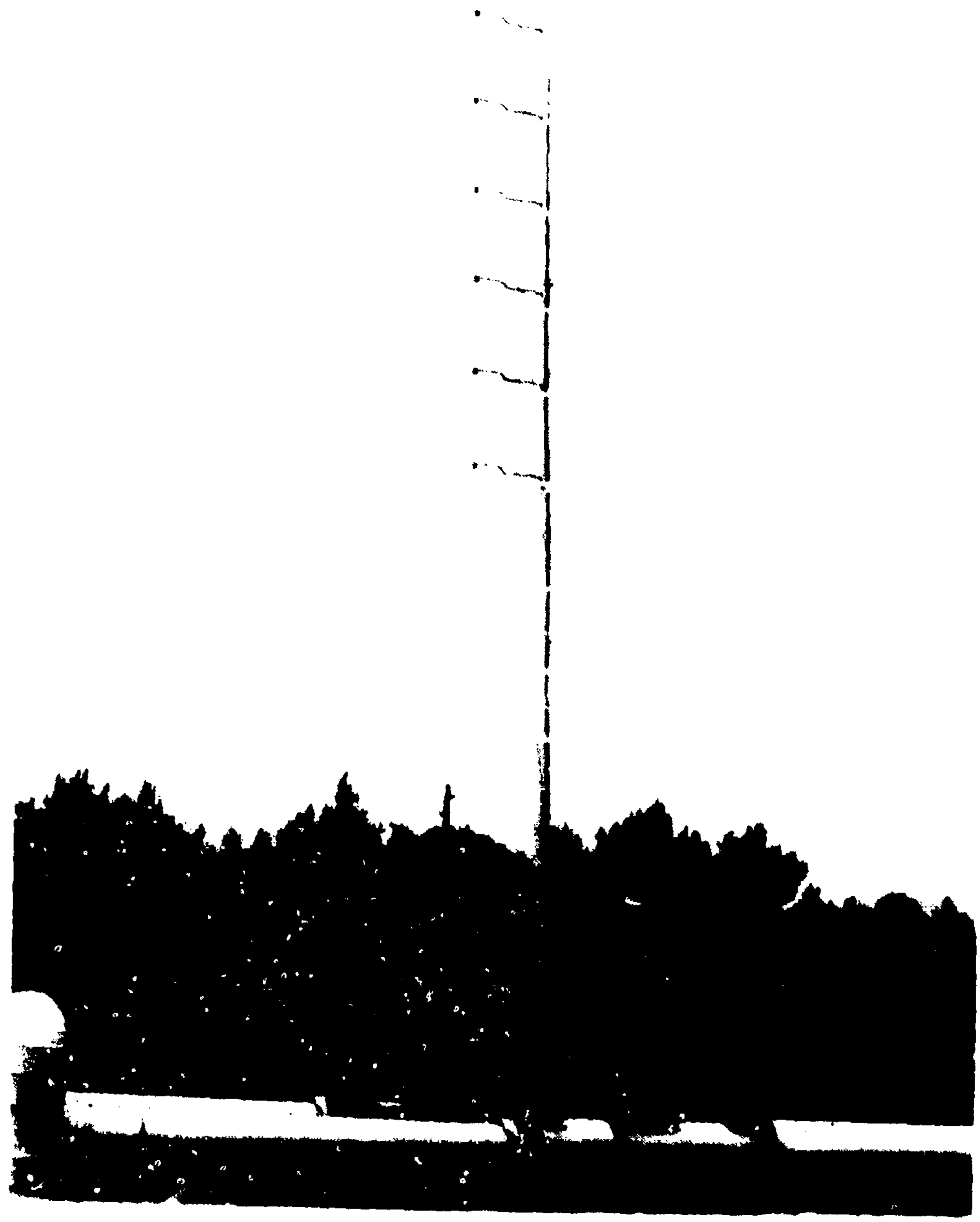

Figure 5. Closeup of mast and trolley assembly.

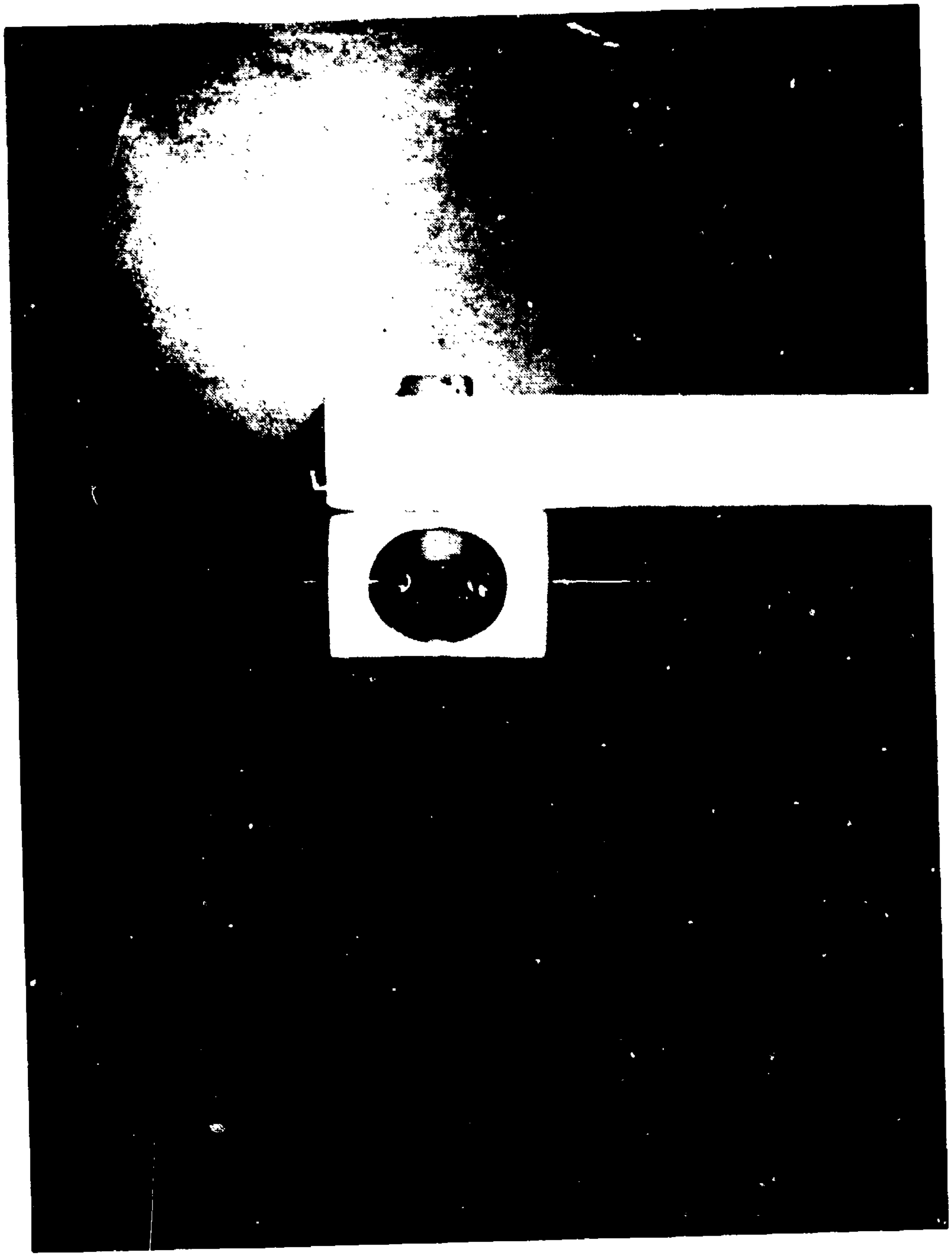

Figure 6. The E-probe and support bracket with carbon-filled (semiconductor) signal lines.

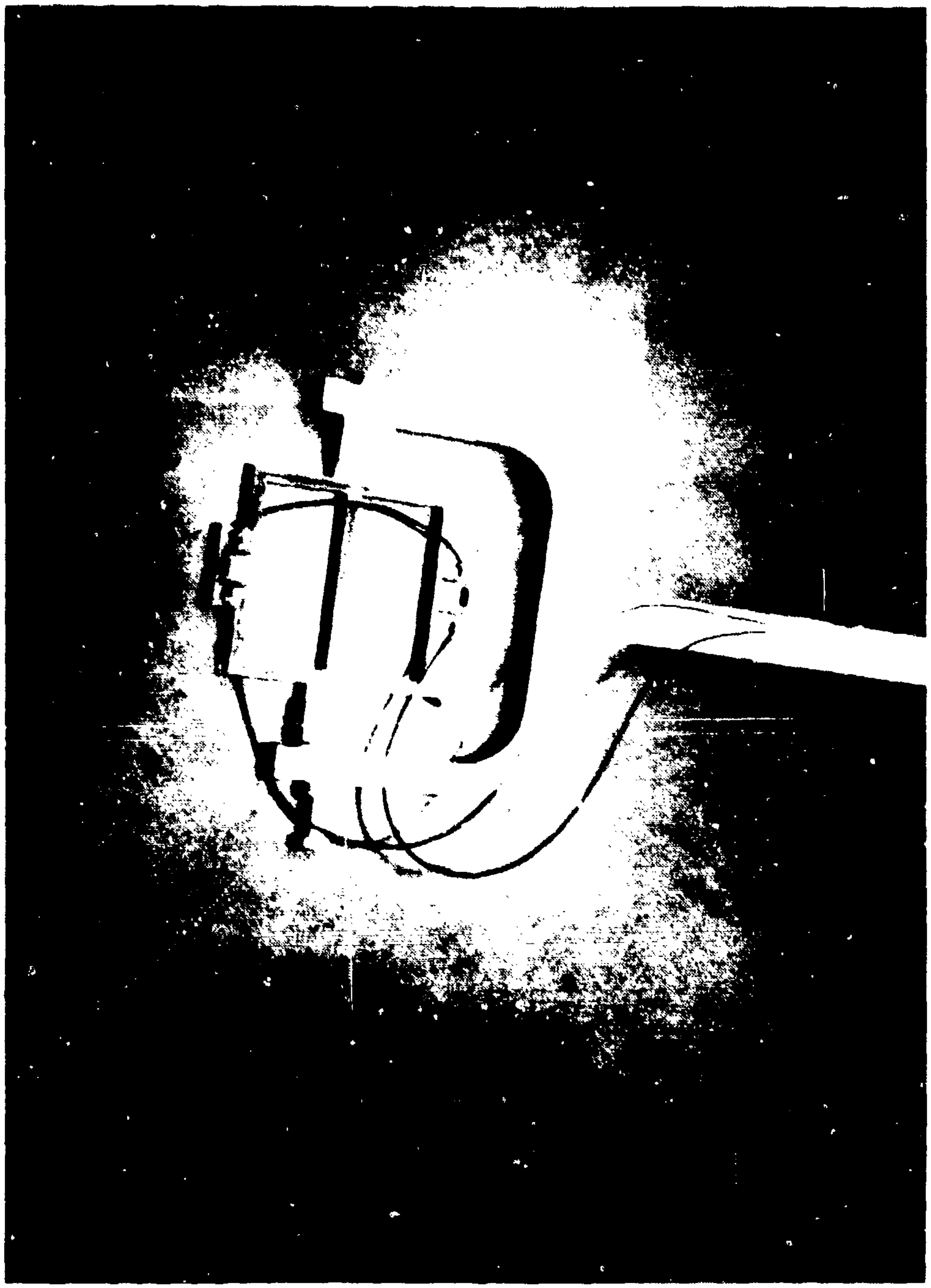

Figure 7. The B dot probe and support bracket.

trolley at a slow constant speed rather than stopping and starting gave much more accurate measurements. This was due to the springiness of the mast. With the system used, the trolley moves at a speed of 8.48 centimeters-per-second. Position is indicated to the computer using the microswitch system described previously. There are six probes on the mast which makes a total of seven voltages that the computer must recognize and measure for each data point. Data points are every ten centimeters, or approximately one data point every 1.8 seconds. Since the computer requires a very small fraction of this time to make the required measurements, the amount of error is nearly negligible. The error that does exist can be accounted for in the data uncertainties.

Figure 8 is a system block diagram of the test setup. The Hewlett-Packard 9825 Microcomputer is utilized to control the operation and the Hewlett-Packard Interface Bus is used throughout the system. Complete analysis of the computer system would serve no purpose here as it is the subject of another report, as is the resulting data.

Design and construction of a low interference probe positioner is feasible. There is considerable demand for such devices in the field of electromagnetic research and several proposals for its utilization already exist.

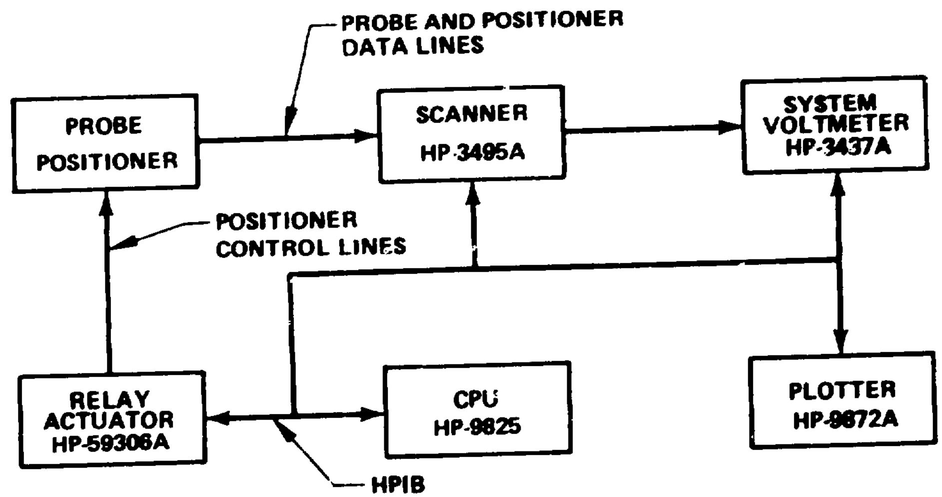

Figure 8. System block diagram.

REFERENCES

1. Edlin, George R. and Wayne T. Hudson, "The Design and Development of a Gap Loop B Dot Sensor", US Army MICOM Technical Report RG-75-23, 1 December 1974.

2. Taggart, Harold E., and John L. Workman, "Calibration Principles and Procedures for Field Strength Meters (30 MHz to 1 GHz)", National Bureau of Standards Technical Note 370, March 1969.

3. Discussions with Dr. Thomas H. Shumpert, Department of Electrical Engineering, Auburn University and Mr. George R. Edlin, Electrical Engineer, Test & Evaluation Directorate, US Army Missile Laboratory, US Army Missile Command, Redstone Arsenal, Alabama.

4. Narda Microwave Corporation, Plainview, New York, Test Data certification and procedural literature for Model 8801 TEM cell.

5. Edlin, George R., "Calibration and Use of B Dot Probes for Electromagnetic Measuring", A Thesis, Southeastern Institute of Technology, Huntsville, Alabama, September 1977.

APPENDIX D

ANALYTICAL DERIVATION OF THE APERTURE DISTRIBUTION MODEL

APPENDIX D

ANALYTICAL DERIVATION OF THE APERTURE DISTRIBUTION MODEL

The E-field aperture distribution used for the theoretical model is the waveguide TE_{01}, i.e., the E-field is described using a quadratic phase term and a cosine amplitude term. This aperture distribution is used with vector Smythe-Kirchhoff formula for diffraction to develop the spatial representation of the radiated E-field. The vector Smythe-Kirchhoff is given in equation (D-1),

$$\vec{E}(x,y,z) = \frac{1}{2\pi}\nabla x \int_{Aper} (\hat{n} X \bar{E}) \frac{e^{-jkR}}{R} \, da' \quad . \tag{D-1}$$

Figure 1 shows the horn geometry and aperture associated coordinate system.

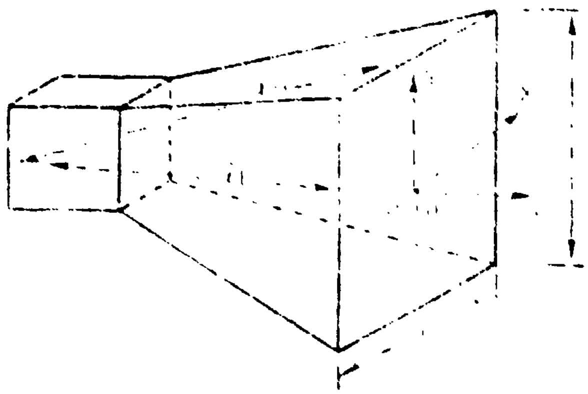

Figure 1. Geometry and Coordinate System of UHF Pyramidal Horn.

The TE_{01} Waveguide E-field distribution is given by equation (D-2).

$$\vec{E}(x,y,0) = E_o \cos\frac{\pi x}{a} \exp\left[-jk\left(\frac{x^2}{2\ell_H} + \frac{y^2}{2\ell_E}\right) \quad \hat{U}_y\right] . \tag{D-2}$$

Let $\hat{n} = \hat{U}_z$ then:

$$\hat{n} X \vec{E} = -\hat{U}_x \, E_o \cos\frac{\pi x}{a} \exp\left[-jk\left(\frac{x^2}{2\ell_H} + \frac{y^2}{2\ell_E}\right)\right] \quad .$$

The relationship of $\vec{R}$, $\vec{r}$, $\vec{r}'$, and z are shown in Figure 2.

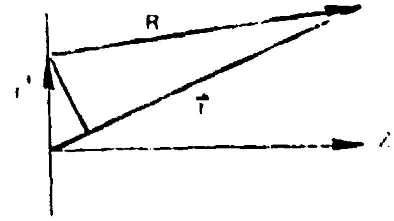

Figure 2. Source - observation coordinate system.

Where:

$$R = |\vec{r} - \vec{r}'| \quad , \quad R = \left[z^2 + (x-x')^2 + (y-y')^2\right]^{1/2} \quad . \tag{D-3}$$

Where (x,y,z) is the observation point and (x',y',o) is the source point, then we have

$$\vec{E}\,(x,y,z) = -\frac{E_o}{2\pi}\,\nabla x \int_{-\frac{a}{2}}^{\frac{a}{2}} \int_{-\frac{b}{2}}^{\frac{b}{2}} U_x \cos\frac{\pi x'}{a}$$

$$\exp \frac{\left[-jk\left(\frac{x'^2}{2\ell_H} + \frac{y'^2}{2\ell_E} - \left(z^2 + (x-x')^2 + (y-y')^2\right)^{1/2}\right)\right]}{(z^2 + (x-x')^2 + (y-y')^2)^{1/2}}\, dx'dy' \quad . \tag{D-4}$$

$$\text{Let } \vec{A} = \hat{U}_x \cos\frac{\pi x'}{a} \exp\left[-jk\left(\frac{x'^2}{2\ell_H} + \frac{y'^2}{2\ell_E} - (z^2 + (x-x')^2 + (y-y')^2)^{1/2}\right)\right]$$

$$\left[z^2 + (x-x')^2 + (y-y')^2\right]^{1/2} \quad . \tag{D-5}$$

$$\text{If } K = \cos\frac{\pi x'}{a} \exp\left[-jk\left(\frac{x'^2}{2\ell_H} + \frac{y'^2}{2\ell_E}\right)\right] \tag{D-6}$$

then substituting K in equation (D-5) yields:

$$\vec{A} = \hat{U}_x \frac{K \exp\left[-jk(z^2 + (x-x')^2 + (y-y')^2)^{1/2}\right]}{\left[z^2 + (x-x')^2 + (y-y')^2\right]^{1/2}} \quad . \tag{D-7}$$

Therefore:

$$\nabla X\vec{A} = \frac{\partial A_x}{\partial z}\hat{U}_y - \frac{\partial A_x}{\partial y}\hat{U}_z \tag{D-8}$$

and

$$\frac{\partial A_x}{\partial z} = K\,\frac{jkz\,e^{-jkR}}{R^2} - \frac{Kze^{-jkR}}{R^3} \tag{D-9}$$

and

$$\frac{\partial A_x}{\partial y} = \frac{Ke^{-jkR}jk(y-y')}{R^2} - \frac{K(y-y')e^{-jkR}}{R^3}\ . \tag{D-10}$$

Thus

$$\nabla x\ \bar{A} = K\left[\hat{U}_y\left(\frac{jkze^{-jkR}}{R^2} - \frac{ze^{-jkR}}{R^3}\right) + U_z\left(\frac{K(y-y')e^{-jkR}}{R^3} - \frac{jk(y-y')e^{-jkR}}{R^2}\right)\right] \tag{D-11}$$

The curl is taken inside the integral by the application of the Leibnitz rule.

$$\vec{E}(x,y,z) = -\frac{E_o}{2\pi}\iint \nabla x\vec{A}dx'dy'\ . \tag{D-12}$$

Substituting $\nabla X\vec{A}$ into equation (D-12) and taking the negative sign inside yields:

$$\vec{E}(x,y,z) = \frac{E_o}{2\pi}\int_{x'=-a/2}^{a/2}\int_{y'=-b/2}^{b/2} K\left[\hat{U}_y\left(\frac{ze^{-jkR}}{R^3} - \frac{jkze^{-jkR}}{R^2}\right) + \hat{U}_z\left(\frac{jk(y-y')e^{-jkR}}{R^2} - \frac{(y-y')e^{-jkR}}{R^3}\right)\right] dx'dy' \tag{D-13}$$

where

$$R = \left[z^2 + (x - x')^2 + (y - y')^2\right]^{1/2}\ , \tag{D-14}$$

$$R' = jkRy - y - jkRy' + y' = (y - y') + j(kRy - kRy')\ , \tag{D-15}$$

$$R_2 = z - jkRz \tag{D-16}$$

$$K' = Ke^{-jkR} \tag{D-17}$$

$$K' = \cos\frac{\pi x'}{a}\left\{\cos\left[k\left(\frac{x'^2}{2\ell_H} + \frac{y'^2}{2\ell_E} - R\right)\right] - j\sin\left[\left(\frac{x'^2}{2\ell_H} + \frac{y'^2}{2\ell_E} - R\right)\right]\right\} \tag{D-18}$$

$$B = k\left(\frac{x'^2}{2\ell_H} + \frac{y'^2}{2\ell_E} - R\right) \tag{D-19}$$

$$\vec{E}(x,y,z) = \frac{E_o}{2\pi}\hat{U}_y \int_{x'=-a/2}^{a/2}\int_{y'=-b/2}^{b/2} \frac{K'R_2}{R^3}\,dx'dy' +$$

$$\frac{E_o}{2\pi}\hat{U}_z \int_{x'=-a/2}^{a/2}\int_{y'=-b/2}^{b/2} \frac{K'R'}{R^3}\,dx'dy' \tag{D-20}$$

$$K'R_2 = z\cos\frac{\pi x'}{a}\left\{[\cos B - kR\sin B] - j\,[\sin B + kR\cos B]\right\} \tag{D-21}$$

$$K' = \cos\frac{\pi x'}{a}(\cos B - j\sin B) \tag{D-22}$$

$$K'R' = \cos\frac{\pi x'}{a}\Big\{[(\cos B)(y' - y) + (\sin B)(kRy - kRy')] +$$

$$j\,[(kRy - kRy')(\cos B) - (y' - y)(\sin B)]\Big\}. \tag{D-23}$$

Let

$$B_1 = \cos\frac{\pi x'}{a}\cos B \tag{D-24}$$

$$B_2 \quad \cos\frac{\pi x'}{a}\sin B \tag{D-25}$$

$$B_3 = R^3 \tag{D-26}$$

$$B_4 = (y - y')\ kR \quad . \tag{D-27}$$

Substituting these expressions into equation (D-20) produces

$$\bar{E}(x,y,z) = \frac{E_o}{2\pi}\hat{U}_y \int_{x'=-a/2}^{a/2} \int_{y'=-b/2}^{b/a} \frac{z}{B_3}\left(B_1 - kRB_2\right) dx'dy'$$

$$\left. - j \int_{x'=-a/2}^{a/2} \int_{y'=b/2}^{b/2} \frac{z}{B_3}\left(B_2 + kRB_1\right)\ dx'dy' \right]$$

$$+ \frac{E_o}{2\pi}\hat{U}_z \left[\int_{x'=-a/2}^{a/2} \int_{y'=-b/2}^{b/2} \left(\frac{y - y'}{B_3}\right)\left[-B_1 + kRB_2\right] dx'dy' \right.$$

$$\left. + j \int_{x'=-a/2}^{a/2} \int_{y'=-b/2}^{b/2} \left(\frac{y - y'}{B_3}\right)\left[B_2 + kRB_1\right]\ dx'dy' \right] \quad . \tag{D-28}$$

For further simplification the following functions are defined:

$$F_1 = \frac{z}{2\pi B_3}\left(B_1 - kRB_2\right) \tag{D-29}$$

$$F_2 = -\frac{z}{2\pi B_3}\left(B_2 + kRB_1\right) \tag{D-30}$$

$$F_3 = \left(\frac{y - y'}{2\pi B_3}\right)\left[-B_1 + kRB_2\right] \tag{D-31}$$

$$F_4 = \left(\frac{y - y'}{2\pi B_3}\right)\left[B_2 + kRB_1\right] \quad . \tag{D-32}$$

Substituting the above functions into equation (D-28), one obtains

$$\vec{E}(x,y,z) = \bar{E}_o \left\{ \hat{U}_y \left[\iint_{Aper} F_1 \, dx'dy' + j \iint_{Aper} F_2 \, dx'dy' \right] \right.$$

$$\left. + \hat{U}_z \left[\iint_{Aper} F_3 \, dx'dy' + j \iint_{Aper} F_4 \, dx'dy' \right] \right\} . \qquad \text{(D-33)}$$

Using the following relationship for the magnetic field the expression for the theoretical H field is developed.

$$\bar{H} = \frac{j}{\omega\mu} \left[\left(\frac{\partial E_z}{\partial y} - \frac{\partial E_y}{\partial z} \right) \hat{U}_x + \left(\frac{-\partial E_z}{\partial x} \right) \hat{U}_y + \left(\frac{-\partial E_y}{\partial x} \right) \hat{U}_z \right] . \qquad \text{(D-34)}$$

Rearranging equation (D-13) and substituting the values for K' and R yields

$$E_y = \frac{E_o}{2\pi} \iint_{Aper} \cos \frac{\pi x'}{a} \, \frac{e^{-jkB} \, z(1-jkR)}{R^3} \, dx'dy' \qquad \text{(D-35)}$$

$$E_z = \frac{E_o}{2\pi} \iint_{Aper} \cos \frac{\pi x'}{a} \, \frac{e^{-jkB} (y' - y) \, (1 - jkR)}{R^3} \, dx'dy' \qquad \text{(D-36)}$$

where

$$R = \left[z^2 + (x - x')^2 + (y - y')^2 \right]^{1/2} \qquad \text{(D-37)}$$

$$B = \left[\frac{x'^2}{2\ell_H} + \frac{y'^2}{2\ell_E} - R \right] , \qquad \text{(D-38)}$$

Taking the partial derivative of E_z with respect to y produces

$$\frac{\partial E_z}{\partial y} = \frac{E_o}{2\pi} \iint_{Aper} \cos \frac{\pi x'}{a} \, \frac{e^{-jkB}}{R^3} \left[(y-y')^2 \left(k^2 - \frac{3}{R^2} + j3\frac{k}{R} \right) + 1-jkR \right] dx'dy' . \qquad \text{(D-39)}$$

Similarly,

$$\frac{\partial E_y}{\partial z} = \frac{E_o}{2\pi} \iint_{Aper} \cos\frac{\pi x'}{a} \frac{e^{-jkB}}{R^3} \left[z^2\left(k^2 - \frac{3}{R^2} + \frac{j3k}{R}\right) + 1 - jkR \right] dx'dy' \qquad (D-40)$$

$$\frac{\partial E_z}{\partial x} = \frac{E_o}{2\pi} \iint_{Aper} \cos\frac{\pi x'}{a} \frac{e^{-jkB}}{R^3} (y-y')\ (x-x') \left(k^2 - \frac{3}{R^2} + \frac{j3k}{R}\right) dx'dy' \qquad (D-41)$$

$$\frac{\partial E_y}{\partial x} = \frac{E_o}{2\pi} \iint_{Aper} \cos\frac{\pi x'}{a} \frac{e^{-jkB}}{R^3}\, z\ (x-x') \left(k^2 - \frac{3}{R^2} + \frac{j3k}{R}\right) dx'dy' \quad . \qquad (D-42)$$

From equation (D-24) the expression for the horizontal component of the magnetic field (H_x) is

$$H_x = \frac{j}{\omega\mu} \left[\frac{\partial E_z}{\partial y} - \frac{\partial E_y}{\partial z} \right] . \qquad (D-43)$$

Substituting equations (D-39) and (D-40) into equation (D-43) yields

$$H_x = \frac{jE_o}{2\pi\omega\mu} \left\{ \iint_{Aper} \cos\frac{\pi x'}{a} \frac{e^{-jkB}}{R^3} \left\{ \left(k^2 - \frac{3}{R^2} + 3j\frac{k}{R}\right) (y-y')^2 - z^2 \right.\right.$$

$$\left.\left. + \left(1 - jkR\right) \right\} dx'dy' \right\} \quad . \qquad (D-44)$$

Where the vertical magnetic field (H_y) is

$$H_y = \frac{-j}{\omega\mu} \frac{\partial E_z}{\partial x} \quad . \qquad (D-45)$$

Then,

$$H_y = \frac{jE_o}{2\pi\omega\mu} \iint_{Aper} \cos\frac{\pi x'}{a} \frac{e^{-jkB}}{R^3} (y-y')\ (x-x') \left(k^2 - \frac{3}{R^2} + \frac{j3k}{R}\right) dx'dy' . \qquad (D-46)$$

From equation (D-34) the radial magnetic field (H_z) is

$$H_z = \frac{j}{\omega\mu}\left(\frac{\partial E_y}{\partial x}\right) \quad . \tag{D-47}$$

Using equation (D-42) with (D-47) gives

$$H_z = \frac{jE_o}{2\pi\omega\mu} \iint_{\text{Aper}} \cos\frac{\pi x'}{a} \frac{e^{-jkB}}{R^3} z\ (x-x') \left(k^2 - \frac{3}{R^2} + \frac{j3k}{R}\right) dx'dy' \quad . \tag{D-48}$$

Equations (D-35), (D-36), (D-44), (D-46), and (D-48) represent the EM fields predicted by the aperture model.

APPENDIX E

EXPERIMENTAL DETERMINATION OF THE ELECTROMAGNETIC FIELD IN THE NEAR-ZONE OF A HIGH POWER UHF PYRAMIDAL HORN ANTENNA

This entire appendix appeared as a paper in the Proceedings of IEEE Southeastcon 1981, pages 503-507, Thomas H. Shumpert, Thomas A. Blalock and George R. Edlin.

EXPERIMENTAL DETERMINATION OF THE ELECTROMAGNETIC FIELD IN THE NEAR-ZONE OF A HIGH POWER UHF PYRAMIDAL HORN ANTENNA

ABSTRACT

The far zone characteristic (directive gain, main lobe beamwidth, side lobe structure, etc.) of pyramidal horn antennas are fairly well-known and, for the most part, easily predictable. However, as the observation point moves within the 'so-called" far zone boundary (often taken to be $2D^2/\lambda$), predicting the radiated field characteristics becomes much more difficult. This paper presents preliminary results of an intensive effort utilizing electrically small electric (dipoles) and magnetic (loops) probes to map the field in the region immediately in front of a high power UHF pyramidal horn antenna. The measured values are compared with values obtained from a theoretical model. Application of these data to electromagnetic hazard considerations are discussed.

INTRODUCTION

In the area of testing for electromagnetic radiation hazards (EMRH), electromagnetic compatibility (EMC), electromagnetic interference (EMI), accurate knowledge of the electromagnetic (EM) field into which the test item (or system) is to be immersed is of essential importance. Most common tests of these types include several apriori assumptions. First, the test item does not interfere (couple) with the mechanism for producing and maintaining the EM field environment, i.e., the radiating antenna structure, the parallel plate transmission line, the anechoic chamber walls, etc. Second, the impinging EM field is commonly assumed to be planar and uniform (true plane waves do not fall off with distance from the source). Third, the EM environment is accurately calibrated at various amplitude levels and predetermined frequencies of interest. Although the assumptions are usually dismissed as routine and well understood, the test engineer in EMRH, EMC, and EMI work is (or should be) all too familiar with the severe problems that arise upon violation of any of these simplifying statements. As expected, these assumptions apply quite well when the test item is sufficiently removed from the EM source (i.e., the test item is truly in the far zone of the EM source structure.) However, this "sufficient" separation is all too often compromised in actual test configurations. However, these compromises are not made out of ignorance or stupidity but are rather forced on the test engineer out of real necessity. Such considerations as limited real estate, limited radiating power, and large test items contribute significantly to this problem.

The purpose of this paper is to discuss measurement techniques and results of the application of these techniques to the situations in which one or more of these assumptions must be compromised. Specifically, this paper addresses the experimental determination of the EM field environment in the immediate region in front of a high power UHF pyramidal horn antenna.

UHF HORN CHARACTERISTIC

The specific horn antenna which is addressed in this paper is presently in use at the US Army Missile Command (MICOM) EM and Nuclear Effects facility at Redstone Arsenal, AL. The horn is of a similar design to commercially available standard gain horns such as those supplied by the Narda Microwave Corporation or Scientific Atlanta. It is constructed of sheet aluminum with all seams formed with a heli-arc technique. The aperture dimensions are 2.44m by 1.8m and the overall feed-to-aperture dimension is approximately 4m. This antenna is designed to operate in the fundamental TE_{01} mode radiation pattern over the UHF frequency range from 300 MHz to 550 MHz. The feed mechanism is coaxial-to-waveguide adapter with a "tear-shaped" stub for better broadband operation. The horn is mounted such that its center line is located approximately 4.6m (15 feet) above the ground, and it is oriented for vertical electric field polarization. The electric field pattern is the standard gain horn pattern with E and H plane 3dB beamwidths of approximately 22°. The nominal gain over the recommended band of operation is 18dB.

ANALYTICAL MODEL

For purposes of analyzing and comparing the measured EM fields with predicted values, a rather simple analytical model of this horn was developed for calculating the radiating properties. Figure 1 is a sketch of the horn geometry with the associated coordinate system.

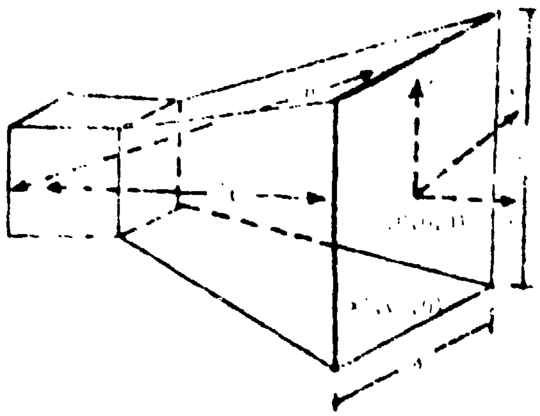

Figure 1. Geometry of UHF pyramidal horn antenna and associated dimensions and coordinate system.

The radiation model assumes a fairly simple aperture distribution as defined below

$$\bar{E}(x',y') = U_y E_0 \cos\left(\frac{\pi x'}{a}\right) \exp\left[jk\left(\frac{x'^2}{2\ell_H} + \frac{y'^2}{2\ell_E}\right)\right] \quad . \tag{1}$$

This may be recognized as the TE_{01} mode amplitude distribution with a quadratic phase term. Several investigators[1,2] have utilized this type of aperture function successfully. The radiated electric field intensity is then given by

$$\bar{E}(x,y,z) = \frac{1}{2\pi} \nabla \times \iint_{\text{Aperture}} [\hat{n} \times \bar{E}(x',y') \frac{e^{-jkR}}{R} dx'dy' \tag{2}$$

where

$$R = [(x-x')^2 + (y-y')^2 + z^2]^{1/2} \quad . \tag{3}$$

The evaluation of the curl and cross product operators yields the following

$$E_x\ (x,y,z) = 0 \tag{4}$$

$$E_y(x,y,z) = \int_{-a/2}^{a/2} \int_{-b/2}^{b/2} \cos\left(\frac{\pi x'}{a}\right) \exp\ (-jkb)z \quad .$$

$$(1-jkR)\ \frac{1}{R^3}\ dx'dy' \tag{5}$$

$$E_z(x,y,z) = \int_{-a/2}^{a/2} \int_{-b/2}^{b/2} \cos\left(\frac{\pi x'}{a}\right) \exp\ (-jkb) \quad .$$

$$(y-y')\ (1-jkR)\ \frac{1}{R^3}\ dx'dy' \tag{6}$$

where

$$b = \frac{x'^2}{\ell_H} + \frac{y'^2}{\ell_E} - R \quad .$$

Substitution of equations (4)-(6) into Maxwell's equations yields the corresponding magnetic field components. Equations (4)-(6) and the corresponding ones for the magnetic field components were evaluated numerically. The results of these calculations and their comparisons to measured data are discussed in a later paragraph.

NEAR-FIELD MEASUREMENT TECHNIQUES

In order to map (measure) the EM field in the immediate vicinity of this UHF pyramidal horn, several pieces of experimental equipment were developed. Probably the most important development was the fabrication of electric and magnetic probes. These probes are electrically small, diode-loaded dipoles and loops. Their general design has been discussed in several National Bureau of Standards technical reports[3,4]. The specific probes utilized in this effort are discussed in great detail in another technical paper in this same meeting[5]. For this discussion, it is sufficient to describe them as electrically small, field-type selective, polarization selective, and of non-perturbing design and construction. The electric and magnetic probes were mounted on a moveable carriage which was computer controlled. Measurements from each of these probes was obtained at points in a symmetric volume located directly in front of the horn antenna. With reference to the coordinate system of the model, this volume occupied the space defined by the coordinates: $-1.5 \leq x \leq 1.5$, $-1.2 \leq y \leq 1.2$, $0 \leq z \leq 4.6$. Resolution of these spatial variations was 0.1m. All probe outputs were fed into the computer controlled data acquisition system, and the actual measured results, the corresponding physical locations, and the field component type and orientation were stored together on a magnetic disk. The moveable carriage was constructed almost entirely of polyvinyl chloride (PVC) pipes. The actual probes and associated circuit components were mounted on low-loss "G-10" dielectric sheets. All electrical leads from the probes to the monitoring voltmeters were high resistance (carbon-filled) lines to minimize their interaction with the field to be measured. This measurement technique produced a set of six fundamental quantities (the rms magnitude of E_x, E_y, E_z, H_x, H_y, H_z) at each of the 36,425 unique spatial locations contained within this previously defined test volume. Preliminary results gleaned from this large mass of data are presented in the following paragraph.

PRELIMINARY ANALYTICAL AND EXPERIMENTAL RESULTS

As was pointed out in the introductory paragraph, measurement or analytical prediction of the EM field in the region far removed from the source is quite straightforward. Near zone measurements and predictions usually are much more difficult. However, as a check on both the analytical and experimental techniques, far zone fields were predicted and measured. As expected, these predicted and measured fields were in very close agreement. Gain, E and H plane beamwidths, and $\frac{1}{r}$ spatial variations were very close to those previously predicted for horn antennas of this type. Consequently, all of the results discussed here will be near-zone analytical predictions and measurements. Furthermore all predictions and measurements were performed at 400 MHz.

Since it was assumed in the analytical model that the aperture distribution was of the TE_{01} amplitude variation, an interesting plane for measured observation is near the actual horn aperture (the z=0 plane). Figure 2 presents both the measured and predicted vertical electric field amplitude (rms $|E_y|$) as a function of x for a constant value of y and z (y=0, z=0.1). All analytical data has been amplitude normalized to match the average value of the measured data on the aperture center line (x=0, y=0). As can be seen, this variation is indeed the expected cosinusoidal distribution. Figure 3 presents similar data for the horizontal magnetic field amplitude (rms $|H_x|$). This also displays the expected cosinusoidal variation with x. Due to space limitations, the variations of these important aperture fields with y are not shown. However, both the analytical and measured curves for E_y and H_x vs. y show the expected uniformity of the assumed TE_{01} mode distribution. Figures 4 and 5 present identical data except that the plane of observation has been moved out to the z=4.6 plane. Here as expected, the plots of E_y and H_x show the typical far-zone variations, i.e., consinusoidal in both x and y variations about the z-axis. Plots of the various other less significant field components as a function of x, y, or z have been made, but are not included due to space limitations. Figure 6 compares the measured vertical electric field on the horn axis (x=0, y=0) with both the predicted field and a superimposed $\frac{1}{r}$ fallout. All of these values are normalized to coincide at the point farthest from the horn (z=4.6). It is interesting and somewhat disturbing that the measured field does not exhibit the expected standing wave behavior as evidenced in the deep null in the analytical results near the aperture. This discrepancy continues to be an area of investigation. Finally, a plot of the z-directed wave impedance of the radiated EM field predicted by the numerical model is included. It demonstrates the expected asymptotic behavior toward 377 ohms as the observation point recedes from the aperture. However, its unexpected reversal of slope at points less than $z \doteq 0.75$ suggest to these investigators that even the numerical model probably has significant deficiencies within a wavelength of the aperture.

CONCLUSIONS

The EM field in the near-zone of a high-power UHF pyramidal horn antenna has been determined both experimentally and analytically. The preliminary results suggest that the techniques employed and the resulting EM field measurements have yielded valuable data for characterizing the near field of the antenna. Much work still remains in analyzing the large quantity of experimental data. A technical report presenting the complete data analysis will be available in the near future.

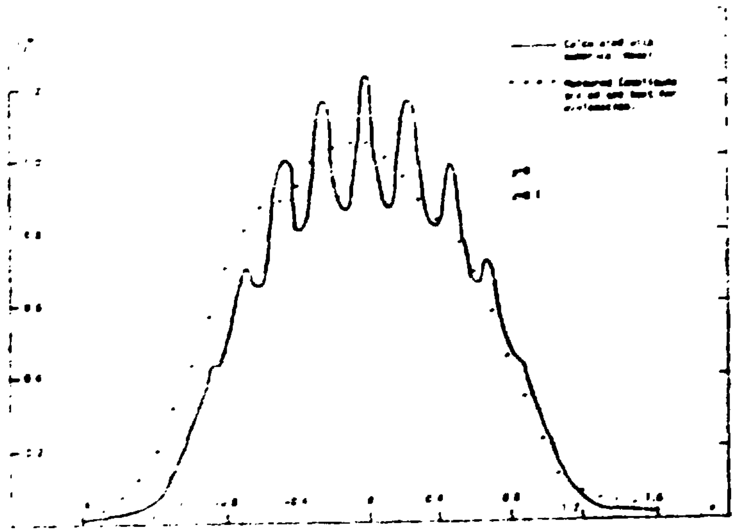

Figure 2. RMS magnitude of the vertical electric field component vs. x in the z=0.1 plane for y=0.

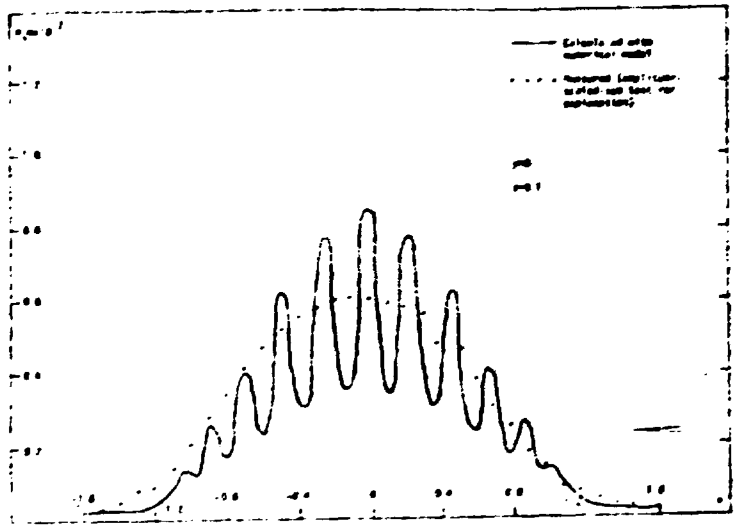

Figure 3. RMS magnitude of the horizontal magnetic field component vs. x in the z=0.1 plane for y=0.

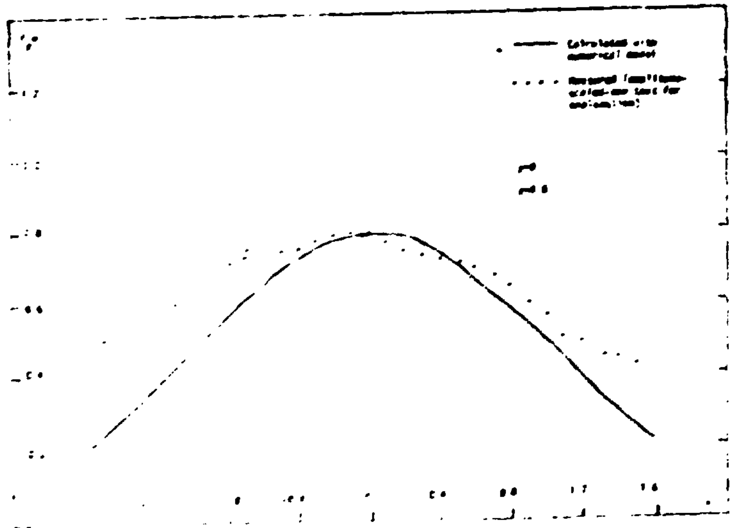

Figure 4. RMS magnitude of the vertical electric field component vs. x in the z=4.6 plane for y=0.

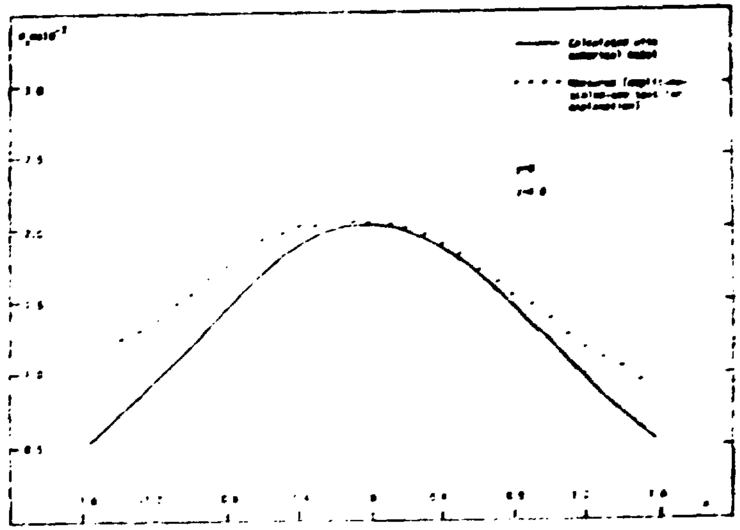

Figure 5. RMS magnitude of the horizontal magnetic field component vs. x in the z=4.6 plane for y=0.

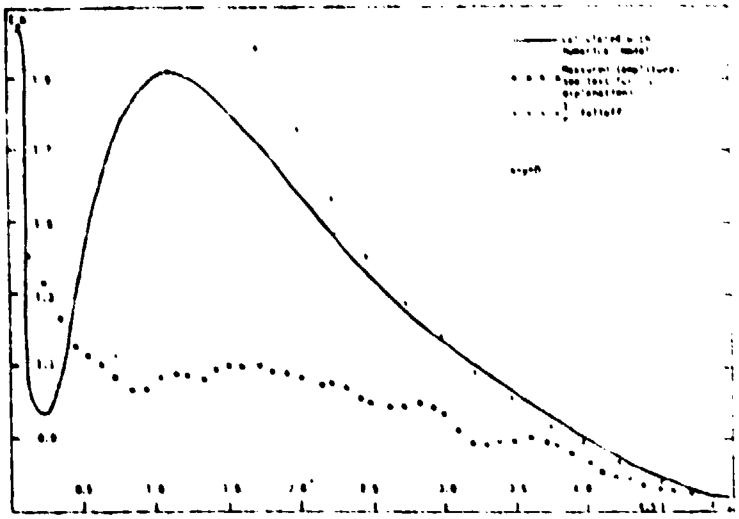

Figure 6. Analytical and experimental vertical electrical field component (rms magnitude) vs. z on the horn axis (x=y=0).

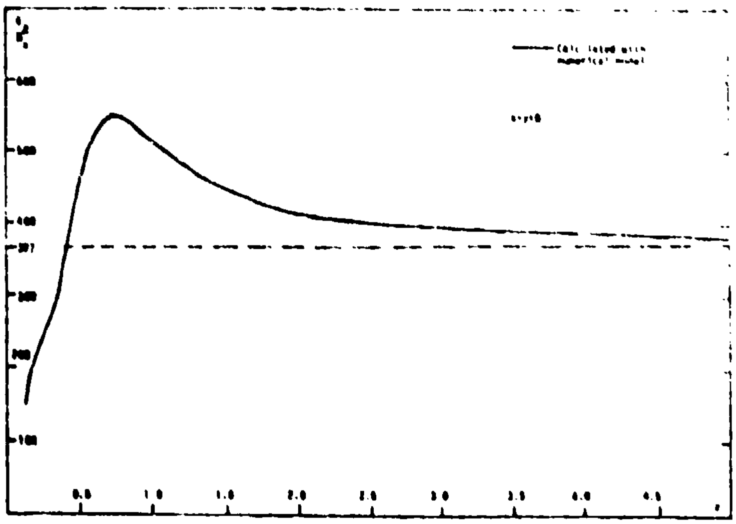

Figure 7. Z-directed wave impedance (analytical model only) vs. z.

REFERENCES

1. Chu, T. S. and R. A. Semplak, "Gain of Electromagnetic Horns," Bell System Tech. Jour., Vol. 44, p. 527-537, March 1965.

2. Muehldorf, E. I., "The Phase Center of Horn Antennas," IEEE Trans. Antennas Propagation, Vol. AP-8, pp. 753-760, November 1970.

3. Green, F. M., "Development of Electric and Magnetic Near-Field Probes," National Bureau of Standards Technical Note 658, January 1975.

4. Wacker, P. E. and R. R. Bowman, "Quantifying Hazardous Electromagnetic Fields: Scientific Basis and Practical Considerations," IEEE Trans. Microwave Theory and Techniques, Vol. MII-19, No. 2, February 1971.

5. Strickland, B. R., G. R. Edlin, and T. H. Shumpert, "Design, Construction, and Calibration of Pseudo-Transparent Non-interfering Electric and Magnetic Field Sensors," to be presented, 1981 Southeastcon Symposium, Huntsville, AL, April 1981.

APPENDIX F

DERIVATION OF THE MULTIPOLE MODEL

APPENDIX F

DERIVATION OF THE MULTIPOLE MODEL

It is desirable from the engineering standpoint to have simple models which can be used to predict E fields in the near-zone of standard gain horn antennas. Review of some selected references (Stratton, 162; Jackson, 136) suggests that complex field problems can be solved using infinite series expansion techniques. This method of field solution utilizes the superposition of the so-called dipole, quadrupole, octupole, and N pole terms, where $n = 4$ to ∞. In addition, examination of the measured data demonstrates that the classical $1/r$ far field relationship does not hold close to the horn aperture. Thus the experimental data confirms the need for additional terms. Therefore, using the idea of the series expansion and truncating it at the third term, one has terms involving $1/r$, $1/r^2$ and $1/r^3$. By incorporating the appropriate constants with each of the terms, we have the dipole (A_1/r), quadrupole (A_2/r^2) and octupole (A_3/r^3) terms. Finally, incorporating the square root of the input power yields a model that can also relate the E field to the input power.

The assumed form for the multipole model is given as:

$$E = \left(\frac{A_1}{r} + \frac{A_2}{r^2} + \frac{A_3}{r^3}\right) \sqrt{P} \quad . \tag{F-1}$$

The constants A_1, A_2 and A_3 are determined experimentally using measured data. The procedure is to choose three different distances and substitute these values along with the corresponding values of E into the generalized equation yielding three equations with three unknowns, which can then be easily solved simultaneously to give the proper values for A_1, A_2 and A_3. These values can then be normalized by dividing by the test power used in the original measurement. The final equation becomes:

$$E = \left(\frac{A_1}{r} + \frac{A_2}{r^2} + \frac{A_3}{r^3}\right) \left[P \text{ (Watts)}\right]^{1/2} \tag{F-2}$$

where

E = E field (in V/m)

A_1, A_2, A_3 = antenna constants

r = distance from the aperture to the field observation point (in meters)

P = power to the antenna (in Watts).

This simplified function can easily be programmed into a hand-held programmable calculator which will allow the determination of the near-zone E field at any distance from the aperture greater than $D^2/4\lambda$. The normalized equation for the 300-500 MHz test horn operating at 400 MHz is:

$$E = \left(\frac{44.95}{r} - \frac{46.17}{r^2} + \frac{1.46}{r^3}\right) P^{1/2} \quad . \tag{F-3}$$

This simplified equation can predict the field amplitude to approximately ±0.5 dB across the entire band of the horn antenna. If greater accuracy is required, the field must be carefully measured using calibrated probes. This model does not predict the E field at all frequencies. It is limited to the frequency range for which it is developed.

APPENDIX G

DEVELOPMENT OF THE ENGINEERING MODEL

APPENDIX G

DEVELOPMENT OF THE ENGINEERING MODEL

The engineering model is developed utilizing the following methodology.

The measured data is read at $2D^2/\lambda$, D^2/λ, $D^2/2\lambda$, and $D^2/4\lambda$. The equivalent far field gain is calculated and the effective gain plotted versus distance.

Observation of this graph suggests that the gain reduction in the near-zone would fit an exponential decay curve of the form:

$$G_{\eta\lambda} = G \left\{ 1 - \exp \left[-\alpha r / (2D^2/\lambda) \right] \right\} \qquad \text{(G-1)}$$

where

$G_{\eta\lambda}$ = wavelength dependent near-zone corrected numerical gain

G = far field numerical gain

D = largest dimension of the aperture (in meters)

λ = wavelength (in meters)

α = gain attenuation constant.

For the horn utilized in this experiment, the approximate value for G is 58.8. Substituting into Eq. (G-1), one obtains

$$G_{\eta\lambda} = 58.8 \left\{ 1 - \exp \left[-\alpha r / (2D^2/\lambda) \right] \right\} \qquad \text{(G-2)}$$

when

$$r = D^2/\lambda \quad , \quad G_{\eta\lambda} = 51.3 \quad , \quad \alpha = 3.86$$

$$r = D^2/2\lambda \quad , \quad G_{\eta\lambda} = 39.5 \quad , \quad \alpha = 4.30 \quad .$$

From the above calculations using the measured data and equation (G-2), one observes that $\alpha = 4$ is a good choice for the gain attenuation constant. Putting this value into equation (G-2) produces:

$$G_{\eta\lambda} = 58.8 \left\{ 1 - \exp \left[-4r / (2D^2/\lambda) \right] \right\} \quad . \qquad \text{(G-3)}$$

This equation for the corrected near-field gain may be utilized in the standard far field formula. The following is the standard formula for the far field power density:

$$P_d = G_T P_T / 4\pi r \qquad \text{(G-4)}$$

where

P_d = power dencity (in Watts/m^2)

G_T = numerical gain of the transmitting antenna

P_T = power of the transmitter (in Watts)

r = distance from the antenna (in meters).

The following is the relationship between the E field and the power density:

$$E = (P_d 377)^{1/2} \tag{G-5}$$

where 377 is the free space wave impedance.

To develop the final form, the expression for $G_{\eta\lambda}$ is substituted into equation (G-4). This expression for P_d with the corrected gain is substituted into equation (G-5). This result gives the complete expression for E in the near-zone, as shown in equation (G-6):

$$E = \left\{ G_m \left[\frac{1 - \exp(-4r/(2D^2/\lambda))}{4\pi r^2} \right] P_T 377 \right\}^{1/2} . \tag{G-6}$$

APPENDIX H

MEASURED FIELD DATA

(VERTICAL ELECTRIC FIELD ONLY)

APPENDIX H

MEASURED FIELD DATA (VERTICAL ELECTRIC FIELD ONLY)

This appendix contains a complete set of vertical E field data. The remaining five orthogonal components are not included due to the large volume of data. All components were measured with polarization selective, nonperturbing E and H field probes. These probes are described in detail in Appendix B. These electric and magnetic probes were mounted on a computer-controlled carriage which permitted a space of 3 meters x 2.4 meters x 4.8 meters to be covered with a resolution of 10 cm. The following coordinate system defines the rectangular parallelopiped mapped: $-1.5 \leq X \leq 1.5$, $-1.2 \leq Y \leq 1.2$, $0 \leq Z \leq 4.8$ (Figure 1).

The data are identified by the type E or H and by the specific component, i.e., radial, horizontal or vertical. At the beginning of each set of data, the position of the probe is given. For example, if the top probe position is 11 and one wishes to see the centerline data, the probe output to observe is Probe 4 which is at $y = -1$, as shown in Figure 2. Any desired vertical position relative to the center line of the horn can be identified by using Figure 2. Appendix C describes the probe positioner in detail.

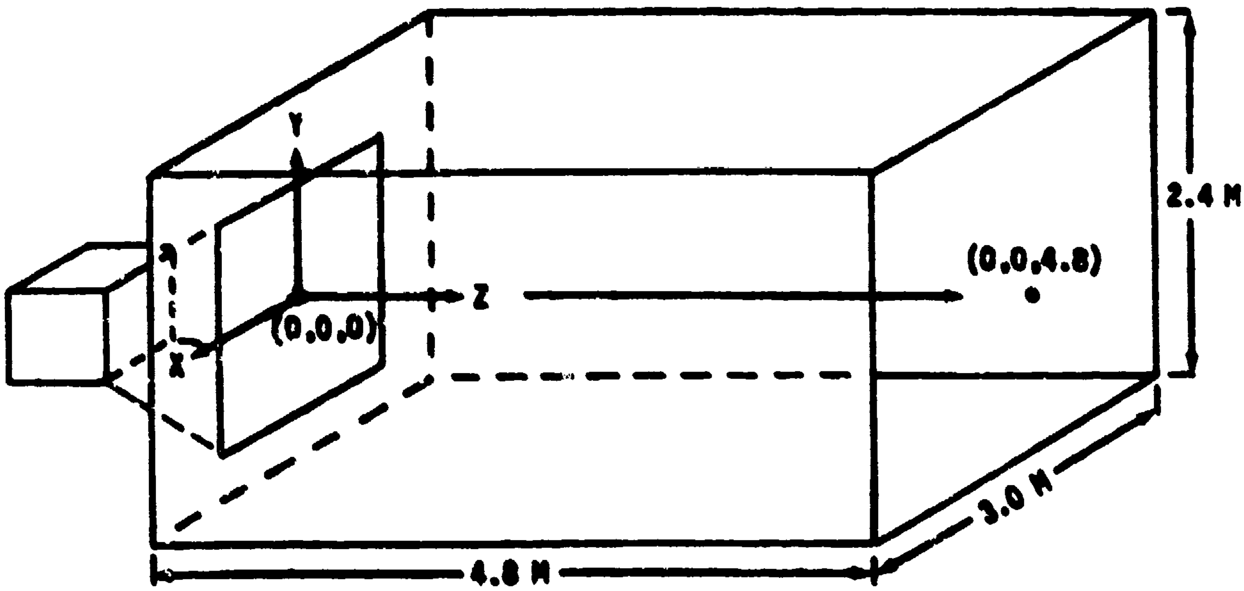

Figure 1. Volume of spatial E and H field measurements.

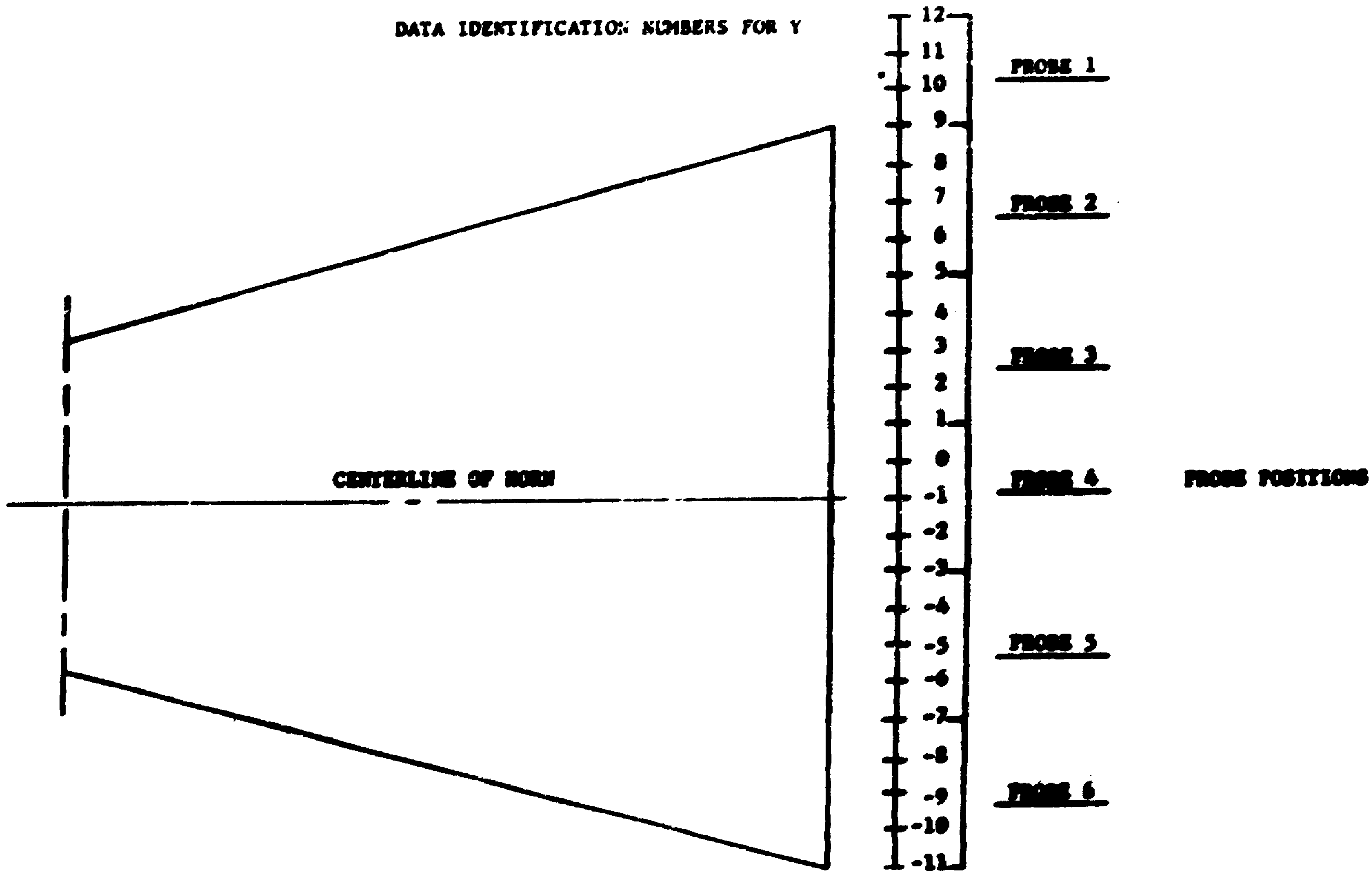

Figure 2. Vertical position of the magnetic and electric field probes relative to the horn antenna.

VERTICAL ELECTRIC FIELD
STARTING COORDINATES

PROBE #	X	Y	Z
1.00	-15.00	12.00	0.00
2.00	-15.00	8.00	0.00
3.00	-15.00	4.00	0.00
4.00	-15.00	0.00	0.00
5.00	-15.00	-4.00	0.00
6.00	-15.00	-8.00	0.00

Z	P(1)	P(2)	P(3)	P(4)	P(5)	P(6)
0.000	1.130	2.215	3.920	3.281	3.136	2.952
0.100	1.760	3.016	5.393	3.640	4.393	3.315
0.200	1.006	4.029	6.413	4.737	6.736	5.106
0.300	1.006	4.324	6.959	4.937	6.780	3.924
0.400	2.126	5.128	7.076	5.340	6.789	6.106
0.500	2.301	6.011	8.202	7.201	7.127	5.970
0.600	3.034	6.604	9.246	9.262	8.651	6.603
0.700	2.909	6.970	9.653	9.103	8.366	6.559
0.800	3.530	7.323	9.962	10.340	9.630	7.021
0.900	4.429	8.276	10.169	10.919	9.985	9.073
1.000	5.007	8.776	9.977	11.422	9.779	9.473
1.100	5.141	8.151	10.169	12.700	9.757	8.939
1.200	5.007	7.016	10.167	13.660	10.134	8.995
1.300	5.539	8.413	11.241	14.673	11.160	9.650
1.400	6.552	9.524	12.420	15.943	12.305	10.354
1.500	7.255	9.014	[illegible]	16.706	12.505	10.376
1.600	7.643	9.670	12.470	16.777	12.305	10.100
1.700	7.643	8.735	12.420	16.706	12.904	10.444
1.800	7.339	8.405	13.365	17.662	14.004	10.837
1.900	7.121	8.904	14.492	18.533	14.096	11.109
2.000	7.773	9.014	15.530	19.174	14.735	10.003
2.100	8.272	10.434	15.761	17.099	14.627	11.146
2.200	8.117	10.579	15.120	18.604	14.627	11.502
2.300	7.200	9.900	14.417	18.117	15.050	11.320
2.400	7.575	10.107	15.071	18.760	15.317	11.050
2.500	7.599	10.046	16.503	19.690	16.376	11.042
2.600	8.117	11.708	17.462	20.770	17.011	12.846
2.700	7.016	11.175	16.607	20.072	16.099	12.965
2.800	7.969	11.270	15.910	18.609	16.113	12.103
2.900	7.909	11.339	15.501	17.730	15.012	11.400
3.000	7.903	11.740	16.021	17.662	14.550	11.233
3.100	7.060	11.992	16.243	18.153	15.050	11.495
3.200	8.550	13.007	17.073	18.073	15.011	11.797
3.300	9.345	14.093	17.066	20.721	16.936	12.535
3.400	9.663	14.073	17.645	20.770	17.455	13.909
3.500	9.322	13.290	17.057	20.370	17.491	14.076
3.600	9.151	13.007	16.296	19.005	17.040	14.771
3.700	9.705	12.926	16.243	19.099	16.825	14.665
3.800	9.570	13.000	16.200	18.496	16.409	14.454
3.900	8.900	12.277	15.761	18.042	16.000	14.977
4.000	8.024	12.310	16.132	17.920	15.925	14.454
4.100	9.033	13.290	16.835	18.420	16.226	14.370
4.200	9.760	13.652	17.535	18.533	16.469	14.623
4.300	9.076	13.093	17.535	18.420	16.707	14.707
4.400	9.450	14.033	17.462	18.302	16.707	14.665
4.500	10.426	14.970	17.602	18.777	16.973	14.301
4.600	11.104	15.721	18.305	19.211	16.973	14.033

VERTICAL ELECTRIC FIELD
STARTING COORDINATES

PROBE #	X	Y	Z
1.00	-14.00	12.00	0.00
2.00	-14.00	8.00	0.00
3.00	-14.00	4.00	0.00
4.00	-14.00	0.00	0.00
5.00	-14.00	-4.00	0.00
6.00	-14.00	-8.00	0.00

Z	P(1)	P(2)	P(3)	P(4)	P(5)	P(6)
0.000	1.577	2.637	3.073	3.477	3.000	3.106
0.100	1.715	3.207	4.531	3.322	3.701	3.600
0.200	2.036	3.960	6.413	4.176	5.966	3.400
0.300	2.186	4.715	8.512	6.378	7.477	4.960
0.400	2.500	6.011	9.759	7.063	8.324	6.692
0.500	2.717	7.230	10.361	7.000	9.001	7.002
0.600	3.305	8.067	10.204	8.610	7.766	7.731
0.700	3.530	8.234	10.077	10.300	10.002	7.597
0.800	4.380	8.776	11.692	12.042	10.763	8.265
0.900	4.705	9.656	12.533	13.475	12.305	9.630
1.000	5.009	10.601	13.139	14.596	12.983	10.700
1.100	6.001	10.550	12.605	15.290	12.305	10.400
1.200	5.552	10.194	12.154	15.943	12.063	10.072
1.300	6.321	9.097	12.647	16.938	12.944	10.576
1.400	6.815	10.145	13.742	18.307	14.004	11.900
1.500	7.773	10.846	14.717	19.361	14.704	11.364
1.600	8.677	11.961	15.352	19.678	14.934	10.700
1.700	9.194	11.384	15.240	19.908	14.538	10.576
1.800	9.100	10.681	15.202	19.773	15.508	11.364
1.900	8.205	10.109	15.501	20.146	16.386	11.538
2.000	8.249	10.640	16.613	20.869	16.750	11.408
2.100	9.022	11.502	17.029	21.598	16.936	11.538
2.200	9.194	12.196	18.132	21.443	16.713	12.016
2.300	8.292	11.666	17.020	20.444	16.638	11.906
2.400	8.162	11.175	16.354	19.960	16.526	11.233
2.500	8.636	11.707	16.903	20.778	17.011	11.475
2.600	8.894	12.562	18.305	21.830	17.596	12.750
2.700	9.022	13.007	19.072	22.359	18.077	13.450
2.800	8.507	13.007	18.342	21.598	17.586	12.965
2.900	8.765	12.769	17.976	20.709	17.059	12.378
3.000	8.593	13.007	17.241	19.773	16.564	12.276
3.100	8.335	12.683	16.903	18.873	16.000	12.103
3.200	8.593	13.209	17.314	19.061	15.962	11.736
3.300	9.363	14.253	18.342	20.221	16.386	11.736
3.400	10.130	15.208	18.962	21.111	17.301	12.664
3.500	10.173	14.851	18.634	21.516	17.675	13.649
3.600	9.960	14.692	18.232	21.350	18.085	14.116
3.700	10.300	14.652	17.792	20.936	18.224	14.205
3.800	11.058	14.413	17.602	20.704	18.042	14.537
3.900	10.637	14.233	17.351	19.923	17.538	14.749
4.000	10.357	13.652	17.093	19.399	17.233	14.707
4.100	10.603	13.491	17.314	17.399	17.122	14.454
4.200	10.469	14.213	17.756	19.136	17.122	14.116
4.300	10.764	14.333	18.049	19.399	17.301	14.378
4.400	10.311	14.973	18.269	19.361	17.602	14.977
4.500	10.469	15.247	18.378	19.736	17.749	14.707
4.600	10.932	15.602	18.634	19.811	17.932	14.623

VERTICAL ELECTRIC FIELD
STARTING COORDINATES

PROBE #	X	Y	Z
1.00	-13.00	12.00	0.00
2.00	-13.00	8.00	0.00
3.00	-13.00	4.00	0.00
4.00	-13.00	0.00	0.00
5.00	-13.00	-4.00	0.00
6.00	-13.00	-8.00	0.00

Z	P(1)	P(2)	P(3)	P(4)	P(5)	P(6)
0.000	1.531	4.662	5.591	6.229	4.593	5.151
0.100	1.852	5.295	7.270	6.733	6.547	5.834
0.200	2.080	5.800	9.207	7.167	8.090	6.015
0.300	2.581	6.684	11.317	8.114	9.725	6.378
0.400	3.124	8.318	12.761	9.761	11.739	7.686
0.500	3.575	9.483	13.854	11.113	13.379	9.361
0.600	4.159	10.475	14.080	12.003	14.045	10.752
0.700	4.383	10.928	14.155	13.163	13.772	10.336
0.800	4.829	[illegible]	14.192	14.325	13.458	10.136
0.900	5.584	11.788	14.866	15.866	14.375	11.014
1.000	6.509	12.926	15.538	17.472	15.773	12.319
1.100	7.860	13.048	15.798	18.571	15.849	12.707
1.200	8.076	12.764	15.240	19.061	15.165	12.232
1.300	8.378	12.399	15.202	19.661	15.279	12.405
1.400	7.903	12.196	15.463	20.593	16.264	13.179
1.500	8.507	12.196	16.169	21.590	17.085	13.435
1.600	9.065	12.440	17.425	22.322	16.862	12.621
1.700	10.088	13.411	18.195	22.468	16.936	12.362
1.800	10.173	13.249	17.976	22.395	17.455	12.965
1.900	9.960	12.277	17.645	22.103	18.152	13.050
2.000	9.322	11.380	17.756	22.759	18.406	12.535
2.100	9.450	12.115	19.181	23.049	18.479	12.707
2.200	9.833	13.370	20.124	23.735	18.914	13.435
2.300	9.705	13.773	19.943	23.447	19.022	13.606
2.400	9.108	13.411	18.671	22.372	18.261	12.836
2.500	9.493	13.169	18.451	22.103	17.932	12.362
2.600	9.748	13.853	19.181	22.795	18.370	12.965
2.700	9.705	14.333	20.232	23.663	19.810	13.946
2.800	9.535	14.692	20.557	23.986	20.520	14.031
2.900	10.045	14.970	20.485	23.807	20.626	14.138
3.000	9.833	14.732	20.088	23.049	19.846	14.243
3.100	9.365	14.053	19.144	21.737	18.914	14.243
3.200	9.578	14.253	18.451	20.518	17.096	13.649
3.300	9.663	14.692	18.997	20.593	17.602	12.836
3.400	10.130	15.524	19.290	21.369	17.602	13.179
3.500	10.553	15.992	19.617	22.140	17.932	13.819
3.600	10.890	15.918	19.472	22.176	18.479	14.370
3.700	11.603	16.192	19.653	22.614	18.877	14.665
3.800	11.728	16.427	19.798	22.504	19.453	15.295
3.900	11.686	15.957	19.435	22.176	19.560	15.837
4.000	11.728	15.287	18.962	21.773	19.309	15.920
4.100	11.811	15.129	18.525	21.037	18.660	15.462
4.200	11.770	15.287	18.561	20.444	18.370	15.043
4.300	11.603	14.930	18.525	19.923	18.370	15.169
4.400	11.[illegible]	15.129	18.378	19.848	18.443	15.336
4.500	11.352	15.642	18.561	20.072	18.677	15.336
4.600	11.519	16.036	18.962	20.370	18.568	15.503

VERTICAL ELECTRIC FIELD
STARTING COORDINATES

PROBE #	X	Y	Z
1.00	-12.00	12.00	0.00
2.00	-12.00	8.00	0.00
3.00	-12.00	4.00	0.00
4.00	-12.00	0.00	0.00
5.00	-12.00	-4.00	0.00
6.00	-12.00	-8.00	0.00

Z	P[1]	P[2]	P[3]	P[4]	P[5]	P[6]
0.000	1.097	8.276	9.092	10.533	7.916	8.188
0.100	2.353	8.943	11.926	11.732	10.798	9.117
0.200	2.717	9.566	14.117	12.158	13.261	9.827
0.300	3.170	9.649	15.202	11.925	14.336	9.361
0.400	3.735	10.558	16.317	12.429	14.973	9.473
0.500	4.651	12.359	17.462	14.016	16.364	10.771
0.600	5.451	13.652	18.195	16.058	18.152	12.750
0.700	5.805	14.053	18.122	17.129	18.370	13.563
0.800	6.245	14.093	17.351	17.548	17.381	12.965
0.900	6.684	14.253	17.314	18.344	17.196	13.050
1.000	7.252	15.010	18.195	20.258	18.406	14.328
1.100	8.507	15.642	18.817	22.213	19.331	15.001
1.200	9.876	15.642	18.889	22.795	18.950	15.001
1.300	10.511	15.642	18.408	22.977	18.334	14.876
1.400	10.003	15.049	18.342	23.302	18.660	15.169
1.500	10.008	14.213	18.159	24.201	19.489	15.545
1.600	10.215	13.853	19.217	24.879	19.703	15.001
1.700	11.100	14.811	20.521	25.622	19.703	14.665
1.800	11.645	15.247	20.918	25.657	20.024	15.043
1.900	11.728	15.049	20.357	25.056	20.449	14.918
2.000	11.016	13.732	19.580	24.451	20.237	14.243
2.100	11.058	13.531	20.052	24.736	20.272	14.031
2.200	10.890	14.213	21.672	25.587	20.802	14.791
2.300	10.595	15.366	22.200	25.868	21.258	15.378
2.400	10.600	15.326	21.349	24.950	20.767	14.791
2.500	10.595	15.247	20.196	24.094	19.453	13.776
2.600	10.637	14.851	20.377	25.007	19.202	13.946
2.700	10.257	14.851	21.098	24.237	20.158	14.412
2.800	10.806	15.760	21.994	25.162	21.328	14.497
2.900	10.890	16.349	22.530	25.692	21.805	14.749
3.000	11.352	16.271	22.316	25.778	22.267	15.670
3.100	11.142	15.996	21.743	25.056	21.701	16.168
3.200	10.732	15.642	20.666	23.627	20.661	15.837
3.300	10.806	16.036	20.465	22.432	19.802	15.043
3.400	11.058	16.427	20.465	22.359	19.166	14.749
3.500	11.016	16.875	20.629	22.650	18.841	15.127
3.600	11.058	17.245	20.593	23.013	18.986	15.211
3.700	12.103	17.631	21.134	23.403	19.433	15.253
3.800	12.683	17.824	21.600	23.843	20.059	15.670
3.900	12.559	17.824	21.277	23.807	20.626	16.292
4.000	12.766	17.554	20.882	23.555	20.626	16.501
4.100	13.219	17.283	20.629	22.759	20.343	16.375
4.200	13.055	16.778	20.232	22.322	20.059	16.292
4.300	12.890	16.466	19.726	21.590	19.739	16.127
4.400	12.476	15.957	19.653	21.105	19.703	16.292
4.500	12.352	16.388	19.617	21.222	19.632	16.292
4.600	12.518	17.089	19.798	21.140	19.596	16.334

VERTICAL ELECTRIC FIELD
STARTING COORDINATES

PROBE #	X	Y	Z
1.00	-11.00	12.00	0.00
2.00	-11.00	8.00	0.00
3.00	-11.00	4.00	0.00
4.00	-11.00	0.00	0.00
5.00	-11.00	-4.00	0.00
6.00	-11.00	-8.00	0.00

Z	P(1)	P(2)	P(3)	P(4)	P(5)	P(6)
0.000	2.262	12.602	14.230	16.097	12.904	12.707
0.100	3.350	13.209	17.241	17.434	16.038	13.073
0.200	4.249	14.053	19.399	17.952	18.950	14.158
0.300	4.740	13.853	20.124	17.205	20.075	14.031
0.400	4.918	13.813	20.449	16.765	19.810	13.007
0.500	5.362	14.811	20.990	16.977	20.130	13.179
0.600	6.509	16.310	21.779	19.099	21.503	14.707
0.700	7.208	17.167	21.958	21.148	22.508	15.920
0.800	7.903	17.322	21.457	21.590	21.712	15.753
0.900	8.076	17.051	20.918	21.810	20.696	15.837
1.000	8.464	17.245	20.882	22.704	21.258	16.375
1.100	9.151	17.322	21.241	24.701	22.370	17.320
1.200	10.553	17.785	21.564	26.114	22.301	17.279
1.300	11.853	18.208	21.672	26.464	21.443	17.115
1.400	12.061	18.016	21.561	26.464	21.153	17.197
1.500	11.853	17.012	20.846	26.674	21.831	17.401
1.600	11.603	16.153	20.774	27.161	22.059	17.320
1.700	11.770	16.036	21.994	27.680	21.746	16.746
1.800	12.311	16.584	22.992	27.853	21.712	16.623
1.900	13.013	16.973	23.170	27.542	22.163	16.375
2.000	13.013	16.310	22.280	27.161	22.301	15.878
2.100	12.518	15.445	21.958	26.707	21.816	15.462
2.200	12.144	15.247	22.743	27.091	22.197	15.961
2.300	11.811	15.957	23.702	27.438	22.807	16.664
2.400	11.728	16.934	23.702	27.438	23.093	16.540
2.500	11.519	16.875	22.814	26.813	22.024	15.837
2.600	11.519	16.584	21.958	26.149	21.293	15.712
2.700	11.477	16.192	21.851	25.410	20.943	15.753
2.800	11.728	16.875	22.280	25.233	21.398	15.253
2.900	11.853	16.662	22.743	25.939	22.197	15.035
3.000	11.728	17.554	23.596	26.918	22.807	15.920
3.100	12.476	17.862	23.844	27.057	23.503	17.197
3.200	12.144	17.438	23.134	26.324	23.196	17.564
3.300	12.144	17.554	22.565	25.021	22.405	17.238
3.400	11.895	17.361	21.958	24.416	21.537	16.910
3.500	11.477	17.515	21.743	23.986	20.696	16.951
3.600	11.911	17.631	21.349	23.914	20.166	16.664
3.700	12.269	18.170	21.743	24.094	19.988	16.127
3.800	12.318	18.323	22.101	24.237	20.130	16.210
3.900	12.972	18.819	22.387	24.451	21.013	16.664
4.000	13.548	18.781	21.994	24.523	21.108	17.158
4.100	13.793	18.629	21.958	24.130	21.108	17.279
4.200	14.283	18.629	21.815	23.986	21.293	17.401
4.300	13.834	18.016	21.600	23.266	21.293	17.361
4.400	13.629	17.785	20.970	22.686	21.048	17.197
4.500	13.752	17.901	20.918	22.249	20.661	17.074
4.600	13.793	17.978	20.702	22.322	20.343	17.033

VERTICAL ELECTRIC FIELD
STARTING COORDINATES

PROBE #	X	Y	Z
1.00	-10.00	12.00	0.00
2.00	-10.00	8.00	0.00
3.00	-10.00	4.00	0.00
4.00	-10.00	0.00	0.00
5.00	-10.00	-4.00	0.00
6.00	-10.00	-8.00	0.00

Z	P(1)	P(2)	P(3)	P(4)	P(5)	P(6)
0.000	2.989	18.205	20.521	23.338	19.775	17.97[illegible]
0.100	4.115	18.093	22.830	23.483	21.735	17.40[illegible]
0.200	5.451	18.438	25.113	23.591	24.809	18.21[illegible]
0.300	6.552	18.933	26.339	23.158	26.397	18.43[illegible]
0.400	7.034	18.705	26.514	22.176	26.233	17.76[illegible]
0.500	7.164	18.743	25.499	21.316	25.430	16.93[illegible]
0.600	7.513	19.123	25.394	22.468	25.665	17.40[illegible]
0.700	8.464	20.067	25.780	24.594	26.632	18.25[illegible]
0.800	9.578	21.260	26.625	25.903	26.366	18.97[illegible]
0.900	10.257	20.963	25.464	26.217	25.330	19.01[illegible]
1.000	10.300	20.404	24.303	26.569	24.960	19.33[illegible]
1.100	10.553	20.142	24.056	27.818	25.464	19.73[illegible]
1.200	11.811	20.104	24.162	29.122	25.397	19.776
1.300	13.013	20.366	24.902	30.006	24.893	19.377
1.400	13.834	21.000	25.253	29.938	24.319	19.612
1.500	14.283	20.516	24.620	29.972	24.691	19.855
1.600	14.038	19.237	23.702	30.006	24.589	19.33[illegible]
1.700	13.424	18.016	23.914	29.972	24.048	18.617
1.800	13.548	18.170	25.078	30.108	24.048	18.234
1.900	14.079	18.771	26.060	30.446	24.426	18.214
2.000	14.687	19.047	25.464	30.006	24.792	17.8[illegible]
2.100	14.038	17.978	24.515	29.326	24.014	17.13[illegible]
2.200	13.424	17.012	24.338	28.951	23.730	17.401
2.300	13.178	17.554	25.218	29.238	24.356	17.930
2.400	13.178	18.629	25.815	29.958	25.330	18.133
2.500	13.342	19.009	25.639	27.767	24.994	17.870
2.600	13.383	18.819	25.043	29.224	24.251	17.930
2.700	12.972	18.285	24.338	28.163	23.435	17.049
2.800	13.137	18.285	23.737	26.918	23.058	17.136
2.900	12.766	18.323	23.985	26.569	22.887	16.127
3.000	13.137	18.705	24.761	27.404	23.571	16.340
3.100	13.178	19.085	25.639	28.575	24.691	18.011
3.200	13.670	19.426	25.604	28.814	25.330	18.018
3.300	13.548	19.540	25.043	28.094	25.027	18.818
3.400	12.972	19.199	24.373	27.265	24.251	18.898
3.500	12.518	19.275	23.418	26.743	23.367	18.938
3.600	12.848	19.123	22.814	25.939	22.474	18.737
3.700	12.931	18.895	22.779	25.445	21.677	18.092
3.800	13.013	19.380	22.850	25.162	21.398	17.646
3.900	13.260	19.728	23.134	25.092	21.607	17.605
4.000	13.793	19.728	23.347	25.622	22.059	18.133
4.100	14.405	20.217	23.702	25.351	22.232	18.214
4.200	14.851	19.879	23.631	24.692	22.646	18.254
4.300	14.851	19.653	23.560	25.198	22.646	18.436
4.400	15.214	19.313	23.063	24.638	22.784	18.335
4.500	15.254	19.502	22.743	24.237	22.197	18.032
4.600	15.093	19.313	22.244	23.843	21.816	17.971

VERTICAL ELECTRIC FIELD
STARTING COORDINATES

PROBE #	X	Y	Z
1.00	-9.00	12.00	0.00
2.00	-9.00	8.00	0.00
3.00	-9.00	4.00	0.00
4.00	-9.00	0.00	0.00
5.00	-9.00	-4.00	0.00
6.00	-9.00	-8.00	0.00

Z	P(1)	P(2)	P(3)	P(4)	P(5)	P(6)
0.000	3.260	23.382	[illegible]	[illegible]	26.798	23.171
0.100	5.318	21.960	[illegible]	28.232	26.964	21.351
0.200	6.640	21.481	28.979	27.196	28.745	20.567
0.300	7.686	22.186	30.907	27.473	31.034	21.312
0.400	8.722	22.510	31.768	27.404	[illegible]	21.565
0.500	8.851	22.070	30.600	26.289	31.132	20.999
0.600	8.980	21.703	28.806	25.692	29.761	20.291
0.700	9.791	22.363	28.495	27.230	29.957	20.606
0.800	10.974	23.310	29.256	29.224	30.088	21.234
0.900	11.519	23.527	28.841	27.836	29.335	21.383
1.000	11.911	23.128	27.767	29.559	27.999	21.468
1.100	12.269	22.619	26.444	30.209	27.791	21.390
1.200	12.766	21.960	26.304	31.357	27.824	21.585
1.300	13.466	21.740	26.967	32.197	27.527	21.624
1.400	14.120	22.217	27.469	32.365	26.798	21.624
1.500	15.214	22.363	27.176	32.566	26.898	21.507
1.600	15.697	21.960	26.304	32.466	26.698	20.920
1.700	15.174	20.254	25.639	31.996	25.979	20.033
1.800	14.364	19.199	26.304	31.794	25.464	19.577
1.900	14.729	19.615	27.176	32.097	26.133	19.657
2.000	15.254	19.992	27.697	31.996	26.499	19.330
2.100	15.335	19.691	26.504	31.256	25.365	18.415
2.200	14.667	18.705	25.850	30.142	24.825	18.011
2.300	14.364	18.476	26.060	30.006	25.128	18.294
2.400	14.120	19.161	26.549	30.717	25.966	18.697
2.500	13.793	19.728	26.730	31.155	26.333	18.770
2.600	13.957	20.292	26.063	31.256	26.033	19.250
2.700	13.711	19.916	26.549	30.460	25.498	19.416
2.800	13.793	19.691	25.990	29.361	24.960	18.737
2.900	13.500	19.577	25.394	28.120	23.700	17.524
3.000	13.301	19.237	24.972	27.853	23.044	[illegible]
3.100	13.711	19.766	25.639	28.506	24.623	18.032
3.200	14.120	20.179	26.304	29.224	25.665	18.978
3.300	14.283	20.404	26.269	29.224	25.799	19.218
3.400	13.916	20.628	25.850	28.643	25.631	19.577
3.500	13.793	20.591	25.253	28.403	25.330	20.133
3.600	13.875	20.479	24.550	27.887	24.522	20.251
3.700	13.997	19.992	23.879	26.987	23.605	20.014
3.800	13.588	19.916	23.808	26.044	22.646	19.338
3.900	13.834	20.067	23.667	26.044	22.789	18.778
4.000	13.997	20.217	24.891	26.149	22.853	18.818
4.100	14.445	20.292	24.020	26.079	22.794	18.536
4.200	15.012	20.665	24.197	25.868	22.818	18.577
4.300	15.496	20.665	24.444	25.798	23.230	18.697
4.400	15.697	20.254	24.091	25.481	23.469	18.858
4.500	15.737	20.441	23.750	25.373	23.161	18.617
4.600	15.857	20.553	23.347	24.843	22.887	18.697

VERTICAL ELECTRIC FIELD
STARTING COORDINATES

PROBE #	X	Y	Z
1.00	-8.00	12.00	0.00
2.00	-8.00	8.00	0.00
3.00	-8.00	4.00	0.00
4.00	-8.00	0.00	0.00
5.00	-8.00	-4.00	0.00
6.00	-8.00	-8.00	0.00

Z	P(1)	P(2)	P(3)	P(4)	P(5)	P(6)
0.000	3.440	28.719	33.243	36.267	33.962	29.171
0.100	5.937	25.423	32.111	32.734	32.401	25.600
0.200	7.426	24.211	32.523	30.311	32.596	23.248
0.300	8.937	24.926	34.649	30.784	35.135	23.325
0.400	10.003	25.848	36.814	31.962	37.586	24.548
0.500	10.680	25.919	35.919	31.034	37.062	24.463
0.600	10.511	25.352	33.243	29.836	34.776	23.402
0.700	10.774	25.530	32.351	30.379	33.962	23.210
0.800	11.936	26.060	32.694	32.432	34.418	23.062
0.900	12.040	26.096	32.592	33.606	33.735	24.282
1.000	13.916	25.990	31.493	33.505	32.043	23.976
1.100	14.526	26.060	30.187	33.304	31.164	23.709
1.200	15.053	25.104	29.497	34.143	30.936	23.709
1.300	14.405	23.779	29.186	34.546	30.153	23.747
1.400	14.931	23.273	29.270	34.579	29.335	23.477
1.500	16.177	24.318	29.635	35.016	29.106	23.240
1.600	17.447	24.426	29.566	35.387	29.303	22.594
1.700	17.051	22.765	28.495	34.747	28.417	22.013
1.800	16.057	21.037	28.114	33.908	27.791	21.505
1.900	15.857	20.814	28.910	33.975	28.551	21.507
2.000	16.575	21.555	29.635	34.445	28.778	21.234
2.100	16.416	21.703	29.463	33.740	28.232	20.330
2.200	15.937	20.014	28.460	32.701	26.898	19.657
2.300	15.616	20.404	28.114	32.097	26.732	19.657
2.400	15.214	20.479	27.906	32.063	27.196	19.935
2.500	14.972	20.665	27.975	32.097	27.262	19.855
2.600	14.405	21.111	28.114	32.600	27.229	20.014
2.700	14.567	21.334	28.399	32.801	27.360	20.327
2.800	15.295	21.[illegible]	28.703	32.029	27.659	20.567
2.900	14.010	20.000	27.419	30.649	26.665	19.657
3.000	14.364	20.329	26.409	29.395	25.430	18.098
3.100	14.364	20.479	26.584	27.190	25.430	18.938
3.200	14.010	20.963	26.967	29.599	26.033	19.378
3.300	15.053	21.555	27.419	29.735	26.399	19.458
3.400	14.689	21.740	27.315	29.936	26.665	19.774
3.500	15.295	21.850	27.246	30.207	26.964	20.001
3.600	15.214	21.924	26.723	30.289	26.698	21.780
3.700	15.093	21.813	25.920	29.361	25.966	21.741
3.800	14.091	21.260	25.289	28.403	24.960	21.273
3.900	14.445	20.926	25.183	27.818	24.589	20.645
4.000	14.567	20.740	25.007	27.891	24.082	20.291
4.100	14.972	21.000	24.726	26.813	23.708	19.657
4.200	15.496	20.851	24.761	26.639	23.401	19.378
4.300	15.576	20.963	25.113	26.359	23.708	19.377
4.400	15.777	21.260	25.148	26.359	24.251	19.617
4.500	16.137	21.518	25.007	26.184	24.149	19.577
4.600	16.217	21.444	24.972	25.149	24.149	19.617

VERTICAL ELECTRIC FIELD
STARTING COORDINATES

PROBE #	X	Y	Z
1.00	-7.00	12.00	0.00
2.00	-7.00	8.00	0.00
3.00	-7.00	4.00	0.50
4.00	-7.00	0.00	0.00
5.00	-7.00	-4.00	0.00
6.00	-7.00	-8.00	0.00

Z	P(1)	P(2)	P(3)	P(4)	P(5)	P(6)
0.000	4.115	32.326	37.918	41.513	39.220	33.777
0.100	6.640	28.708	36.332	37.154	37.291	29.971
0.200	8.162	27.185	36.366	33.807	36.734	26.407
0.300	9.876	27.255	37.953	33.706	38.903	25.726
0.400	10.890	28.093	40.214	35.050	41.964	26.861
0.500	11.561	28.093	39.515	34.310	41.495	27.098
0.600	12.186	28.093	37.193	33.036	38.936	26.067
0.700	12.559	28.232	36.057	33.539	38.013	25.002
0.800	12.807	28.232	35.005	35.252	38.112	26.045
0.900	13.752	27.900	35.164	36.505	37.455	26.710
1.000	15.053	28.050	34.580	36.301	35.754	26.331
1.100	16.774	28.708	33.757	36.471	34.501	25.953
1.200	17.091	28.050	32.763	36.914	33.930	26.264
1.300	16.137	26.060	31.207	36.710	32.726	26.029
1.400	15.616	24.712	30.737	36.437	31.132	25.195
1.500	17.368	25.300	31.493	36.903	30.071	24.071
1.600	18.054	26.166	31.071	37.600	31.340	24.518
1.700	18.623	24.997	31.001	37.291	30.773	23.747
1.800	17.762	23.237	30.221	35.826	29.663	23.133
1.900	17.604	22.656	30.462	35.691	29.990	22.709
2.000	17.919	23.120	31.562	36.301	30.050	22.632
2.100	17.525	23.201	31.734	36.165	30.610	22.204
2.200	17.249	22.619	31.115	35.353	29.597	21.702
2.300	17.012	22.437	30.324	34.546	29.073	21.624
2.400	16.774	22.510	29.704	33.773	29.040	21.624
2.500	16.177	21.007	29.152	33.271	28.515	20.960
2.600	15.375	21.813	29.014	33.539	28.252	20.942
2.700	15.057	22.290	30.152	34.143	28.044	21.741
2.800	16.097	23.092	30.565	34.210	29.794	22.324
2.900	15.977	22.838	29.077	33.067	29.139	21.038
3.000	15.697	22.180	28.495	31.626	27.758	20.960
3.100	15.415	21.740	27.871	30.750	27.030	20.330
3.200	15.097	21.850	27.940	30.345	26.732	20.340
3.300	15.977	22.070	28.103	30.142	26.765	20.271
3.400	15.375	22.437	28.287	30.277	26.977	20.449
3.500	15.496	22.838	28.356	30.953	27.639	21.390
3.600	15.737	23.454	28.044	31.290	27.692	22.400
3.700	16.376	23.237	27.305	30.052	27.361	22.671
3.800	15.817	22.619	26.793	30.074	26.790	22.632
3.900	15.576	21.924	26.479	27.393	26.366	22.207
4.000	15.576	21.703	26.025	28.609	25.066	21.017
4.100	15.777	21.850	25.744	27.991	24.960	20.999
4.200	15.857	21.813	25.394	27.438	24.420	20.003
4.300	15.937	21.555	25.639	27.369	24.657	20.665
4.400	16.257	21.007	25.955	27.369	24.954	20.645
4.500	16.336	22.107	25.709	26.987	25.027	20.327
4.600	16.695	21.960	25.015	26.813	24.724	20.330

VERTICAL ELECTRIC FIELD
STARTING COORDINATES

PROBE #	X	Y	Z
1.00	-6.00	12.00	0.00
2.00	-6.00	8.00	0.00
3.00	-6.00	4.00	0.00
4.00	-6.00	0.00	0.00
5.00	-6.00	-4.00	0.00
6.00	-6.00	-8.00	0.00

Z	P(1)	P(2)	P(3)	P(4)	P(5)	P(6)
0.000	4.294	34.675	40.424	44.914	41.428	35.639
0.100	6.015	31.943	40.177	41.476	41.327	33.150
0.200	8.722	30.141	40.494	38.258	41.495	30.009
0.300	10.342	29.890	41.728	36.812	43.313	28.563
0.400	11.811	29.864	42.830	36.948	45.257	27.095
0.500	12.393	29.725	42.366	36.673	44.640	28.981
0.600	13.178	30.141	40.424	35.725	42.334	28.298
0.700	14.079	30.626	39.341	36.369	41.394	28.033
0.800	13.957	30.453	38.507	37.325	41.327	28.412
0.900	14.242	29.413	37.090	37.876	40.028	28.563
1.000	15.656	29.482	36.229	38.154	38.112	28.033
1.100	17.604	30.591	36.435	39.027	37.226	27.757
1.200	18.662	30.591	35.679	39.735	36.767	28.260
1.300	17.525	28.267	33.757	38.921	35.135	27.806
1.400	16.972	26.518	32.523	38.154	33.084	26.899
1.500	17.801	26.834	32.797	38.571	32.564	26.256
1.600	19.824	27.430	33.860	39.735	33.084	26.218
1.700	19.631	26.799	33.175	39.309	32.564	25.460
1.800	19.128	24.997	32.249	37.807	31.099	24.202
1.900	18.895	24.246	32.146	37.051	30.969	23.440
2.000	18.895	24.354	32.832	37.704	31.946	23.440
2.100	18.350	24.354	33.072	37.980	32.369	23.479
2.200	17.919	23.851	32.866	37.394	31.555	23.402
2.300	18.193	23.887	32.454	36.675	31.034	23.171
2.400	17.958	24.175	31.940	36.064	30.936	23.056
2.500	17.525	23.779	30.737	34.915	29.790	22.204
2.600	16.416	23.201	30.255	34.613	29.237	21.858
2.700	16.536	23.237	30.978	34.949	29.728	22.362
2.800	16.933	23.995	31.734	35.353	30.806	23.248
2.900	17.051	24.211	31.528	35.016	30.736	23.075
3.000	16.496	23.815	30.462	33.773	30.120	22.516
3.100	16.257	23.454	29.842	33.036	29.237	22.168
3.200	16.456	23.237	29.532	32.197	28.417	21.935
3.300	16.297	22.983	28.806	31.155	27.738	21.507
3.400	15.977	23.056	28.495	30.818	27.427	21.116
3.500	15.857	23.671	28.564	31.189	27.659	21.385
3.600	16.297	24.246	28.875	31.626	27.824	22.478
3.700	16.814	23.815	28.322	31.626	27.725	23.036
3.800	16.695	23.454	28.114	31.424	27.659	23.171
3.900	16.734	23.092	27.906	30.704	27.923	23.402
4.000	15.575	23.092	27.489	30.142	27.659	23.133
4.100	16.536	22.728	26.897	29.427	26.665	22.394
4.200	16.336	22.327	26.409	28.506	25.765	22.091
4.300	16.297	22.034	26.479	28.163	25.631	21.780
4.400	16.416	22.400	26.374	27.922	25.765	21.429
4.500	16.774	22.473	26.164	27.507	25.464	20.801
4.600	16.376	22.254	25.885	27.230	25.196	20.001

VERTICAL ELECTRIC FIELD
STARTING COORDINATES

PROBE #	X	Y	Z
1.00	-5.00	12.00	0.00
2.00	-5.00	8.00	0.00
3.00	-5.00	4.00	0.00
4.00	-5.00	0.00	0.00
5.00	-5.00	-4.00	0.00
6.00	-5.00	-8.00	0.00

Z	P(1)	P(2)	P(3)	P(4)	P(5)	P(6)
0.000	5.007	33.423	41.586	46.077	42.704	36.567
0.100	7.816	33.478	42.580	44.431	43.618	34.730
0.200	9.960	32.535	44.052	41.476	44.606	32.251
0.300	11.142	31.909	44.487	39.415	46.134	30.469
0.400	12.311	30.972	44.961	38.397	47.510	30.085
0.500	13.055	30.626	44.016	38.154	46.812	29.894
0.600	13.875	31.596	43.045	37.842	45.257	29.627
0.700	15.133	32.535	41.976	38.467	44.162	29.665
0.800	15.375	32.326	40.705	39.062	43.618	29.971
0.900	15.012	31.111	38.750	38.921	41.763	29.730
1.000	15.017	30.383	37.780	39.203	39.597	29.133
1.100	17.997	31.319	37.849	40.308	39.002	29.247
1.200	19.477	32.117	37.573	41.513	38.573	29.569
1.300	19.051	30.349	36.194	41.071	37.062	29.133
1.400	18.428	28.336	34.512	39.735	34.744	28.109
1.500	18.934	28.197	34.237	39.806	34.255	27.379
1.600	19.978	28.441	35.198	40.852	34.581	27.390
1.700	20.362	28.058	35.061	40.961	34.190	26.747
1.800	20.171	26.659	34.169	39.344	32.792	25.309
1.900	20.055	25.671	33.517	33.571	32.108	24.244
2.000	19.940	25.281	33.792	38.327	32.857	24.205
2.100	19.051	24.783	33.699	38.606	33.214	24.014
2.200	18.584	24.390	33.552	38.258	32.661	23.976
2.300	18.584	24.854	33.060	38.084	32.434	23.938
2.400	18.856	25.565	33.963	38.015	32.596	24.129
2.500	18.467	25.139	32.454	36.880	31.685	23.364
2.600	17.368	24.175	31.390	[illegible]	30.349	22.748
2.700	17.210	23.779	31.425	35.286	29.924	22.864
2.800	17.486	24.676	32.317	35.522	30.936	23.210
2.900	17.209	24.569	32.351	35.488	31.490	23.440
3.000	16.933	24.569	32.043	35.185	31.457	23.287
3.100	17.170	24.318	31.390	34.613	31.132	23.440
3.200	17.131	24.211	31.047	33.740	30.480	23.402
3.300	17.051	23.923	30.049	32.497	29.204	22.671
3.400	16.057	23.599	28.875	31.189	28.022	22.052
3.500	16.057	23.959	[illegible]	31.290	27.090	21.974
3.600	16.615	24.246	[illegible]	31.525	27.692	22.246
3.700	17.012	24.461	28.910	31.794	27.626	22.748
3.800	16.655	24.103	28.530	31.640	27.857	23.287
3.900	17.407	24.246	28.841	31.525	28.351	23.632
4.000	17.525	23.923	28.703	31.256	28.449	23.765
4.100	17.210	23.527	27.767	30.412	27.923	23.517
4.200	16.695	22.656	27.072	29.701	27.063	23.018
4.300	16.779	22.363	26.828	28.985	26.499	22.555
4.400	16.814	22.583	26.723	28.369	26.333	22.013
4.500	16.774	22.583	26.549	27.646	25.966	21.439
4.500	16.416	22.290	26.199	27.126	25.397	21.234

VERTICAL ELECTRIC FIELD
STARTING COORDINATES

PROBE #	X	Y	Z
1.00	-4.00	12.00	0.00
2.00	-4.00	8.00	0.00
3.00	-4.00	4.00	0.00
4.00	-4.00	0.00	0.00
5.00	-4.00	-4.00	0.00
6.00	-4.00	-8.00	0.00

Z	P(1)	P(2)	P(3)	P(4)	P(5)	P(6)
0.000	5.362	37.308	43.116	49.246	45.120	38.671
0.100	8.550	34.817	44.415	47.006	45.670	36.227
0.200	10.090	33.583	45.511	43.524	46.327	33.437
0.300	12.393	32.083	46.206	40.998	47.440	31.355
0.400	12.931	32.291	46.845	40.164	49.022	30.545
0.500	12.931	31.666	46.138	39.806	48.907	30.507
0.600	14.201	32.256	44.997	39.309	47.825	30.430
.700	15.737	33.723	44.016	39.664	46.396	30.507
0.800	16.177	33.758	42.616	40.128	45.154	30.814
0.900	15.697	32.674	40.670	40.092	43.414	30.661
1.000	16.137	31.562	38.993	40.236	41.160	30.047
1.100	18.036	31.943	38.646	40.925	39.795	29.933
1.200	20.055	32.639	38.646	42.297	39.928	30.354
1.300	20.669	32.152	38.091	42.524	38.738	30.162
1.400	19.824	30.349	36.435	41.550	36.702	29.133
1.500	19.940	29.448	35.649	41.255	35.819	28.583
1.600	20.703	28.893	35.919	41.997	36.015	28.408
1.700	21.012	28.719	35.908	42.260	35.917	27.920
1.800	21.241	27.709	36.126	41.402	34.841	26.672
1.900	20.974	27.220	35.576	40.561	34.320	25.839
2.000	21.203	26.659	35.061	39.771	34.418	25.423
2.100	20.324	25.840	34.512	37.274	34.073	24.853
2.200	17.120	25.032	34.135	38.711	33.507	24.434
2.300	19.266	25.459	34.603	38.816	33.409	24.472
2.400	19.438	26.377	34.992	38.992	33.097	24.815
2.500	18.662	26.060	34.340	38.327	33.344	24.739
2.600	18.115	25.352	32.777	36.948	31.816	23.900
2.700	17.644	24.676	32.043	35.920	30.643	23.287
2.800	17.762	24.604	32.100	35.793	30.806	23.287
2.900	17.644	24.703	32.592	35.725	31.653	23.133
3.000	17.447	25.104	32.832	35.970	31.978	23.517
3.100	17.722	25.175	32.866	35.962	32.401	23.976
3.200	17.079	25.104	32.386	35.353	32.043	24.202
3.300	17.325	24.712	31.104	33.900	30.858	23.900
3.400	16.933	24.103	30.324	32.633	29.597	23.133
3.500	16.655	24.319	27.601	32.161	28.770	22.941
3.600	16.893	24.961	29.470	32.130	28.186	22.707
3.700	17.170	24.604	29.221	31.693	27.824	22.702
3.800	16.972	24.747	29.117	31.559	27.758	23.095
3.900	17.603	24.533	29.117	31.626	26.153	23.287
4.000	18.350	24.961	29.236	31.794	28.548	23.747
4.100	17.079	24.202	28.633	31.034	28.515	23.900
4.200	17.603	23.671	28.079	30.345	28.007	23.670
4.300	17.406	22.910	27.732	27.036	27.659	23.171
4.400	17.447	23.052	27.246	29.224	27.361	22.864
4.500	17.249	23.019	26.828	28.236	26.665	22.160
4.600	16.814	22.765	26.584	27.803	26.133	22.052

VERTICAL ELECTRIC FIELD
STARTING COORDINATES

PROBE #	X	Y	Z
1.00	-3.00	12.00	0.00
2.00	-3.00	8.00	0.00
3.00	-3.00	4.00	0.00
4.00	-3.00	0.00	0.00
5.00	-3.00	-4.00	0.00
6.00	-3.00	-8.00	0.00

Z	P(1)	P(2)	P(3)	P(4)	P(5)	P(6)
0.000	5.981	38.840	45.805	50.633	47.790	40.009
0.100	8.008	35.495	45.504	49.107	47.405	37.342
0.200	11.142	33.373	45.953	44.995	47.265	34.039
0.300	12.807	32.003	47.219	42.222	48.201	32.016
0.400	13.219	33.163	48.354	41.439	50.196	31.433
0.500	13.466	32.569	47.974	40.993	50.492	31.433
0.600	14.120	32.674	45.877	39.985	48.563	31.200
0.700	15.456	33.548	44.415	39.878	46.847	30.930
0.800	16.734	34.463	43.800	40.670	45.808	31.239
0.900	16.814	34.181	42.759	41.661	44.538	31.549
1.000	16.575	32.639	40.459	41.210	42.300	30.930
1.100	18.076	32.500	38.993	41.439	40.660	30.776
1.200	19.824	33.163	39.063	42.260	40.227	31.007
1.300	21.008	32.908	39.271	43.446	39.633	30.892
1.400	20.860	31.492	38.126	43.213	37.940	30.239
1.500	20.703	30.141	36.435	42.260	36.757	29.399
1.600	20.898	29.586	35.954	42.406	36.440	29.093
1.700	21.335	29.066	36.332	42.714	36.440	28.525
1.800	21.507	28.371	36.779	42.448	36.001	27.730
1.900	21.545	28.232	37.159	41.805	35.609	27.012
2.000	21.658	27.849	36.366	41.181	35.656	26.634
2.100	20.974	26.403	35.438	40.236	35.102	25.412
2.200	19.901	25.884	34.683	39.557	34.060	24.853
2.300	19.554	25.813	35.267	39.415	34.190	25.271
2.400	19.709	26.589	35.747	39.735	34.744	25.915
2.500	19.012	26.510	35.061	39.593	34.646	25.764
2.600	18.623	25.954	34.032	39.397	33.117	25.119
2.700	18.545	25.742	33.175	37.257	31.978	24.320
2.800	18.350	25.175	32.969	36.301	31.653	24.053
2.900	18.115	25.104	32.694	35.894	31.598	23.517
3.000	17.762	25.494	32.969	35.691	31.816	23.555
3.100	18.115	25.671	33.106	35.826	32.304	24.053
3.200	18.504	25.990	33.243	35.962	32.336	[illegible]
3.300	18.154	25.308	32.454	35.084	31.913	[illegible]
3.400	17.328	25.068	31.322	33.807	31.067	24.396
3.500	17.328	25.281	30.531	33.203	30.302	24.232
3.600	17.328	25.308	29.911	32.969	29.335	24.129
3.700	16.814	24.783	29.152	32.063	29.120	23.335
3.800	17.012	24.497	28.841	31.660	27.527	23.018
3.900	17.368	24.961	29.146	31.593	27.494	22.864
4.000	18.271	24.997	29.447	31.593	28.120	23.325
4.100	18.467	24.854	29.186	31.222	28.235	23.555
4.200	18.115	24.390	28.564	31.054	28.351	23.900
4.300	18.232	24.031	28.668	30.615	28.219	23.362
4.400	18.076	24.031	28.148	29.904	28.120	23.594
4.500	17.762	23.671	27.767	29.156	27.626	23.210
4.600	17.091	23.273	26.932	28.472	27.030	22.594

VERTICAL ELECTRIC FIELD
STARTING COORDINATES

PROBE #	X	Y	Z
1.00	-2.00	12.00	0.00
2.00	-2.00	8.00	0.00
3.00	-2.00	4.00	0.00
4.00	-2.00	0.00	0.00
5.00	-2.00	-4.00	0.00
6.00	-2.00	-8.00	0.00

Z	P(1)	P(2)	P(3)	P(4)	P(5)	P(6)
0.000	6.025	40.227	48.392	52.243	49.377	41.155
0.100	9.194	36.395	47.445	51.763	48.916	37.756
0.200	11.436	33.969	47.032	46.077	48.669	34.771
0.300	13.137	33.583	49.813	44.252	49.803	32.831
0.400	14.120	34.428	50.800	42.524	50.832	32.526
0.500	14.038	34.004	50.053	42.222	52.032	32.447
0.600	13.875	33.023	46.695	40.092	49.164	31.794
0.700	15.012	33.373	44.633	39.628	46.917	31.007
0.800	16.774	34.724	44.560	41.218	46.327	31.471
0.900	17.565	35.200	44.324	42.753	45.800	31.977
1.000	17.249	33.793	42.082	42.448	43.618	31.821
1.100	17.919	32.744	39.515	41.847	41.420	31.433
1.200	19.477	32.900	39.202	42.411	40.760	31.374
1.300	21.127	33.470	39.725	43.994	40.560	31.355
1.400	21.582	32.535	39.585	44.391	39.490	30.814
1.500	21.961	31.353	37.804	43.407	38.013	30.200
1.600	21.885	30.522	36.745	42.905	37.455	29.551
1.700	21.696	29.240	36.642	43.059	37.173	28.905
1.800	21.696	28.500	37.366	43.175	36.832	28.260
1.900	21.810	28.649	37.918	42.791	36.090	27.730
2.000	22.225	28.545	37.676	42.440	36.032	27.163
2.100	21.620	27.465	36.573	41.439	36.407	26.369
2.200	20.783	26.799	35.782	40.380	35.330	25.574
2.300	20.209	26.518	35.816	39.949	34.809	25.688
2.400	19.709	26.834	36.194	40.200	35.461	26.256
2.500	19.593	27.080	36.091	40.200	35.558	26.369
2.600	19.245	27.010	35.404	39.842	34.613	25.953
2.700	19.747	27.115	34.958	39.097	34.028	25.630
2.800	19.477	26.518	34.169	37.807	33.279	25.195
2.900	18.309	25.636	33.449	36.437	32.739	24.510
3.000	17.840	25.459	32.969	35.894	32.141	23.594
3.100	18.350	25.990	33.552	35.962	32.271	23.670
3.200	18.545	26.413	33.723	35.996	32.629	24.434
3.300	18.309	26.272	33.620	35.928	32.824	24.967
3.400	17.879	26.201	32.866	35.307	32.499	25.157
3.500	18.154	26.377	31.940	34.781	31.913	25.195
3.600	18.115	25.884	31.012	33.975	30.871	25.309
3.700	17.249	25.459	30.083	33.170	29.630	24.548
3.800	16.933	24.819	29.186	32.130	28.219	23.709
3.900	17.801	24.819	29.325	31.929	27.870	23.310
4.000	18.193	24.961	29.394	31.660	28.022	23.440
4.100	18.310	25.068	29.635	31.391	28.285	23.632
4.200	18.428	24.676	29.325	31.270	28.252	23.747
4.300	18.779	24.854	29.497	31.133	28.745	23.785
4.400	18.895	24.640	29.359	30.750	28.778	23.785
4.500	18.623	24.282	28.737	30.040	28.219	23.555
4.600	17.879	23.707	27.767	29.292	27.626	23.095

VERTICAL ELECTRIC FIELD
STARTING COORDINATES

PROBE	X	Y	Z
1.00	-1.00	13.00	0.00
2.00	1.00	9.00	0.00
3.00	-1.00	4.00	0.00
4.00	1.00	0.00	0.00
5.00	-1.00	-4.00	0.00
6.00	1.00	-9.00	0.00

Z	P(1)	P(2)	P(3)	P(4)	P(5)	P(6)
0.000	6.157	40.818	48.464	50.006	48.704	40.475
0.100	9.194	37.302	48.169	51.964	48.775	37.531
0.200	11.561	34.428	47.747	47.049	48.634	34.089
0.300	13.137	33.064	49.083	43.915	49.641	33.039
0.400	14.120	34.746	51.317	42.714	51.453	32.644
0.500	14.160	34.428	50.445	41.328	51.417	32.447
0.600	13.875	33.443	46.957	39.344	48.739	31.588
0.700	14.607	33.470	44.378	38.501	46.050	30.833
0.800	16.456	34.959	44.016	40.071	45.154	31.162
0.900	17.565	35.530	44.009	41.307	44.811	31.860
1.000	17.722	34.675	42.118	41.085	43.211	32.212
1.100	17.919	32.953	39.271	40.777	40.726	31.388
1.200	19.203	32.744	38.334	41.402	39.696	31.200
1.300	21.165	33.443	39.028	42.902	39.464	31.007
1.400	21.696	32.744	39.097	43.719	39.068	30.892
1.500	22.225	31.631	37.642	43.059	37.915	30.430
1.600	22.112	30.556	36.160	42.406	37.062	29.509
1.700	21.923	29.621	36.263	42.333	36.767	28.715
1.800	21.582	28.476	36.676	42.109	36.407	28.033
1.900	21.545	27.849	36.083	41.922	36.031	27.428
2.000	21.999	27.988	36.607	41.476	36.211	26.861
2.100	21.847	27.709	36.435	40.998	35.835	26.256
2.200	21.203	26.799	35.541	40.200	34.939	25.650
2.300	19.863	25.998	34.992	39.309	34.060	25.460
2.400	19.477	25.884	34.649	39.062	34.060	25.233
2.500	19.400	26.589	35.095	39.133	34.288	25.498
2.600	19.400	27.220	35.301	39.309	34.385	25.512
2.700	19.245	26.589	34.615	38.536	33.757	25.460
2.800	18.818	26.166	33.997	37.600	33.344	25.195
2.900	18.428	25.423	33.175	36.403	32.401	24.232
3.000	18.154	25.210	32.489	35.084	31.685	23.325
3.100	17.958	25.317	32.454	34.680	31.197	22.364
3.200	17.879	25.423	32.587	34.882	31.555	23.402
3.300	18.036	25.990	32.557	35.217	32.043	24.396
3.400	17.958	25.778	32.420	35.050	32.271	24.815
3.500	17.683	25.813	31.425	34.344	31.457	24.915
3.600	17.368	25.530	30.703	33.841	30.512	24.015
3.700	16.734	25.210	29.532	32.835	29.454	24.701
3.800	17.249	24.533	28.979	32.063	28.515	23.862
3.900	17.368	24.640	28.530	31.256	27.692	23.402
4.000	17.801	24.497	28.564	31.088	27.427	23.210
4.100	17.722	24.175	28.945	30.603	27.560	23.287
4.200	17.919	24.318	28.875	30.412	27.626	22.907
4.300	18.193	24.246	28.806	29.972	27.593	22.594
4.400	18.584	24.282	28.495	29.836	27.560	22.825
4.500	18.115	24.103	28.142	29.463	27.824	23.133
4.600	17.801	23.599	27.419	28.746	27.328	22.748

VERTICAL ELECTRIC FIELD
STARTING COORDINATES

PROBE	X	Y	Z
1.00	0.00	12.00	0.00
2.00	0.00	8.00	0.00
3.00	0.00	4.00	0.00
4.00	0.00	0.00	0.00
5.00	0.00	-4.00	0.00
6.00	0.00	-8.00	0.00

Z	P(1)	P(2)	P(3)	P(4)	P(5)	P(6)
0.000	6.421	41.337	48.392	54.505	49.022	40.057
0.100	9.194	37.456	47.671	51.016	47.730	36.733
0.200	11.260	34.286	47.407	46.364	47.440	33.878
0.300	13.219	33.829	49.044	43.129	48.246	32.172
0.400	14.203	34.392	50.840	41.972	49.982	31.782
0.500	14.445	34.569	50.210	40.015	50.124	31.635
0.600	13.540	33.513	46.770	39.415	48.211	31.239
0.700	14.292	33.373	44.270	38.746	45.843	30.776
0.800	16.057	34.463	43.836	39.557	45.017	31.046
0.900	17.565	35.244	43.475	41.034	44.060	31.355
1.000	18.154	34.782	41.976	41.328	42.334	31.549
1.100	18.467	33.583	39.446	40.779	40.560	31.278
1.200	18.973	32.674	37.804	40.925	39.464	30.814
1.300	20.171	32.535	38.057	42.034	39.137	30.507
1.400	21.317	32.221	38.057	42.600	38.375	30.239
1.500	21.810	31.562	37.366	42.486	37.400	29.771
1.600	22.376	31.007	36.573	42.104	37.226	29.399
1.700	22.489	29.725	36.022	42.184	36.702	28.771
1.800	21.582	28.476	35.954	41.513	36.001	27.655
1.900	21.050	27.535	35.816	41.144	35.558	26.937
2.000	21.355	27.639	36.091	40.925	35.754	26.710
2.100	21.507	27.674	36.160	40.706	35.930	26.445
2.200	20.822	26.985	35.438	40.092	35.200	25.915
2.300	20.017	26.035	34.443	38.711	33.865	25.157
2.400	19.245	25.494	33.826	37.946	33.214	24.701
2.500	18.818	25.919	33.997	38.050	33.540	24.739
2.600	18.740	26.272	34.203	38.432	33.670	25.043
2.700	18.973	26.201	34.615	38.397	33.757	25.157
2.800	18.856	25.990	34.066	37.600	33.442	25.081
2.900	18.232	25.671	33.277	36.403	32.739	24.472
3.000	17.919	24.854	32.180	35.016	31.523	23.248
3.100	17.683	24.533	31.699	34.243	30.806	22.594
3.200	17.840	24.961	31.734	34.109	30.643	22.709
3.300	17.447	25.139	31.699	34.210	31.079	23.325
3.400	17.525	25.530	31.802	34.109	31.327	23.862
3.500	17.525	25.848	31.322	34.243	30.871	24.282
3.600	17.644	25.742	30.875	33.841	30.577	24.663
3.700	17.209	25.494	30.359	33.505	30.000	25.043
3.800	17.407	24.926	29.463	32.399	29.106	24.548
3.900	17.328	24.747	28.633	31.492	28.022	23.670
4.000	17.289	24.067	28.426	30.986	27.494	23.248
4.100	17.249	23.923	28.252	30.345	27.133	22.902
4.200	17.525	23.635	28.114	29.938	26.798	22.168
4.300	17.997	23.707	28.218	29.429	26.655	21.780
4.400	18.310	23.887	27.906	29.292	27.063	22.091
4.500	17.879	23.959	27.371	27.054	27.196	22.400
4.600	17.644	23.743	27.697	28.843	27.063	22.246

VERTICAL ELECTRIC FIELD
STARTING COORDINATES

PROBE #	X	Y	Z
1.00	1.00	12.00	0.00
2.00	1.00	8.00	0.00
3.00	1.00	4.00	0.00
4.00	1.00	0.00	0.00
5.00	1.00	-4.00	0.00
6.00	1.00	-8.00	0.00

Z	P[1]	P[2]	P[3]	P[4]	P[5]	P[6]
0.000	5.716	40.462	47.107	52.478	47.615	40.216
0.100	8.722	36.649	46.175	48.694	45.843	35.890
0.200	10.511	33.899	46.733	44.955	45.326	32.565
0.300	12.766	33.198	48.126	41.997	46.431	31.162
0.400	14.160	33.513	49.121	40.416	47.685	30.584
0.500	14.283	33.633	48.469	37.593	48.035	30.277
0.600	13.711	33.058	46.138	38.886	46.882	30.354
0.700	14.201	33.268	43.980	30.362	45.189	30.334
0.800	15.536	33.653	43.009	38.781	44.094	30.507
0.900	16.893	34.145	42.011	39.593	42.839	30.345
1.000	17.525	33.934	40.775	40.128	40.960	30.239
1.100	18.350	33.373	39.063	40.416	39.862	30.354
1.200	19.283	32.779	37.676	40.561	39.068	30.277
1.300	19.322	31.666	36.848	40.706	38.211	29.742
1.400	19.901	30.591	36.263	40.706	36.767	29.171
1.500	21.050	30.453	35.954	40.888	36.244	28.677
1.600	21.810	30.279	35.816	41.587	36.375	28.260
1.700	22.074	29.462	35.404	41.328	36.015	27.844
1.800	21.127	27.847	34.958	40.236	35.037	26.634
1.900	20.745	26.694	34.718	39.522	34.6[illegible]	25.715
2.000	21.088	26.518	34.855	39.878	35.004	25.991
2.100	21.165	26.834	35.473	39.985	35.428	25.839
2.200	20.630	26.553	34.958	39.344	34.613	25.385
2.300	19.709	25.671	34.066	38.292	33.182	24.815
2.400	19.012	25.352	33.243	37.360	32.629	24.510
2.500	18.545	24.926	32.935	37.120	32.499	24.205
2.600	18.193	24.890	32.832	37.017	32.564	24.053
2.700	18.115	25.210	33.003	37.083	32.396	24.167
2.800	18.350	25.565	33.517	36.948	32.694	24.320
2.900	18.310	25.281	33.209	36.471	32.364	24.205
3.000	17.722	25.032	32.249	35.118	31.848	23.364
3.100	17.447	24.282	31.390	33.874	30.806	22.555
3.200	17.328	24.318	30.840	33.304	30.251	22.129
3.300	16.814	24.211	30.600	32.868	29.757	22.400
3.400	17.051	24.676	30.668	32.801	29.597	22.555
3.500	17.051	25.104	30.462	33.136	29.630	22.864
3.600	17.407	25.494	30.324	33.405	29.728	23.976
3.700	17.486	25.210	30.221	33.405	29.724	24.310
3.800	17.447	24.961	29.566	32.432	29.270	24.282
3.900	17.131	24.282	28.772	31.557	28.219	23.823
4.000	17.210	23.959	28.044	30.952	27.361	23.171
4.100	17.131	23.346	27.975	29.938	26.931	22.825
4.200	16.774	23.273	27.419	29.463	26.366	21.896
4.300	17.249	23.346	27.280	28.746	25.999	21.551
4.400	17.447	23.237	27.106	28.308	26.066	21.468
4.500	17.644	23.273	27.141	28.575	26.432	21.896
4.600	17.722	23.563	27.4[illegible]	28.403	26.599	21.663

VERTICAL ELECTRIC FIELD
STARTING COORDINATES

PROBE #	X	Y	Z
1.00	2.00	12.00	0.00
2.00	2.00	8.00	0.00
3.00	2.00	4.00	0.00
4.00	2.00	0.00	0.00
5.00	2.00	-4.00	0.00
6.00	2.00	-8.00	0.00

Z	P[1]	P[2]	P[3]	P[4]	P[5]	P[6]
0.000	5.628	39.412	45.144	49.951	44.948	38.581
0.100	8.119	36.214	45.290	46.748	43.992	35.100
0.200	9.918	34.075	46.360	43.876	44.401	32.565
0.300	12.103	32.988	47.596	41.103	45.636	30.730
0.400	13.342	32.744	47.822	39.451	46.812	30.200
0.500	14.201	32.988	47.294	38.711	46.639	29.742
0.600	13.957	32.883	45.879	38.467	45.601	29.704
0.700	14.323	33.303	44.270	38.292	44.572	30.200
0.800	14.729	33.163	42.153	38.258	43.279	30.162
0.900	15.737	32.883	40.775	38.606	41.461	29.836
1.000	17.210	32.744	39.969	39.203	39.995	29.437
1.100	18.701	33.128	39.132	40.128	39.431	29.780
1.200	19.283	32.953	37.884	40.308	38.837	29.994
1.300	19.361	31.007	35.816	39.664	37.422	29.437
1.400	18.740	29.586	34.615	39.168	35.493	28.336
1.500	19.670	29.344	34.615	37.522	35.069	27.730
1.600	21.165	29.725	35.164	40.561	35.395	27.655
1.700	21.620	29.066	34.923	40.525	35.330	27.012
1.800	20.822	27.325	33.723	39.133	34.190	25.802
1.900	20.132	25.954	33.312	38.571	33.507	25.031
2.000	20.477	25.990	33.963	38.781	33.930	24.929
2.100	20.362	26.025	34.477	37.168	34.320	25.005
2.200	19.709	25.778	34.100	38.711	33.962	24.979
2.300	19.400	25.423	33.689	38.015	33.052	24.510
2.400	19.400	25.388	33.243	37.222	32.792	24.358
2.500	18.350	24.926	32.317	36.744	32.141	24.129
2.600	17.407	24.175	31.734	35.894	31.490	23.440
2.700	17.447	24.282	31.940	35.657	31.164	23.171
2.800	17.919	24.997	32.694	36.030	31.750	23.440
2.900	17.801	25.104	33.003	36.131	32.466	23.823
3.000	17.801	24.783	32.180	35.151	32.076	23.670
3.100	17.486	24.497	31.425	34.143	31.132	22.702
3.200	16.972	23.887	30.565	33.271	30.251	22.323
3.300	16.972	24.139	30.152	32.633	29.532	22.129
3.400	16.695	24.067	29.566	31.895	28.876	21.974
3.500	16.536	24.139	29.566	31.895	28.518	22.168
3.600	16.575	24.604	29.532	32.566	28.942	23.171
3.700	16.695	24.854	29.566	32.734	29.237	24.053
3.800	17.249	24.676	29.359	32.432	29.073	23.938
3.900	17.012	24.354	28.579	31.761	28.318	23.594
4.000	17.170	24.067	28.218	31.121	27.791	23.517
4.100	17.170	23.310	27.975	30.277	27.427	23.075
4.200	16.972	23.346	27.489	29.463	26.732	22.478
4.300	17.249	22.910	27.246	28.746	25.999	21.507
4.400	17.012	22.619	27.002	28.025	25.866	21.390
4.500	17.091	22.619	26.828	27.818	25.899	21.468
4.600	16.972	22.874	26.863	27.611	25.866	21.312

VERTICAL ELECTRIC FIELD
STARTING COORDINATES

PROBE #	X	Y	Z
1.00	3.00	12.00	0.00
2.00	3.00	9.00	0.00
3.00	3.00	4.00	0.00
4.00	3.00	0.00	0.00
5.00	3.00	-4.00	0.00
6.00	3.00	-8.00	0.00

Z	P[1]	P[2]	P[3]	P[4]	P[5]	P[6]
0.000	5.539	37.419	43.407	47.893	41.863	36.953
0.100	8.033	35.102	44.161	44.631	42.199	34.698
0.200	7.620	33.128	45.400	41.845	43.211	32.408
0.300	11.268	32.326	46.435	39.664	44.777	31.046
0.400	12.890	31.909	46.733	38.501	45.670	30.315
0.500	13.466	32.117	45.916	37.667	45.326	29.475
0.600	14.160	32.500	44.596	37.154	43.924	29.323
0.700	14.201	32.744	42.973	37.291	42.839	29.475
0.800	14.323	32.197	41.092	37.257	41.930	29.742
0.900	14.972	31.700	39.132	37.773	40.260	29.205
1.000	16.575	31.839	38.542	38.292	39.037	28.867
1.100	18.350	32.221	38.022	39.274	38.112	29.171
1.200	19.051	32.291	36.986	39.344	37.240	29.361
1.300	18.662	30.279	35.164	38.781	34.375	28.905
1.400	18.195	28.580	33.655	38.154	34.613	27.768
1.500	19.128	28.476	33.757	38.606	33.997	27.038
1.600	20.132	28.719	34.032	39.274	34.288	27.050
1.700	20.592	27.919	33.752	39.307	34.190	26.483
1.800	20.247	26.553	32.557	38.223	32.797	25.385
1.900	19.786	25.530	32.487	37.463	32.304	24.338
2.000	19.670	25.104	32.763	37.497	32.661	24.891
2.100	19.283	24.604	32.969	37.600	32.922	24.071
2.200	18.956	24.497	32.729	37.017	32.401	23.862
2.300	18.779	24.640	32.763	37.083	32.369	23.938
2.400	18.779	24.926	32.523	37.051	32.269	24.129
2.500	17.801	24.497	31.596	35.928	31.710	23.862
2.600	17.012	23.635	30.737	34.791	30.316	22.864
2.700	16.456	23.346	30.496	34.210	29.630	22.207
2.800	17.051	23.779	31.370	34.613	30.480	22.516
2.900	17.051	24.497	32.043	34.983	31.327	23.095
3.000	17.091	24.067	31.802	34.613	31.555	23.171
3.100	16.814	24.067	31.012	33.740	31.081	22.702
3.200	16.893	23.959	30.703	33.802	30.218	22.594
3.300	16.496	23.635	29.704	32.231	29.499	22.246
3.400	15.977	23.382	28.841	31.525	28.449	21.896
3.500	15.817	23.490	28.356	30.986	27.494	21.624
3.600	16.177	23.671	28.633	31.189	27.626	22.439
3.700	16.217	24.175	28.841	31.660	28.054	22.941
3.800	16.655	24.246	28.564	31.525	28.217	23.171
3.900	17.091	24.103	28.460	31.424	27.791	23.171
4.000	16.933	23.995	28.148	30.919	27.593	23.325
4.100	16.893	23.346	28.114	30.613	27.427	23.479
4.200	17.091	23.201	27.732	29.769	26.964	22.025
4.300	17.210	22.838	27.037	28.643	26.079	21.896
4.400	16.893	22.298	26.618	27.956	25.665	21.429
4.500	16.496	22.187	26.339	27.367	25.430	21.136
4.600	16.814	22.473	26.339	26.987	25.296	20.960

VERTICAL ELECTRIC FIELD
STARTING COORDINATES

PROBE #	X	Y	Z
1.00	4.00	12.00	0.00
2.00	4.00	8.00	0.00
3.00	4.00	4.00	0.00
4.00	4.00	0.00	0.00
5.00	4.00	-4.00	0.00
6.00	4.00	-8.00	0.00

Z	P(1)	P(2)	P(3)	P(4)	P(5)	P(6)
0.000	4.651	35.423	40.565	43.407	39.066	35.017
0.100	7.469	32.744	41.057	40.670	39.332	32.881
0.200	8.722	31.041	41.621	37.738	39.696	30.545
0.300	10.300	30.175	42.545	36.197	41.227	29.323
0.400	11.603	30.141	43.475	35.928	42.637	28.829
0.500	12.642	30.141	43.224	35.303	42.637	28.222
0.600	13.466	30.591	41.657	34.815	40.773	27.693
0.700	13.466	31.007	40.494	34.815	39.729	27.693
0.800	13.793	30.937	38.958	35.286	39.299	27.844
0.900	13.916	30.175	37.055	35.757	38.178	27.306
1.000	15.214	29.864	35.988	36.201	36.571	27.390
1.100	16.774	30.106	35.335	36.778	35.395	27.428
1.200	17.840	30.245	34.752	37.222	35.135	27.579
1.300	17.525	28.927	33.072	36.880	34.150	27.201
1.400	17.447	27.185	31.734	36.471	32.661	26.294
1.500	17.997	26.318	31.528	36.403	32.011	25.612
1.600	18.934	26.694	31.837	36.983	32.271	25.423
1.700	18.934	25.459	31.322	36.880	32.043	25.085
1.800	19.012	24.783	31.012	36.064	31.132	23.938
1.900	18.662	24.211	30.772	35.737	30.675	23.210
2.000	18.467	23.599	30.658	35.438	30.708	22.709
2.100	17.683	22.583	30.324	34.947	30.610	22.400
2.200	17.091	22.546	30.014	34.512	30.218	22.207
2.300	17.170	23.092	30.462	34.680	30.349	22.316
2.400	17.565	23.418	30.806	35.084	30.708	22.364
2.500	16.814	22.510	30.187	34.378	30.022	22.335
2.600	15.977	22.290	29.117	33.002	28.811	21.741
2.700	15.496	21.960	28.495	32.264	28.120	20.760
2.800	15.576	22.180	28.979	32.499	28.581	20.920
2.900	15.937	22.400	29.635	32.499	29.139	21.234
3.000	15.817	22.692	29.704	32.231	29.237	21.468
3.100	15.937	22.546	29.497	32.097	29.172	21.507
3.200	15.897	22.838	29.532	31.996	29.204	21.702
3.300	15.656	22.728	28.841	31.290	28.617	21.624
3.400	15.174	22.327	27.767	30.277	27.361	21.156
3.500	15.254	21.960	26.793	29.497	26.333	20.842
3.600	15.335	22.510	26.793	29.258	25.899	21.077
3.700	15.415	22.692	26.897	29.497	26.066	21.346
3.800	15.817	23.128	26.967	29.599	26.233	21.663
3.900	15.977	23.165	27.176	29.735	26.266	21.858
4.000	16.257	22.656	27.176	29.836	26.466	22.323
4.100	16.217	22.546	26.863	29.497	26.632	22.594
4.200	16.336	22.363	26.653	28.540	26.233	22.013
4.300	16.416	21.776	26.234	27.887	25.363	21.273
4.400	16.057	21.592	25.464	27.057	24.960	20.842
4.500	15.777	21.148	25.324	26.394	24.623	20.724
4.600	15.857	21.260	25.043	25.798	24.217	20.291

VERTICAL ELECTRIC FIELD
STARTING COORDINATES

PROBE #	X	Y	Z
1.00	5.00	12.00	0.00
2.00	5.00	8.00	0.00
3.00	5.00	4.00	0.00
4.00	5.00	0.00	0.00
5.00	5.00	-4.00	0.00
6.00	5.00	-8.00	0.00

Z	P[1]	P[2]	P[3]	P[4]	P[5]	P[6]
0.000	4.294	33.268	38.403	33.308	37.160	33.918
0.100	7.208	30.591	37.884	37.325	36.571	31.200
0.200	8.464	28.962	38.091	34.109	36.081	28.298
0.300	9.493	28.615	39.146	33.403	37.652	27.239
0.400	10.384	28.788	40.916	32.536	40.028	27.428
0.500	11.561	28.545	40.565	33.472	40.129	27.126
0.600	12.393	28.927	39.167	[illegible]	38.309	26.331
0.700	13.096	29.344	37.988	32.902	37.226	25.953
0.800	13.424	29.656	37.193	33.837	37.324	26.445
0.900	13.178	28.754	35.301	34.512	36.342	26.445
1.000	14.283	29.197	33.929	34.546	34.483	25.991
1.100	15.415	28.197	33.003	34.747	33.182	25.764
1.200	16.853	28.510	32.935	35.195	32.954	25.953
1.300	17.131	27.779	31.905	35.488	32.336	25.650
1.400	16.972	26.166	30.634	35.094	31.425	25.119
1.500	17.170	25.388	29.980	34.915	30.480	24.358
1.600	17.447	25.068	29.808	35.016	30.218	23.938
1.700	17.525	24.497	27.670	34.915	30.153	23.632
1.800	18.036	23.779	29.670	34.747	29.663	22.902
1.900	18.232	23.418	29.980	34.512	29.794	22.207
2.000	17.997	22.692	29.635	34.143	29.597	21.858
2.100	17.012	21.629	28.530	33.136	28.876	21.466
2.200	16.057	21.222	28.356	32.835	28.351	20.999
2.300	16.217	21.481	29.152	33.170	28.647	21.312
2.400	16.734	22.437	29.532	33.706	29.139	21.780
2.500	16.177	22.034	29.256	33.371	28.975	21.780
2.600	15.536	21.481	28.183	32.231	28.219	21.351
2.700	15.295	21.297	27.940	31.357	27.560	20.685
2.800	15.254	21.334	27.871	31.121	27.394	20.330
2.900	14.729	20.888	27.802	30.750	27.394	20.093
3.000	14.851	21.260	28.079	30.412	27.560	19.855
3.100	15.133	21.592	28.287	30.717	27.890	20.172
3.200	15.496	22.363	28.633	30.996	28.351	21.038
3.300	15.415	22.363	28.079	30.719	28.219	21.468
3.400	14.770	21.924	27.315	29.836	27.096	21.077
3.500	14.648	21.518	26.234	29.122	26.033	20.488
3.600	14.607	21.850	25.850	28.678	25.162	20.527
3.700	14.810	21.776	25.744	28.300	24.859	20.488
3.800	15.174	21.960	25.990	28.403	24.724	20.506
3.900	15.576	22.107	26.060	28.380	24.994	20.685
4.000	15.616	21.887	26.129	28.472	25.229	21.195
4.100	15.817	21.703	26.164	28.367	25.531	21.798
4.200	16.017	21.740	25.955	27.956	25.464	21.702
4.300	16.257	21.481	25.674	27.542	25.061	21.195
4.400	15.697	21.148	25.499	26.813	24.792	20.920
4.500	15.536	20.702	24.867	26.357	24.420	20.567
4.600	15.375	20.814	24.620	25.622	23.980	20.053

VERTICAL ELECTRIC FIELD
STARTING COORDINATES

PROBE #	X	Y	Z
1.00	6.00	12.00	0.00
2.00	6.00	8.00	0.00
3.00	6.00	4.00	0.00
4.00	6.00	0.00	0.00
5.00	6.00	-4.00	0.00
6.00	6.00	-8.00	0.00

Z	P[1]	P[2]	P[3]	P[4]	P[5]	P[6]
0.000	4.115	30.175	34.203	35.524	33.084	30.430
0.100	6.596	27.430	33.929	33.203	32.661	27.768
0.200	7.989	26.307	34.409	30.717	32.369	25.650
0.300	8.636	26.448	36.160	30.146	34.288	25.005
0.400	9.705	26.869	37.711	30.919	36.605	25.309
0.500	10.257	26.307	37.055	30.412	36.731	25.043
0.600	11.184	26.413	35.438	29.567	34.972	24.014
0.700	11.811	27.010	34.718	30.207	34.020	23.670
0.800	12.393	27.919	34.580	31.391	34.156	24.167
0.900	12.559	27.255	33.140	32.177	33.702	24.472
1.000	14.013	26.060	31.150	32.063	32.011	24.205
1.100	14.120	25.954	30.600	32.264	30.871	23.323
1.200	15.174	26.483	30.565	33.002	30.643	23.976
1.300	15.857	25.990	30.255	33.841	30.382	23.976
1.400	16.297	25.139	29.186	33.505	29.597	23.517
1.500	16.376	24.282	28.426	32.967	28.778	22.787
1.600	16.336	23.273	27.802	32.835	28.120	22.168
1.700	16.057	22.583	27.882	32.868	27.725	21.741
1.800	16.575	22.437	28.218	33.002	28.022	21.351
1.900	17.289	22.180	28.599	32.868	28.022	20.842
2.000	17.289	21.740	28.252	32.365	27.857	20.409
2.100	16.017	20.479	27.072	31.525	27.196	19.735
2.200	15.456	19.954	26.932	31.088	26.665	19.736
2.300	15.093	20.029	27.246	31.323	26.997	19.537
2.400	15.214	21.000	27.906	31.794	27.427	20.172
2.500	15.053	21.148	28.010	31.962	27.672	20.527
2.600	15.053	21.037	27.697	31.424	27.229	20.606
2.700	14.972	20.851	27.106	30.917	26.732	26.133
2.800	14.689	20.254	26.863	30.142	26.366	19.557
2.900	13.997	20.029	26.199	29.156	25.932	18.738
3.000	13.957	20.104	26.384	28.917	25.698	18.577
3.100	14.079	20.441	27.106	29.088	26.333	18.878
3.200	14.648	21.408	27.593	29.701	26.964	19.776
3.300	14.486	21.444	27.350	29.597	27.196	20.567
3.400	14.405	21.481	26.688	29.122	26.698	20.567
3.500	14.405	21.260	25.780	28.607	25.899	20.330
3.600	14.160	21.111	25.499	28.163	24.893	20.053
3.700	13.997	21.111	25.007	27.715	24.183	20.014
3.800	14.242	21.037	24.726	27.265	23.605	19.537
3.900	14.648	21.148	24.550	26.883	23.605	19.577
4.000	14.810	20.888	24.972	27.265	23.944	19.855
4.100	15.254	21.148	24.937	27.057	24.285	20.469
4.200	15.656	21.185	25.078	26.918	24.319	20.645
4.300	15.977	21.111	25.218	26.778	24.454	20.724
4.400	15.817	21.037	25.007	26.464	24.488	20.685
4.500	15.415	20.665	24.726	26.077	24.420	20.251
4.600	15.053	20.516	24.162	25.056	23.571	19.776

VERTICAL ELECTRIC FIELD
STARTING COORDINATES

PROBE #	X	Y	Z
1.00	7.00	12.00	0.00
2.00	7.00	8.00	0.00
3.00	7.00	4.00	0.00
4.00	7.00	0.00	0.00
5.00	7.00	-4.00	0.00
6.00	7.00	-8.00	0.00

Z	P(1)	P(2)	P(3)	P(4)	P(5)	P(6)
0.000	3.575	24.819	28.252	27.803	26.798	23.271
0.100	5.716	23.273	28.703	28.197	27.295	23.317
0.200	7.295	22.910	30.049	27.126	28.286	22.555
0.300	7.860	23.563	31.837	26.813	30.400	22.632
0.400	8.249	23.490	32.592	26.639	31.048	22.671
0.500	8.507	22.546	31.493	25.622	31.508	22.013
0.600	9.407	22.583	30.255	25.339	30.153	21.234
0.700	10.595	23.959	30.600	26.464	29.957	21.195
0.800	11.268	24.997	30.565	28.060	29.990	21.702
0.900	11.016	24.246	29.428	28.712	29.368	21.780
1.000	11.226	23.092	27.558	28.780	28.153	21.663
1.100	12.352	23.237	27.037	29.156	27.540	21.546
1.200	13.424	23.527	27.315	29.972	27.361	21.565
1.300	14.323	23.454	27.280	30.852	27.229	21.624
1.400	14.810	22.728	26.653	30.818	26.698	21.429
1.500	14.770	22.144	26.060	30.514	26.066	20.881
1.600	14.729	21.481	25.464	30.074	25.430	20.093
1.700	14.567	20.591	25.148	30.040	25.196	19.617
1.800	14.770	19.879	25.674	30.243	25.296	19.338
1.900	15.536	20.179	26.129	30.446	25.565	18.898
2.000	15.496	19.879	25.920	30.040	25.330	18.657
2.100	14.931	19.047	25.289	29.429	24.859	18.214
2.200	14.364	18.285	24.761	28.814	24.386	17.849
2.300	13.752	18.285	24.691	28.678	24.149	17.686
2.400	13.711	18.667	25.113	28.985	24.556	18.133
2.500	13.548	19.047	25.218	29.019	24.960	18.577
2.600	13.711	19.464	25.464	29.258	24.994	19.058
2.700	13.629	19.502	25.569	27.122	25.095	18.737
2.800	13.507	19.161	25.043	28.266	24.454	18.294
2.900	13.013	18.208	24.449	27.161	24.082	17.524
3.000	12.848	18.170	24.373	26.778	23.639	17.033
3.100	12.972	18.591	24.585	26.987	23.878	17.461
3.200	12.931	19.275	25.113	27.265	24.386	18.092
3.300	13.013	19.540	24.902	27.196	24.758	18.898
3.400	13 424	19.879	24.902	27.473	24.691	19.338
3.500	13.260	20.142	24.585	27.438	24.454	19.338
3.600	13.219	20.179	24.232	27.091	23.810	19.418
3.700	12.766	19.728	23.454	26.254	23.058	19.178
3.800	13.013	19.540	22.886	25.375	22.024	18.617
3.900	13.629	19.615	22.921	25.304	21.885	18.173
4.000	13.629	19.615	23.134	25.198	21.990	18.254
4.100	13.997	19.351	23.170	25.267	21.955	18.818
4.200	14.486	19.540	23.454	24.950	22.336	19.018
4.300	14.851	19.653	23.702	25.127	22.749	19.218
4.400	14.770	19.916	23.914	25.092	23.127	19.537
4.500	14.607	19.464	23.303	24.665	23.024	19.218
4.600	14.607	19.464	22.814	23.950	22.646	18.770

VERTICAL ELECTRIC FIELD
STARTING COORDINATES

PROBE #	X	Y	Z
1.00	0.00	12.00	0.00
2.00	0.00	8.00	0.00
3.00	0.00	4.00	0.00
4.00	0.00	0.00	0.00
5.00	0.00	4.00	0.00
6.00	0.00	8.00	0.00

Z	P(1)	P(2)	P(3)	P(4)	P(5)	P(6)
0.000	2.717	20.142	22.065	23.627	20.555	20.093
0.100	4.651	18.895	23.409	23.122	21.920	19.010
0.200	6.421	19.502	25.015	22.868	24.149	19.058
0.300	7.121	20.366	27.628	22.577	26.333	19.298
0.400	7.252	17.916	27.409	21.553	26.931	19.258
0.500	6.990	17.047	26.479	20.852	26.299	18.377
0.600	7.946	19.540	26.339	21.443	25.932	18.415
0.700	9.065	21.260	26.063	23.338	26.432	18.617
0.800	9.740	22.290	26.967	24.950	26.399	19.218
0.900	9.076	21.703	25.850	23.410	25.932	19.418
1.000	10.045	21.148	24.867	25.727	25.027	19.412
1.100	10.974	20.963	24.409	26.254	24.657	19.418
1.200	11.053	21.000	24.479	27.369	24.522	19.537
1.300	12.931	21.000	24.656	28.197	24.536	19.438
1.400	13.383	20.665	24.338	28.609	24.285	19.418
1.500	13.916	20.516	24.303	28.643	24.048	19.298
1.600	13.670	19.615	23.667	28.609	23.810	18.898
1.700	13.342	18.705	23.418	28.335	23.401	18.335
1.800	13.424	18.323	23.773	28.163	23.298	17.930
1.900	13.875	18.438	24.056	28.367	23.708	17.646
2.000	14.405	18.285	24.268	28.128	23.810	17.401
2.100	14.120	17.824	23.808	27.887	23.537	17.238
2.200	13.424	17.477	23.418	27.438	23.161	16.992
2.300	13.178	17.128	23.063	26.918	22.543	16.623
2.400	12.476	16.973	23.134	26.778	22.474	16.581
2.500	12.228	17.283	23.383	26.918	22.853	17.115
2.600	12.393	17.901	23.914	27.646	23.367	17.524
2.700	12.725	18.361	24.444	27.715	23.708	17.727
2.800	12.848	17.901	23.985	26.848	23.435	17.401
2.900	12.061	17.438	23.099	26.114	22.990	17.074
3.000	11.978	17.128	22.886	25.516	22.646	16.623
3.100	11.936	17.206	23.134	25.092	22.370	16.334
3.200	11.770	17.438	22.957	24.985	22.267	16.705
3.300	11.895	18.246	23.134	25.092	22.818	17.279
3.400	12.518	18.781	23.347	25.939	23.230	18.133
3.500	12.972	19.313	23.844	26.374	23.469	18.778
3.600	12.518	19.351	23.383	26.324	23.298	19.058
3.700	12.559	18.743	22.316	25.410	22.301	19.058
3.800	12.393	18.514	21.922	24.701	21.746	18.415
3.900	12.807	18.400	21.994	24.416	21.328	17.890
4.000	12.890	18.361	21.958	23.950	21.083	17.686
4.100	13.260	18.323	21.958	23.699	20.872	17.564
4.200	13.466	18.514	21.922	23.663	20.907	17.605
4.300	13.997	18.781	22.601	23.627	21.328	18.611
4.400	13.997	18.667	22.565	23.771	22.024	18.496
4.500	13.875	18.591	22.530	23.517	22.059	18.496
4.600	14.120	18.895	22.387	23.085	21.920	18.254

VERTICAL ELECTRIC FIELD
STARTING COORDINATES

PROBE #	X	Y	Z
1.00	9.00	12.00	0.00
2.00	9.00	8.00	0.00
3.00	9.00	4.00	0.00
4.00	9.00	0.00	0.00
5.00	9.00	-4.00	0.00
6.00	9.00	-8.00	0.00

Z	P[1]	P[2]	P[3]	P[4]	P[5]	P[6]
0.000	1.097	13.893	14.979	15.713	[illegible]	14.031
0.100	3.530	13.732	16.790	13.751	[illegible]	13.330
0.200	5.141	14.051	19.726	16.671	[illegible]	13.734
0.300	5.620	15.602	21.349	16.786	20.272	14.539
0.400	5.620	15.326	21.457	15.790	20.731	14.539
0.500	5.504	15.049	20.990	15.020	20.767	14.497
0.600	6.069	16.075	21.313	17.434	21.363	15.001
0.700	7.513	17.354	22.450	19.324	21.701	15.629
0.800	7.946	18.438	22.280	20.593	21.712	15.878
0.900	8.851	18.361	21.007	21.258	21.363	16.210
1.000	9.236	18.438	21.277	22.030	21.293	16.499
1.100	9.620	18.361	21.385	23.194	21.433	16.787
1.200	9.833	18.016	20.738	23.591	20.978	16.664
1.300	10.732	17.515	20.918	24.273	20.661	16.540
1.400	11.895	17.939	21.098	25.233	20.802	16.828
1.500	12.642	18.285	21.815	25.937	21.328	16.869
1.600	12.559	17.670	21.493	25.657	21.293	16.746
1.700	11.895	16.623	21.134	25.657	20.943	16.168
1.800	12.228	16.153	21.134	25.516	20.837	15.795
1.900	12.228	16.349	21.564	25.410	21.118	15.795
2.000	12.807	16.192	22.208	26.009	21.677	15.670
2.100	12.559	16.192	22.101	26.184	21.677	15.753
2.200	12.393	16.114	22.065	25.692	21.433	15.712
2.300	11.978	15.682	21.600	25.021	20.907	15.462
2.400	11.436	15.247	20.954	24.736	20.343	15.001
2.500	10.806	15.168	20.702	24.237	20.308	15.169
2.600	11.352	16.114	21.851	25.092	21.118	15.545
2.700	11.477	16.701	22.494	25.445	21.503	15.878
2.800	11.603	16.739	22.280	25.233	21.816	16.086
2.900	11.436	16.505	22.173	24.701	21.781	16.127
3.000	11.436	16.388	21.708	23.946	21.398	15.795
3.100	11.184	15.996	21.421	23.591	20.978	15.295
3.200	11.100	15.839	20.990	22.940	20.237	15.085
3.300	10.806	15.957	20.702	22.650	20.272	15.503
3.400	11.352	16.934	21.313	23.555	21.118	16.292
3.500	11.561	17.862	21.807	24.300	21.337	17.197
3.600	11.853	18.246	21.528	24.558	21.537	17.890
3.700	11.645	17.901	21.026	24.130	21.328	18.032
3.800	12.103	17.593	21.134	23.986	20.837	17.930
3.900	12.228	17.747	20.918	23.447	20.449	17.646
4.000	12.228	17.012	20.629	22.723	20.166	17.238
4.100	12.228	16.739	20.160	22.322	19.596	16.746
4.200	12.393	16.701	20.449	21.803	19.202	16.210
4.300	12.642	17.206	20.738	21.737	19.417	16.375
4.400	13.096	17.477	21.026	22.030	20.272	16.951
4.500	13.137	17.361	21.241	22.140	20.535	17.320
4.600	13.301	17.631	20.918	22.030	20.626	17.115

VERTICAL ELECTRIC FIELD
STARTING COORDINATES

PROBE #	X	Y	Z
1.00	-15.00	9.00	0.00
2.00	-15.00	5.00	0.00
3.00	-15.00	1.00	0.00
4.00	-15.00	-3.00	0.00
5.00	-15.00	-7.00	0.00
6.00	-15.00	-11.00	0.00

Z	P(1)	P(2)	P(3)	P(4)	P(5)	P(6)
0.000	2.126	14.891	15.724	16.900	14.240	14.076
0.100	3.375	14.173	17.756	16.633	15.049	14.138
0.200	5.105	15.168	20.521	17.129	18.515	14.581
0.300	6.157	16.271	22.208	17.396	20.907	15.127
0.400	5.628	16.036	21.994	16.556	21.328	15.177
0.500	5.716	15.760	21.672	16.510	21.258	15.159
0.600	6.509	16.310	21.887	17.776	21.781	15.545
0.700	7.469	18.016	22.814	19.085	22.301	16.210
0.800	8.205	18.933	23.099	21.258	22.405	16.499
0.900	8.765	19.009	22.316	21.883	21.990	16.746
1.000	9.493	18.743	22.030	22.759	21.746	17.115
1.100	9.876	18.895	21.708	23.519	21.781	17.197
1.200	10.342	18.093	21.313	24.130	21.293	17.197
1.300	11.100	17.824	21.205	24.808	21.048	17.115
1.400	12.061	18.285	21.779	25.727	21.258	17.442
1.500	12.683	18.438	21.958	26.324	21.372	17.524
1.600	12.601	18.055	21.708	26.429	21.468	17.238
1.700	12.061	17.012	21.349	26.044	21.118	16.664
1.800	12.311	16.466	21.528	25.798	21.048	16.416
1.900	12.807	16.388	22.173	26.149	21.572	16.127
2.000	13.055	16.584	22.280	26.464	21.955	16.127
2.100	12.890	16.544	22.494	26.569	21.816	16.251
2.200	12.807	16.310	22.423	26.184	21.712	16.127
2.300	12.269	15.918	21.815	25.445	21.118	15.761
2.400	11.394	15.326	21.026	24.558	20.485	15.545
2.500	11.058	15.682	21.349	24.772	20.731	15.670
2.600	11.436	16.349	21.887	25.587	21.223	15.920
2.700	11.811	16.701	22.708	25.939	21.816	16.375
2.800	11.811	16.895	22.708	25.551	22.128	16.664
2.900	11.436	16.388	22.101	24.914	22.094	16.540
3.000	11.352	16.349	21.994	24.558	21.781	16.044
3.100	11.519	16.427	21.708	23.950	21.033	15.462
3.200	10.932	16.036	21.098	23.085	20.520	15.336
3.300	11.016	16.584	21.026	23.194	20.731	15.720
3.400	11.519	17.477	21.779	23.807	21.398	16.664
3.500	11.978	18.131	22.200	24.808	21.920	17.685
3.600	11.853	18.361	21.922	24.985	21.712	18.294
3.700	11.978	17.862	21.493	24.630	21.379	18.336
3.800	12.186	17.708	21.098	24.165	20.978	18.254
3.900	12.228	17.631	21.241	23.627	20.626	17.890
4.000	12.559	17.554	20.629	23.013	20.272	17.524
4.100	12.061	17.089	20.341	22.359	19.560	16.751
4.200	12.476	16.856	20.666	22.140	19.417	16.787
4.300	12.890	17.477	21.062	22.103	19.739	16.828
4.400	13.137	17.708	21.349	22.286	20.343	17.401
4.500	13.137	17.939	21.421	22.393	20.802	17.605
4.600	13.301	17.978	21.349	22.249	20.978	17.564

VERTICAL ELECTRIC FIELD
STARTING COORDINATES

PROBE #	X	Y	Z
1.00	9.00	12.00	0.00
2.00	9.00	8.00	0.00
3.00	9.00	4.00	0.00
4.00	9.00	0.00	0.00
5.00	9.00	-4.00	0.00
6.00	9.00	-8.00	0.00

Z	P(1)	P(2)	P(3)	P(4)	P(5)	P(6)
0.000	1.989	14.970	15.724	16.709	14.356	15.001
0.100	3.575	14.093	17.609	16.400	15.807	14.243
0.200	5.096	15.208	20.160	17.396	18.515	14.454
0.300	5.937	16.308	22.280	17.244	20.978	15.211
0.400	5.620	15.996	22.030	16.403	21.223	15.336
0.500	5.620	15.445	21.564	16.400	21.198	15.085
0.600	6.245	16.388	21.897	17.920	21.712	15.587
0.700	7.599	18.170	22.806	19.811	22.508	16.168
0.800	8.292	18.895	23.099	21.295	22.232	16.581
0.900	8.765	19.047	22.458	21.863	21.895	16.751
1.000	9.322	18.857	22.030	22.759	21.781	17.115
1.100	9.960	18.933	21.743	23.627	21.805	17.401
1.200	10.300	18.208	21.457	24.380	21.398	17.320
1.300	11.142	17.862	21.169	24.985	21.048	17.238
1.400	12.103	18.400	21.636	25.798	21.293	17.524
1.500	12.683	18.743	22.101	26.429	21.746	17.605
1.600	12.807	18.246	21.779	25.394	21.607	17.197
1.700	12.186	16.895	21.385	26.079	21.118	16.828
1.800	12.393	16.153	21.493	25.974	21.048	16.458
1.900	12.642	16.623	22.137	26.184	21.607	16.292
2.000	12.972	16.778	22.387	26.534	21.816	16.334
2.100	12.807	16.544	22.458	26.639	21.851	16.210
2.200	12.848	16.192	22.173	26.219	21.712	16.210
2.300	12.228	15.879	21.851	25.410	21.013	16.044
2.400	11.645	15.563	20.990	24.843	20.731	15.587
2.500	11.058	15.642	21.134	24.772	20.802	15.587
2.600	11.352	16.232	21.887	25.516	21.363	16.003
2.700	11.895	16.781	22.330	25.763	21.816	16.499
2.800	11.936	16.895	22.708	25.587	21.920	16.746
2.900	11.645	16.544	22.208	24.879	21.955	16.499
3.000	11.436	16.505	22.101	24.451	21.816	16.168
3.100	11.603	16.388	21.528	23.699	21.093	15.345
3.200	11.268	16.036	21.205	23.158	20.826	15.503
3.300	10.974	16.232	20.990	23.302	20.535	16.003
3.400	11.561	17.477	21.743	23.843	21.328	16.664
3.500	11.936	18.093	22.208	24.736	21.712	17.605
3.600	11.853	18.246	22.030	24.808	21.677	18.294
3.700	11.895	17.939	21.349	24.594	21.293	18.496
3.800	12.103	17.862	21.241	24.237	20.943	18.415
3.900	12.393	17.631	21.026	23.627	20.731	17.971
4.000	12.393	17.203	20.810	23.122	20.237	17.401
4.100	12.103	17.051	20.485	22.249	19.668	16.992
4.200	12.269	16.817	20.593	22.176	19.560	16.664
4.300	13.096	17.322	21.134	22.213	19.703	16.910
4.400	13.137	17.515	21.457	22.249	20.308	17.361
4.500	13.301	17.862	21.241	22.468	20.767	17.686
4.600	13.342	18.055	21.421	22.286	20.907	17.768

VERTICAL ELECTRIC FIELD
STARTING COORDINATES

PROBE #	X	Y	Z
1.00	10.00	12.00	0.00
2.00	10.00	8.00	0.00
3.00	10.00	4.00	0.00
4.00	10.00	0.00	0.00
5.00	10.00	-4.00	0.00
6.00	10.00	-8.00	0.00

Z	P(1)	P(2)	P(3)	P(4)	P(5)	P(6)
0.000	1.669	11.051	10.667	11.151	9.419	10.444
0.100	2.717	10.475	13.025	11.693	11.230	10.136
0.200	4.294	11.788	16.021	12.854	14.279	10.732
0.300	4.740	12.845	18.049	13.320	16.601	11.756
0.400	4.963	13.007	18.305	13.933	17.159	12.276
0.500	4.740	13.088	18.232	13.397	17.749	12.664
0.600	5.274	14.173	18.671	15.174	18.508	13.393
0.700	6.245	15.366	19.399	16.930	19.022	13.789
0.800	7.121	16.075	19.653	18.004	18.805	14.370
0.900	7.606	16.349	19.435	18.986	18.769	14.655
1.000	8.765	16.817	19.544	20.258	19.202	15.420
1.100	8.894	16.895	19.653	21.185	19.525	15.629
1.200	9.151	16.310	18.999	21.810	18.769	15.420
1.300	9.663	15.839	18.598	22.176	18.479	15.420
1.400	10.595	16.232	19.326	23.230	18.877	15.712
1.500	11.728	16.739	20.269	24.273	19.739	15.837
1.600	11.811	16.388	20.269	24.594	19.632	15.670
1.700	11.268	15.524	19.580	23.950	19.130	15.275
1.800	11.436	14.732	19.943	24.072	19.309	15.085
1.900	11.770	14.811	20.269	24.273	19.632	14.876
2.000	11.561	15.366	20.846	24.630	20.308	14.876
2.100	12.020	15.129	21.277	24.914	20.414	15.127
2.200	12.106	15.603	21.098	24.914	20.272	15.253
2.300	11.720	15.089	20.846	24.022	20.095	15.127
2.400	10.890	14.493	20.015	23.411	19.525	14.833
2.500	10.511	14.373	19.979	23.302	19.274	14.623
2.600	10.426	15.089	20.413	23.663	19.703	14.749
2.700	10.932	15.721	21.134	24.022	20.059	15.085
2.800	11.142	15.760	21.421	24.072	20.767	15.587
2.900	10.774	15.910	21.457	24.022	21.133	15.878
3.000	11.142	16.153	21.241	23.627	20.943	15.629
3.100	10.774	15.404	20.774	22.868	20.166	15.043
3.200	10.469	15.366	19.907	21.957	19.345	14.623
3.300	10.384	15.404	19.943	21.883	19.274	14.918
3.400	10.722	15.957	20.485	22.359	19.703	15.670
3.500	11.226	16.856	20.629	22.940	20.272	16.416
3.600	11.268	17.089	20.485	23.230	20.308	17.115
3.700	11.394	17.206	20.521	23.411	20.378	17.727
3.800	11.519	17.089	20.557	23.375	20.343	17.930
3.900	11.895	17.245	20.666	23.049	20.237	17.849
4.000	11.895	16.817	20.124	22.249	19.668	17.238
4.100	11.519	16.349	19.508	21.626	18.930	16.664
4.200	12.020	16.232	19.798	21.111	18.805	16.066
4.300	12.144	16.388	19.834	21.037	18.697	16.251
4.400	12.435	16.505	20.232	21.148	19.238	16.334
4.500	12.603	16.584	20.305	20.926	19.396	16.623
4.600	12.890	16.895	20.269	21.272	19.703	16.767

VERTICAL ELECTRIC FIELD
STARTING COORDINATES

PROBE #	X	Y	Z
1.00	11.00	12.00	0.00
2.00	11.00	8.00	0.00
3.00	11.00	4.00	0.00
4.00	11.00	0.00	0.00
5.00	11.00	4.00	0.00
6.00	11.00	8.00	0.00

Z	P(1)	P(2)	P(3)	P(4)	P(5)	P(6)
0.000	1.394	6.810	5.983	6.192	5.100	5.788
0.100	1.760	6.474	8.589	7.393	6.851	6.378
0.200	2.943	7.858	11.393	8.381	9.588	6.966
0.300	3.665	9.026	13.403	9.223	11.730	8.314
0.400	4.070	9.566	14.117	9.415	12.904	9.251
0.500	4.115	10.599	14.917	10.340	13.772	9.759
0.600	4.338	11.420	14.904	11.654	14.781	10.664
0.700	4.651	11.992	15.277	13.087	15.008	11.189
0.800	5.407	12.377	15.314	14.094	14.820	11.625
0.900	6.684	13.411	16.206	15.636	15.432	12.039
1.000	7.556	14.652	16.798	17.320	16.113	12.793
1.100	7.860	14.771	16.909	18.344	16.264	13.222
1.200	7.903	13.652	15.910	18.647	15.811	13.272
1.300	8.335	13.290	15.798	19.324	15.660	13.222
1.400	9.279	13.732	16.872	20.444	16.264	13.691
1.500	10.257	14.732	17.719	21.700	17.005	13.319
1.600	10.553	14.213	17.756	21.957	17.122	13.691
1.700	10.130	13.853	17.572	21.700	16.787	13.350
1.800	10.469	13.491	17.792	21.663	17.233	13.307
1.900	10.215	13.008	18.159	21.957	17.491	13.136
2.000	10.257	13.128	18.634	22.140	18.005	13.272
2.100	10.384	13.330	18.089	22.504	18.070	13.393
2.200	10.600	13.933	19.689	22.904	18.588	14.031
2.300	10.764	13.973	19.435	22.650	18.660	14.243
2.400	9.076	13.612	18.598	21.957	18.042	13.776
2.500	9.279	12.926	18.305	21.553	17.602	13.264
2.600	9.578	13.169	18.488	21.516	17.712	13.272
2.700	9.876	13.773	19.217	21.083	17.896	13.563
2.800	9.705	14.293	19.617	21.863	18.660	14.031
2.900	9.833	14.612	19.726	22.249	19.453	14.339
3.000	10.469	15.049	19.943	22.432	19.882	14.623
3.100	10.595	14.732	19.544	21.047	19.417	14.328
3.200	10.088	14.413	19.035	20.852	18.588	14.116
3.300	9.620	14.173	18.451	20.295	17.932	13.904
3.400	9.535	14.493	18.707	20.333	17.822	14.031
3.500	10.003	15.445	18.598	20.015	18.115	14.749
3.600	9.960	15.682	18.634	21.000	18.261	15.387
3.700	10.300	15.682	19.035	21.847	18.677	16.334
3.800	11.058	16.153	19.544	22.103	19.202	16.787
3.900	11.058	16.308	19.617	22.066	19.058	16.951
4.000	11.058	15.800	19.072	21.250	18.805	16.581
4.100	11.058	15.563	18.853	20.667	18.443	16.003
4.200	11.142	15.168	18.707	20.184	17.896	15.670
4.300	11.561	15.287	18.707	19.694	17.675	15.211
4.400	11.226	15.129	18.378	19.211	17.528	15.127
4.500	11.519	15.247	18.561	19.174	18.078	15.336
4.600	11.728	15.910	18.817	19.661	18.297	15.336

VERTICAL ELECTRIC FIELD
STARTING COORDINATES

PROBE #	X	Y	Z
1.00	12.00	12.00	0.00
2.00	12.00	8.00	0.00
3.00	12.00	4.00	0.00
4.00	12.00	0.00	0.00
5.00	12.00	-4.00	0.00
6.00	12.00	-8.00	0.00

Z	P(1)	P(2)	P(3)	P(4)	P(5)	P(6)
0.000	1.302	3.691	3.783	3.818	2.945	3.552
0.100	1.006	4.202	5.026	4.392	4.346	4.036
0.200	2.126	5.126	8.163	5.340	5.505	4.741
0.300	2.626	6.263	9.900	6.192	8.393	6.015
0.400	3.079	7.481	10.514	6.753	9.630	6.875
0.500	3.305	8.067	11.508	8.000	10.467	7.731
0.600	3.530	8.735	11.678	9.262	11.332	8.542
0.700	3.710	9.026	11.736	10.031	11.639	9.117
0.800	4.383	9.566	12.230	10.958	11.780	9.606
0.900	5.407	10.928	13.214	12.739	12.585	10.092
1.000	6.728	12.440	14.305	14.634	13.379	10.796
1.100	6.946	12.196	14.005	13.828	13.458	11.277
1.200	6.552	11.584	13.440	15.770	12.983	11.233
1.300	7.077	11.257	13.440	16.595	13.142	11.277
1.400	7.860	11.752	14.717	17.728	13.089	11.842
1.500	8.094	12.237	15.463	18.906	14.704	11.842
1.600	9.151	11.992	15.612	19.361	14.820	11.712
1.700	9.450	11.952	15.947	19.436	14.838	11.756
1.800	9.493	11.870	16.466	19.773	15.432	11.573
1.900	9.236	11.584	16.429	17.511	15.622	11.669
2.000	8.900	11.134	16.095	19.511	15.811	11.493
2.100	9.108	11.298	16.724	20.072	15.925	11.799
2.200	9.748	12.399	17.939	20.630	16.707	12.578
2.300	9.960	12.764	17.902	20.852	17.085	13.050
2.400	9.065	12.562	17.278	20.221	16.713	12.879
2.500	8.507	11.911	16.835	19.848	16.151	12.405
2.600	8.679	12.196	16.687	19.698	15.962	12.016
2.700	8.593	12.033	17.204	19.397	16.076	12.016
2.800	8.335	12.196	17.462	19.546	16.750	12.440
2.900	8.851	12.764	18.232	20.146	17.433	12.793
3.000	9.450	13.773	18.598	20.555	18.115	13.179
3.100	9.535	13.853	18.598	20.518	17.896	13.478
3.200	9.322	13.491	17.976	19.848	17.307	13.435
3.300	8.593	13.048	17.351	19.286	16.936	13.350
3.400	8.808	13.491	17.204	18.986	16.376	13.093
3.500	9.065	13.933	16.983	18.722	16.139	13.307
3.600	9.279	13.933	16.904	18.948	16.189	13.861
3.700	9.407	14.133	17.093	19.923	16.787	14.749
3.800	10.003	14.771	17.829	20.401	17.233	15.378
3.900	10.595	14.771	18.159	20.221	17.491	15.545
4.000	10.553	14.771	18.012	19.848	17.528	15.712
4.100	10.342	14.533	17.682	19.511	17.675	15.378
4.200	10.680	14.253	17.939	19.511	17.418	14.959
4.300	10.637	14.053	17.425	18.571	16.342	14.454
4.400	10.257	13.572	17.204	17.852	16.414	14.116
4.500	10.342	13.692	17.167	17.852	16.451	14.138
4.600	10.637	14.652	17.609	18.080	16.825	14.201

VERTICAL ELECTRIC FIELD
STARTING COORDINATES

PROBE #	X	Y	Z
1.00	13.00	12.00	0.00
2.00	13.00	8.00	0.00
3.00	13.00	4.00	0.00
4.00	13.00	0.00	0.00
5.00	13.00	4.00	0.00
6.00	13.00	8.00	0.00

Z	P(1)	P(2)	P(3)	P(4)	P(5)	P(6)
0.000	1.394	2.594	2.400	2.452	2.561	2.865
0.100	1.486	2.890	4.177	2.902	3.421	3.002
0.200	1.715	3.269	5.669	3.287	4.593	3.552
0.300	2.126	4.156	6.842	4.212	5.920	4.421
0.400	2.581	5.505	8.047	5.157	7.171	5.333
0.500	2.807	6.726	8.976	6.303	7.916	6.151
0.600	2.898	7.230	9.516	7.091	8.866	6.830
0.700	2.807	7.230	9.439	7.886	8.951	7.417
0.800	3.215	7.397	9.708	8.878	9.249	7.956
0.900	4.696	9.068	10.706	10.726	10.050	8.672
1.000	5.672	10.228	11.736	12.623	10.881	9.295
1.100	5.849	10.434	11.546	13.397	11.291	9.517
1.200	5.981	9.566	11.355	13.746	11.004	9.738
1.300	6.377	9.483	11.660	14.325	11.291	9.783
1.400	6.990	10.104	12.496	15.405	11.739	10.180
1.500	7.295	10.228	13.101	16.430	12.385	10.136
1.600	7.773	10.104	13.478	17.015	12.864	10.136
1.700	8.378	10.358	14.230	17.700	13.221	10.356
1.800	8.808	10.764	14.904	18.004	13.889	10.620
1.900	8.292	10.434	14.829	17.548	13.767	10.576
2.000	7.773	9.566	14.530	17.320	13.011	10.356
2.100	7.989	10.063	14.941	17.852	14.279	10.664
2.200	8.765	11.093	16.280	18.910	15.203	11.451
2.300	8.808	11.543	16.687	17.324	15.736	12.016
2.400	8.464	11.461	16.317	19.061	15.660	12.016
2.500	8.162	11.461	15.872	18.722	15.279	11.886
2.600	8.292	11.134	15.761	18.344	15.050	11.408
2.700	7.903	11.216	15.724	18.117	14.858	11.233
2.800	7.643	10.846	15.724	17.700	15.126	11.277
2.900	7.903	11.707	16.466	18.382	15.811	11.451
3.000	8.679	12.359	17.278	19.099	16.713	12.016
3.100	9.065	12.845	17.462	19.249	16.973	12.664
3.200	8.636	12.481	17.093	18.986	16.526	12.965
3.300	8.335	12.481	16.687	18.307	16.264	12.965
3.400	8.292	12.643	16.895	18.042	15.849	12.621
3.500	8.249	12.805	15.501	17.358	15.241	12.491
3.600	8.507	12.764	15.277	17.662	14.973	12.922
3.700	8.593	13.169	15.724	18.042	15.279	13.321
3.800	9.194	13.451	16.650	18.722	15.622	13.989
3.900	9.833	13.652	16.761	18.609	16.038	14.328
4.000	9.833	13.612	16.946	18.533	16.414	14.665
4.100	9.960	13.813	17.093	18.647	16.862	14.876
4.200	10.130	13.933	17.020	18.797	16.713	14.749
4.300	10.173	13.491	16.946	17.776	16.301	14.201
4.400	9.833	12.926	16.132	17.129	15.849	13.606
4.500	9.748	12.967	16.280	16.633	15.698	13.563
4.600	10.173	13.411	16.392	16.747	15.387	13.478

VERTICAL ELECTRIC FIELD
STARTING COORDINATES

PROBE #	X	Y	Z
1.00	14.00	12.00	0.00
2.00	14.00	8.00	0.00
3.00	14.00	4.00	0.00
4.00	14.00	0.00	0.00
5.00	14.00	-4.00	0.00
6.00	14.00	-8.00	0.00

Z	P[1]	P[2]	P[3]	P[4]	P[5]	P[6]
0.000	1.302	1.668	1.925	1.639	2.077	2.177
0.100	1.394	2.005	3.112	2.111	2.609	2.498
0.200	1.440	2.426	4.059	2.315	3.231	2.819
0.300	1.897	3.185	5.199	3.076	4.360	3.461
0.400	2.308	4.198	6.139	4.033	5.054	4.284
0.500	2.581	5.295	7.076	5.120	6.011	4.923
0.600	2.535	5.927	7.465	5.709	6.772	5.652
0.700	2.353	5.632	7.309	6.303	7.083	6.197
0.800	3.034	6.221	7.620	7.355	7.479	6.695
0.900	4.159	7.272	8.744	8.916	8.134	7.146
1.000	4.918	8.318	9.554	10.301	8.823	7.821
1.100	5.185	8.318	9.708	11.267	9.164	8.180
1.200	5.185	8.318	9.516	11.848	9.292	8.404
1.300	5.849	8.485	9.939	12.390	9.546	8.338
1.400	6.069	8.401	10.591	13.475	9.883	8.672
1.500	6.025	8.443	10.897	13.823	10.259	8.538
1.600	6.552	8.443	11.546	14.827	10.757	8.672
1.700	7.643	9.026	12.685	15.790	11.699	9.206
1.800	8.076	9.524	13.553	16.058	12.465	9.428
1.900	7.556	9.151	12.987	15.790	12.305	9.206
2.000	6.946	8.443	12.761	15.559	12.264	8.939
2.100	7.295	8.776	13.591	16.135	12.705	9.584
2.200	7.903	9.897	14.567	17.015	13.340	10.224
2.300	7.903	10.269	15.128	17.472	14.084	10.796
2.400	7.686	10.311	14.792	17.510	14.517	10.971
2.500	7.816	10.517	14.866	17.396	14.356	11.189
2.600	7.903	10.517	14.904	17.472	14.162	10.883
2.700	7.513	10.187	14.492	16.671	13.772	10.488
2.800	6.990	10.021	14.342	16.097	13.576	10.268
2.900	7.208	10.475	14.904	16.518	14.240	10.312
3.000	8.076	11.502	15.798	17.244	14.935	10.977
3.100	8.335	11.870	16.021	17.510	15.546	11.712
3.200	8.033	11.666	15.947	17.852	15.660	12.276
3.300	7.903	11.911	15.687	17.700	15.546	12.405
3.400	7.946	12.155	15.277	17.205	15.050	12.276
3.500	7.643	11.788	14.492	16.480	14.201	12.016
3.600	7.599	11.666	14.042	16.250	13.772	12.016
3.700	8.033	12.033	14.342	16.633	13.673	12.276
3.800	8.292	12.196	14.866	16.786	14.123	12.448
3.900	9.022	12.318	15.277	17.053	14.472	13.050
4.000	9.151	12.643	15.501	17.320	15.203	13.691
4.100	9.450	12.886	16.206	17.548	15.962	13.861
4.200	9.791	13.128	16.354	17.700	15.962	14.031
4.300	9.620	12.926	16.132	16.977	15.470	13.606
4.400	9.236	12.318	15.612	16.518	15.279	13.179
4.500	9.151	12.196	15.426	15.943	15.050	12.722
4.600	9.407	12.481	15.314	15.866	15.088	12.750

VERTICAL ELECTRIC FIELD
STARTING COORDINATES

PROBE #	X	Y	Z
1.00	15.00	12.00	0.00
2.00	15.00	8.00	0.00
3.00	15.00	4.00	0.00
4.00	15.00	0.00	0.00
5.00	15.00	-4.00	0.00
6.00	15.00	-8.00	0.00

Z	P[1]	P[2]	P[3]	P[4]	P[5]	P[6]
0.000	1.440	1.542	2.004	1.406	2.174	2.039
0.100	1.486	1.458	2.400	1.572	2.319	2.131
0.200	1.486	1.878	2.914	1.840	2.609	2.452
0.300	1.669	2.552	4.138	2.452	3.363	3.048
0.400	2.034	3.438	5.160	3.357	4.360	3.644
0.500	2.171	4.704	5.787	4.320	4.870	4.193
0.600	2.308	4.999	6.295	5.010	5.557	4.832
0.700	2.034	4.831	6.178	5.524	5.920	5.333
0.800	2.762	4.915	6.413	6.117	5.920	5.743
0.900	3.485	6.347	7.153	7.620	6.594	6.106
1.000	4.249	6.894	7.892	8.725	7.391	6.569
1.100	4.606	7.062	8.008	9.915	7.716	7.146
1.200	5.007	7.439	8.551	10.610	7.960	7.552
1.300	5.229	7.481	8.899	10.996	8.177	7.641
1.400	5.185	7.523	9.092	11.538	8.479	7.641
1.500	5.318	7.062	9.323	12.274	9.037	7.597
1.600	5.849	7.146	10.015	12.971	9.334	7.597
1.700	6.903	8.067	11.393	14.209	10.259	7.756
1.800	7.164	8.359	12.116	14.364	10.963	8.314
1.900	6.990	7.983	11.698	14.055	11.250	8.225
2.000	6.333	7.732	11.698	14.055	11.168	8.046
2.100	6.465	7.732	12.078	14.750	11.455	8.448
2.200	6.728	8.485	12.987	15.328	11.902	8.984
2.300	6.552	8.984	13.629	15.866	12.465	9.606
2.400	6.771	9.400	13.817	15.905	13.063	9.915
2.500	7.295	10.063	14.080	16.441	13.261	10.224
2.600	7.469	9.980	14.042	16.288	13.300	10.224
2.700	6.946	9.441	13.742	15.520	13.063	9.871
2.800	6.465	8.860	13.176	14.866	12.705	9.339
2.900	6.552	9.441	13.553	15.020	12.963	9.384
3.000	7.426	10.104	14.305	15.751	13.458	9.650
3.100	7.513	10.599	14.642	16.097	13.967	10.444
3.200	7.339	10.805	14.866	16.556	14.472	11.320
3.300	7.469	11.502	14.979	16.938	14.627	11.712
3.400	7.773	11.420	14.605	16.518	14.434	12.016
3.500	7.469	11.257	14.005	15.751	13.693	11.669
3.600	7.077	10.928	13.440	15.636	13.182	11.451
3.700	7.339	11.051	13.478	15.636	12.745	11.564
3.800	7.946	11.339	13.930	15.597	12.824	11.451
3.900	8.162	11.420	14.230	15.751	13.182	11.773
4.000	8.378	11.543	14.492	15.981	13.772	12.491
4.100	8.894	11.952	15.091	16.556	14.743	12.922
4.200	9.194	12.440	15.649	16.556	15.050	13.050
4.300	9.236	12.440	15.463	16.173	15.050	13.136
4.400	9.065	11.788	14.829	15.866	14.781	12.750
4.500	8.679	11.992	14.734	15.367	14.508	12.787
4.600	8.894	11.992	14.455	15.251	14.434	12.405

DISTIRBUTION LIST

	No. of Copies
US Army Materiel Systems Analysis Activity ATTN: DRXSY-MP Aberdeen Proving Ground, Maryland 21005	1
DRSMI-R	1
DRSMI-LP, Mr. Voigt	1
DRSMI-RPR	5
DRSMI-RPT	1
DRSMI-RT, Mr. Edlin	20